FATIGUE CRACKING FROM STRESS CONCENTRATIONS IN MILD STEEL

by

ANTHONY RICHARD JACK

A THESIS SUBMITTED TO THE
UNIVERSITY OF ASTON IN BIRMINGHAM
FOR THE DEGREE OF
DOCTOR OF PHILOSOPHY

FEBRUARY 1971

I certify that to the best of my knowledge no part of the work described in this thesis was done in collaboration, unless specifically so described, and that the work has not been submitted for any other award.

A. R. Jack

February 1971.

SUMMARY

Pulsating tension fatigue tests have been carried out on edge notched specimens of a mild steel. An electrical potential drop technique was used to determine the number of cycles taken to initiate cracks and the rate at which the cracks grew across the specimen. The results could be described by the range of stress intensity factor, which for crack initiation was modified to take account of the notch root radius.

Analysis of elastic stress distributions at cracks and notches and models of plasticity at crack tips are used to discuss the results. Limited evidence in the literature indicates that the fracture mechanics approach may provide a general description of crack initiation and growth in notched specimens, and a simple graphical method of calculating fatigue lives is described.

The results are used to illustrate the effects of specimen size and geometry on the fatigue life of notched specimens. The relevance of the work to the assessment of the significance of defects in welds is discussed.

ACKNOWLEDGEMENTS

My thanks are due to my supervisors, Dr. A. T. Price of the C. E. G. B. and Dr. J. T. Barnby of the University of Aston in Birmingham for many helpful discussions and for their encouragement during this work; to my employers, C. E. G. B. (Midlands Region) for their permission to submit this thesis which is the result of work carried out for the C. E. G. B.; to my colleagues Mr. D. E. Yeldham, Mr. M. J. Siverns and Dr. G. J. Neate for helpful discussions and advice and to Messrs. J. A. Mullins and A. Davis who assisted with the experimental work in its later stages.

My thanks are also due to my wife for her continued encouragement and support.

CONTENTS

1. INTRODUCTION

In modern power generating plant, a recurring problem (Burgess and Glossop 1970) is the failure of butt welds in mild steel boiler tubes due to the extension of weld defects under fatigue conditions resulting from thermally induced stresses during plant start-up. These failures have led to increased inspection for the detection and measurement of defects and efforts to reduce their frequency by the adoption of suitable inspection standards. Historically, these standards have been based on experience and considerations of good welding practice and as yet standards based on fitness for purpose have not been widely adopted.

The traditional approach to assessing the significance of defects has been to carry out tests on notched specimens and to compare fatigue endurances with those of un-notched specimens on the basis of the elastic stress concentration factors at the notch. Interpretation of this data is often difficult because the full stress concentration factor is usually not realised, especially for sharp notches, and size effects are observed.

An alternative approach, which has been applied particularly to air-frames in recent years, is to design on the basis of crack growth rates which are usually determined on large sheet specimens. This has been stimulated by the observation (Paris and Erdogan 1963) that crack growth rates can be related to the crack tip stress intensity factor so that the techniques of linear elastic fracture mechanics can be used to predict crack growth rates in many practical circumstances. Design on this

basis assumes that fatigue crack initiation takes place on the first cycle of loading. However, several investigations (Weibull 1961, Hoeppner 1967) have shown that initiation, even from sharp notches, takes a finite number of cycles. Recently, a model of the plastic relaxation at a crack tip (Bilby, Cottrell and Swinden 1963) has been used to derive an expression relating the number of cycles taken to initiate a fatigue crack from a sharp notch or crack to the stress intensity factor (Weertman 1966, Bilby and Heald 1968). There are as yet insufficient data available to test this expression experimentally, but it would appear that it may be possible to develop a unified approach to crack initiation and propagation in notched specimens using a fracture mechanics approach.

The present study is concerned with the initiation and propagation of fatigue cracks in notched mild steel specimens at room temperature, and is part of a wider investigation currently in progress within the C. E. G. B. whose aim is to specify realistic inspection standards for butt welds in mild steel economiser tubes. These tubes are subjected to fatigue loading equivalent to a frequency of 0.33 Hz at temperatures up to 350^{o}C, and have a life requirement of 10^{4} cycles. There are few data available for crack propagation under these conditions and none at all for crack initiation, while the effects of specimen size, particularly thickness, and mean stress have received little attention. The aim of the present work was to obtain data and develop expressions describing crack initiation and propagation in annealed mild steel at room temperature. These results were to provide a basis for the extension of the work to welded material both at room temperature and at 350^{o}C, which would then be applied to the specification of realistic inspection standards.

2. LITERATURE REVIEW

The literature on fatigue is extensive and covers many aspects of the subject. In order to limit this review to sensible proportions, only the literature which is directly relevant to the present study is included and much interesting work on related topics has been left out. For convenience, the survey is divided into four sections - a general description of fatigue crack initiation and growth, a more detailed historical survey of the various models and laws of fatigue crack growth, a brief "state of the art" statement and a final section dealing with fracture mechanics.

2.1 General Description of Fatigue Crack Initiation and Growth

The first systematic study of fatigue was reported by Ewing and Humfrey (1903) who carried out metallographic examinations of fatigued Swedish iron. Prior to this time it had been thought that the fatigue process involved a "loosening of the intercrystalline cement". The work of Ewing and Humfrey demonstrated that the fatigue process involved the development of coarse slip bands which eventually broadened into cracks. Failure was by the spreading and linking up of these cracks.

For many years after this work, research in fatigue was concentrated on the development of slip bands (Gough and Hanson 1923) and it was not until 1939 that attention turned to the process of fatigue cracking when Orowan (1939) published his theory of fatigue crack growth. Even at this time there had been few reported observations of the physical features of crack initiation and growth and it was not until 1961 that Forsyth (1961)

developed a modern classification of fatigue cracking which he based on work during the previous decade.

Forsyth (1961) divided fatigue cracking into three stages - initiation, Stage I or slip-band growth and Stage II growth on planes normal to the maximum tensile stress. As was noted by Ewing and Humfrey (1903) the process of crack initiation in plane specimens takes place at slip bands. In studies of these slip bands in fatigued specimens, Forsyth (1956) observed that metal was extruded from the slip bands ("extrusions") and at the same time fine crevices, generally termed intrusions, were formed within the bands. These intrusions developed into cracks and crack initiation was loosely defined as the formation of a 'viable' crack from a slip band intrusion. While little attention has been paid to the number of cycles taken to initiate cracks in plane specimens per se, it has been shown that initiation occupies the majority of the life in high cycle fatigue (Thomson, Wadsworth and Louat, 1956). It is known that surface condition greatly influences the fatigue life, rough surfaces giving shorter lives than smooth surfaces and this is attributed to the presence of favourable sites for the early formation of slip bands at stress concentrations such as surface scratches. Several mechanisms for the formation of extrusions and intrusions have been proposed and have been summarised by Kennedy (1962). These mechanisms, although differing in detail, postulate reversed slip mechanisms on planes of maximum resolved shear stress. While there have been many investigations concerned with the effect of notches on fatigue life, crack initiation in notched or pre-cracked specimens has been almost entirely neglected, it being generally assumed that crack initiation takes

place immediately at sharp cracks and after a small porportion of the fatigue life from blunt notches. Exceptions to this are the investigations of Weibull (1961) and Hoeppner (1967), who showed that crack initiation could occupy a significant proportion of the fatigue life of notched specimens.

Stage I fatigue crack growth occurs on planes of maximum resolved shear stress and it is considered by Forsyth (1961) to be an extension of the reversed slip process responsible for crack initiation. This mode of growth can continue for an appreciable proportion of the life in plain specimens, particularly under torsional loading, but is generally assumed to be absent in notched tension specimens and will not be considered further in this review.

Stage II crack growth takes place on planes normal to the applied stress, and is generally thought to be controlled by the maximum principle stress operating in the region of the crack tip (Forsyth 1961). Stage II crack growth is characterised by microscopic features, known as fatigue striations, on the fracture surface. These features were first observed by Zappfe and Worden (1951) who wrongly connected them with some micro-cellular structure in metals. Many authors have since studied these striations, which appear as markings or lines on the fracture surface at right angles to the direction of propagation, and it has been shown (Laird and Smith 1962, Forsyth and Ryder 1961) that they are associated with the complex plastic deformation processes occuring at the crack tip. In general, each striation is produced by one cycle of the fatigue load (Forsyth and Ryder 1960, McMillan and Pelloux 1967).

The early part of Stage II propagation in sheet specimens is generally on a plane normal to both the applied tensile stress and the plane of the sheet, but as crack length increases the crack may rotate to a plane at 45° to the plane of the sheet but still normal to the applied stress (Weibull 1963). Weibull referred to propagation on the plane normal to the sheet as the tensile mode; while propagation on the 45° plane was termed the shear mode. Liu (1964) has correlated the transition from the tensile mode to the shear mode with the size of the plastic zone ahead of the crack tip, and showed that Weibull's (1963) results could be predicted from the ratio of the plastic zone size to the specimen thickness. The transition from the tensile mode to the shear mode has been variously reported to involve no change in the crack growth rate (Forsyth and Ryder 1961, Liu 1961 a) or to involve a change to a reduced rate in the shear mode (McEvily and Johnston 1967). Stage II crack propagation has been the subject of many papers, and will be considered in more detail in the next section. The rate of crack propagation is dependent principally on the alternating stress and crack length. Mean stress is usually found to have a small effect compared with that of the alternating stress (Frost and Dugdale 1958, Broek and Schijve 1963, Forman et al 1966); in one case mean stress was found to have no measurable effect on the crack growth rate for mild steel (Frost and Dugdale 1958).

An interesting phenomenon in notched fatigue tests is the formation of non-propagating cracks (Fenner, Owen and Phillips 1951, Frost 1955). Such cracks apparently form in notched specimens within a narrow range of applied alternating stress. Above this range, cracks,

propagate to failure while below this range cracks do not form.

2.2 Models of Crack Growth and Crack Growth Laws.

Orowan (1939) published a theory of fatigue which adopted a physical model based on work hardening at the crack tip. Orowan's concept was that the stress at the tip of a pre-existing crack or defect increased due to cyclic work hardening until eventually the fracture strength of the material was exceeded. Fracture of this hardened material caused the crack to advance an incremental distance into unhardened material where the stress did not exceed the fracture stress. The crack then remained dormant for a sufficient number of cycles for the stress at the new crack tip to increase to the fracture stress, when a further incremental advance occurred. This process was repeated until final fracture of the specimen. Orowan predicted that the rate of crack propagation would depend only on the applied stress, apparently neglecting the fact that the stress at the crack tip would increase as the crack extended due to the increased stress concentration effect. Although Orowan's model was based on increasing stress due to cyclic work hardening, it has since been generally viewed as an exhaustion of work hardening model in which the criterion for crack extension is an increase in local strain beyond the fracture strain.

Orowan's concept of fatigue was used by Head (1953) Weibull (1954, 1956) and McEvily and Illg (1958) to derive crack propagation laws. Head (1953) employed a mechanical model which considered rigid-plastic work

hardening elements ahead of the crack tip and predicted a law

$$\frac{da}{dN} = \frac{C_1 \sigma^3 a^{\frac{3}{2}}}{(\sigma_y - \sigma) r_p^{\frac{1}{2}}} \qquad (1)$$

where C_1 is a constant depending on the strain hardening modulus, the yield stress and the fracture stress,

σ_y is the yield stress

σ is the applied stress

a is the crack length

and r_p is the size of the plastic zone ahead of the crack tip which Head considered to be constant during crack propagation. Experimental evidence was presented to support the theoretical dependence of growth rate on crack length, but the value of the constant terms in equation 1 differed from that found experimentally by two or three orders of magnitude.

Weibull (1954, 1956) suggested that the crack growth rate depended only on the net section stress and predicted a law

$$\frac{da}{dN} = C\sigma_{net}^{n} \qquad (2)$$

Weibull presented experimental evidence to support this equation obtained from data in which the maximum load in zero-tension tests on aluminium alloys was reduced as the crack propagated to keep the net section stress constant. In a later paper Weibull (1961) analysed the results of tests on geometrically similar specimens of 24S-T aluminium alloy. Both crack initiation and crack growth data were presented. Again the crack growth data was claimed to agree with equation 2. The crack

initiation data were analysed in terms of net section stress and Weibull found that increased specimen size led to reduced values of N_i, the number of cycles taken to initiate a crack. He attempted, unsuccessfully, to rationalise the data by correlating N_i with the concentrated stresses at the crack tip as calculated by Neuber's (1958) methods.

Weibull's equation is supported by tests on mild steel reported by Rolfe and Munse (1963). Rolfe and Munse carried out tension-compression tests on centre notched mild steel plates in which the tensile load was reduced as the crack length increased so as to keep the net tensile stress constant. The compressive load was kept constant throughout, and Rolfe and Munse argued that since the crack closed completely on the compressive half-cycle the net compressive stress also remained constant. Rolfe and Munse found that in these tests the crack growth rate remained constant for the major part of crack growth.

McEvily and Illg (1958) argued that, since the concentrated stress at the crack tip increased as crack length increased (Neuber 1958) even at constant net section stress, the rate of crack growth should depend on this concentrated stress and proposed a law

$$\frac{da}{dN} \propto f\left(K_N \sigma_{net}\right) \qquad (3)$$

where K_N is the elastic stress concentration factor. McEvily and Illg showed that both Head's (1953) and Weibull's (1954, 1956) results agreed with equation 3 at least as well as with equations 1 and 2 respectively and presented additional experimental justification for this equation.

The first departure from Orowan's concept was by Frost and Dugdale (1958) who assumed that fatigue crack growth was a continuous, rather than a two stage process. They assumed, on elasticity considerations, that the crack remained geometrically similar as it propagated. They also demonstrated experimentally that in thin sheets the size of the plastic zone at the crack tip was proportional to the crack length provided that the crack was small compared to the sheet width. They concluded that, apart from stress, the only independent variable was crack length to which, they reasoned, the crack growth rate should be proportional. Experimental evidence was given to support this and they found that the crack growth rate could be expressed as

$$\frac{da}{dN} = C\sigma^{3}a \qquad (4)$$

where C is a constant

σ is the gross stress

provided that the crack length did not exceed $W/8$ where W is the specimen width. Notwithstanding the different physical concepts adopted in Head's (1953) work and their own, Frost and Dugdale pointed out that if in Head's equation the plastic zone size was assumed to be proportional to crack length equation 1 reduced to a form very similar to equation 4. Frost and his co-workers (Frost 1955, Frost and Dugdale 1958, Frost and Greenan 1964, Frost and Denton 1966, Frost and Dixon 1967) have reported studies of crack growth for a variety of materials. All of their data is analysed in terms of equation 4. Mean stress was found to affect only the value of the constant C in this equation, but in the case of mild steel Frost and Dugdale (1958) found that mean stress had no effect.

Frost (1955) also found the parameter $\sigma^3 a$ useful in analysing data on non-propagating cracks and concluded that this parameter had a critical value below which, even if cracks formed, they would not propagate.

Liu (1960) restated Frost and Dugdale's geometrical similarity hypothesis, and, using a somewhat more rigorous dimensional analysis, again concluded that the crack growth rate should be proportional to the crack length. In a subsequent paper Liu(1961b) using an idealised elastic-plastic stress-strain diagram and assuming that the hysteresis energy absorption to failure was constant, derived an expression

$$\frac{da}{dN} = C\sigma^2 a \qquad (5)$$

Again, experimental evidence was provided to support this equation.

The most recent approach to fatigue crack propagation is that using fracture mechanics proposed by Paris and his co-workers (Paris, Gomez and Anderson 1961, Paris and Erdogan 1963) in which crack growth rates are related to Irwin's (1958) stress intensity factor. Paris suggested that the stress intensity factor, being a unique description of the stress field at a crack tip, should control the rate of fatigue crack growth. Paris and Erdogan (1963) analysed data for 2024-T3 aluminium alloy, obtained from several sources, and found that an equation

$$\frac{da}{dN} = A\Delta K^4 \qquad (6)$$

where ΔK is the range of the crack tip stress intensity factor, provided

a good description of the data. In a critical review of previous crack propagation laws, Paris and Erdogan (1963) demonstrated that the stress intensity factor was equivalent to McEvily and Illg's (1958) $K_N\sigma_{net}$ approach for the specimen configuration used by McEvily and Illg. It can also be shown that the constant net section stress used by Rolfe and Munse (1963) leads to a constant stress intensity factor over much of the range that they considered.

Since Paris first proposed that crack growth data could be correlated using the stress intensity factor, many authors have demonstrated experimentally that this approach gives a good description of their data (e. g. Bellow and Long 1966, Carman and Katlin 1966, Brothers and Yukawa 1966, Brothers 1968), although the scatter in crack growth rates is generally large. The value of the exponent in equation 6 is commonly found to be about 4, but values within the range 2 - 6 have been observed (Miller 1968). Theoretical explanations for this correlation have been given by Krafft (1964, 1965), McClintock (1963), Weertman (1966), Bilby and Heald (1968) and Ham (1966). Krafft (1964, 1965) developed a concept of a fracture process zone to show that the fatigue crack growth rate should be proportional to $(\Delta K)^n$, where n should be in the range 2 - 4. Krafft concluded that the fourth power relationship should hold at low values of ΔK; at higher values of ΔK the exponent should fall to a value between 2 and 4. McClintock (1963) considered that, since fatigue is essentially a plastic flow phenomen, the crack growth rate should be proportional to the plastic zone size at the crack tip. McClintock proposed two possible mechanisms for crack growth - a) by damage and repeated crack initiation ahead of the crack tip, in which

case the growth rate should be proportional to the square of the plastic zone size and b) growth by irreversible plastic deformation at the crack tip in which case the growth rate should be directly proportional to the plastic zone size. The radius of the plastic zone can be expressed in terms of the square of the stress intensity factor (ASTM 1960), so that depending on which mechanism operated the growth rate should be proportional to either ΔK^4 or ΔK^2. McClintock found experimental evidence for both theories, although the majority of the data corresponded to crack growth by damage ahead of the crack tip.

Weertman (1966) and Bilby and Heald (1968) have used a model of the plastic relaxation at a crack tip (Bilby et. al. 1963) to derive expressions for the number of cycles to initiate a crack and the rate at which the crack grows after initiation. Both authors used this model to obtain the plastic displacement Φ at the crack tip after each cycle of the fatigue load. It was assumed that when the sum of the plastic displacements at the crack tip exceeded a critical value Φ_c the crack would extend, leading to an expression (Bilby and Heald 1968) for the number of cycles taken to initiate a crack

$$N_i = \frac{2\gamma G}{\pi a \sigma^2} \qquad (7)$$

where $\gamma = \Phi_c \sigma_y$ is a measure of the plastic work done per unit area of fracture

and G is the shear modulus.

After initiation, the crack will grow provided that the displacement at the crack tip exceeds the critical value Φ_c and an expression

$$\frac{da}{dN} = \frac{5}{3}\left(\frac{\pi}{4}\right)^3 \frac{\sigma^4 a^2}{G\gamma\sigma_y^2} \tag{8}$$

was obtained for the crack growth rate. For the geometry considered,

$$K = \sigma a^{\frac{1}{2}} \tag{9}$$

and $$N_i \propto K^{-2} \tag{10}$$

$$\frac{da}{dN} \propto K^4 \tag{11}$$

which is the relationship proposed by Paris (1963). Ham (1966) considered that, during crack extension on the tensile stroke of the fatigue cycle, the volume of the material within the plastic zone is conserved and on goemetrical considerations the crack growth rate should be given by

$$\frac{da}{dN} \propto \left(\frac{K}{E}\right)^4 \tag{12}$$

where E is Young's modulus. This result is in close agreement with the experimental observations of Pearson (1966) who found that, for a variety of materials

$$\frac{da}{dN} \propto \frac{\Delta K}{E}^{3.6} \tag{13}$$

Several authors have considered the effect of mean stress on fatigue crack growth rates as expressed in equation 6. Broek and Schijve (1963) carried out tests on aluminium alloy sheets and proposed an empirical relationship

$$\frac{da}{dN} = C_1 e^{-C_2 R} \sigma_{max}^3 a^{3/2} \left\{1 + 10\left(\frac{a}{W}\right)^2\right\} \tag{14}$$

where R is the ratio of minimum to maximum stress and C_1 and C_2 are constants. Forman et. al. (1966) pointed out that any equation which includes mean stress should predict an infinite crack growth rate when K_{max} reaches the fracture toughness and proposed a relationship

$$\frac{da}{dN} = \frac{C(\Delta K)^n}{[(1-R)K_c - \Delta K]^m} \qquad (15)$$

where K_c is the fracture toughness

and m is unity in Foreman's equation

which satisfied this condition and gave a good fit to data obtained on aluminium alloys. Hudson and Scardina (1969), again working with aluminium alloys, found that equation 15 gave a good fit to their data whereas equation 14 did not. Pearson (1969) has investigated the effect of mean stress on two aluminium alloys. He pointed out that the condition that the growth rate should be infinite when $K_{max} = K_c$ was satisfied by equation 15 for any value of the exponent m, and fount that a value $m = \frac{1}{2}$ gave a better fit to his data than the value m = 1 proposed by Forman.

Weertman (1969) has considered the effect of mean stress on his model (1966) of fatigue crack growth. He concluded that mean stress has very little effect on crack growth rates except when the maximum stress is comparable with the fracture stress σ_f, when the crack growth rate will increase rapidly as the limiting condition of $\sigma_{max} = \sigma_f$ is approached.

The fracture mechanics approach has been used by Harrison (1969) to correlate data on non-propagating cracks. Harrison found that for several materials there is a minimum value of the stress intensity factor below which cracks will not propagate. He also showed that if this critical value were

expressed in terms of K/E, then the results for a number of materials fell within a narrow scatter band.

2.3 Present State of the Art

The fracture mechanics approach is now widely used to correlate fatigue crack growth data and there is encouraging progress on the theoretical treatment of crack growth. The confusion that existed between earlier methods of correlation has been largely removed; the fracture mechanics approach not only provides a method by which virtually all crack growth data can be described but is readily applicable to many practical problems. However, there are many areas where there is disagreement between various investigators - for example (a) the value of the exponent in the equation proposed by Paris (1961, 1963); (b) the effect of mean stress, particularly in mild steel; (c) the transition from the tensile to the shear mode of propagation and any effect of this transition on crack growth rates, and (d) the effect of material properties on the value of the constant in the Paris equation. It should be noted that the commonly used plot of $\log da/dN$ Vs $\log \Delta K$ can hide a large amount of scatter - an order of magnitude variation in da/dN is covered by less than a factor of 2 in ΔK - and this can lead to small but significant effects on the crack growth rate being neglected. With specific reference to mild steel, there is a wealth of reported crack growth data which can be applied to practical problems in spite of the areas of lack of knowledge mentioned above. With regard to crack initiation, there is an almost complete lack of data; the only reliable measurements of N_i are for an aluminium alloy (Weibull 1961)

and too few results are available for satisfactory analysis. Theoretical treatments of fatigue crack growth have indicated that the stress intensity factor might be useful in describing crack initiation from pre-existing cracks, but there is no indication as to how far this approach could be used to describe crack initiation from notches of various root radii.

2.4 The Stress Intensity Factor

The stress intensity factor arises out of Westergaard's (1939) treatment of the stress analysis of a crack. Westergaard defined an Airy stress function which satisfied the equilibrium and compatibility equations for the case of a crack of length 2a in an infinitely wide sheet under a uniform tensile stress (Fig. 1). The crack tip stress field at a point $P(r, \theta)$ where r is small compared with the crack length (Irwin 1960), is given by

$$\sigma_x = \frac{K}{(2\pi r)^{\frac{1}{2}}} \cos \theta/2 \left[1 - \sin \theta/2 \sin \frac{3\theta}{2}\right] \quad (16)$$

$$\sigma_y = \frac{K}{(2\pi r)^{\frac{1}{2}}} \cos \theta/2 \left[1 + \sin \theta/2 \sin \frac{3\theta}{2}\right. \quad (17)$$

$$\tau_{xy} = \frac{K}{(2\pi r)^{\frac{1}{2}}} \sin \theta/2 \cos \theta/2 \cos \frac{3\theta}{2} \quad (18)$$

where K, termed the stress intensity factor is given by

$$K = \sigma(\pi a)^{\frac{1}{2}} \quad (19)$$

for the geometry shown in Fig. 1.

The stress intensity factor K uniquely defines the stress field around the crack tip and Irwin (1960) has shown that K is related to the force G tending to cause crack extention by the relationships

$$K^2 = EG \text{ in plane stress} \tag{20}$$

$$K^2 = \frac{EG}{(1 - \nu^2)} \text{ in plane strain} \tag{21}$$

where ν is Poisson's ratio.

For the geometry shown in Fig. 1., equations 19 and 20 give

$$\sigma = \sqrt{\frac{2EG}{\pi a}} \tag{22}$$

which is similar to the Griffith (1920) equation for the fracture stress of a brittle solid containing a crack length of 2a.

$$\sigma_f = \sqrt{\frac{2E\gamma}{\pi a}} \tag{23}$$

where γ is the surface energy.

The Griffith equation is valid only for a completely brittle solid; for metals where crack extension is accompanied by plastic flow the increase in surface energy considered in the Griffith equation is several orders of magnitude less than the energy expended in plastic deformation. Irwin (1948) and Orowan (1950) developed a modified Griffith theory in which the energy of plastic deformation or crack extension force G replaced the surface energy as the controlling factor in brittle fracture. Irwin's concept was that fracture occurred when, on increase in stress, the crack extension force as defined in equation 22 reached a critical value G_c which he termed the critical strain energy release rate or the fracture toughness. The stress intensity factor K has now replaced G as the parameter used to describe the onset of brittle fracture. The critical value K_c is dependent on the condition of stress at the crack tip and is higher in plane stress than in plane strain. The plane strain value, termed K_{1c} is found to be constant

for a particular material and is extensively used in specifying maximum tolerable defect sizes in structures and in materials selection.

The stress intensity factor relating to geometries other than that shown in Fig. 1 can be obtained by similar analyses (Irwin 1960); e. g. for a semi-infinite plate containing an edge crack of length a under uniform tension

$$K = 1.1\,\sigma\,(\pi a)^{\frac{1}{2}} \qquad (24)$$

For finite plate widths it is necessary to include a correction factor in equations 19 and 24 to take account of interactions between the crack and the free surface of the plate. This is usually expressed in the form of a polynominal in a/W (Brown and Srawley 1966), where W is the plate width, and the stress intensity factor is expressed as

$$K = \sigma a^{\frac{1}{2}}\, f(a/W) \qquad (25)$$

$$\text{where } f(a/W) = A_0 + A_1(a/W) + A_2(a/W)^2 + A_3(a/W)^3 + A_4(a/W)^4 \qquad (26)$$

and the constants $A_0 - A_4$ depend on the geometry. Several methods are available for computing $f(a/W)$ including conformal mapping (Bowie and Neal 1965), boundary collocation procedures (Srawley and Gross 1967), and finite element analysis (Dixon and Pook 1969). Alternatively, the crack extension force G can be determined experimentally (Sullivan 1967) since Irwin (1960) has shown that

$$G = \frac{P^2}{2B} \quad \frac{d}{da} \quad \left(\frac{1}{M}\right) \qquad (27)$$

where P is the load on the specimen

B is the specimen thickness

$\frac{1}{M}$ is the compliance i. e. Extension/load.

3. EXPERIMENTAL

3.1 Outline of Experimental Work

While the principal aim of the project was to provide information on the initiation and propagation of fatigue cracks from notches in annealed mild steel at room temperature, it was clear that the major topic requiring investigation was the initiation of fatigue cracks since there is a wealth of data on the propagation of cracks. The experimental work, therefore, was designed primarily to study the factors affecting crack initiation, such as applied stress range, mean stress, notch depth, notch root radius, specimen width and specimen thickness. Concurrently sufficient information would be obtained from these tests to resolve some of the questions that existed regarding crack growth rates.

In order to simplify experimental observations and the interpretation of data, rectangular cross section specimens with single edge notches were used. Testing was carried out on controlled lead screw movement testing machines at the frequency dictated by the basic cyclic frequency to which boiler tubes are subjected in service, i.e. 0.33 Hz. Most of the tests were continued to final fracture so as to provide the maximum information on crack growth.

3.2 Material

The material used throughout this work was mild steel to BS. 3602-27, which is extensively used in C. E. G. B. boiler plant and is commonly referred to as 27 ton mild steel. It was obtained in the form of hot-rolled strip at thicknesses in the range 0. 25 in. - 2 in.; some of the thicker material was

subsequently hot-rolled down to 0. 25 in. since the majority of the specimens tested were machined from the thinner material. The composition of the material is given in Table I.

In service, the material is used in the form of electrical resistance welded tube, and a typical structure is shown in Fig. 2. It was decided that data would be obtained on material with a similar structure. Some experiments showed that this was produced by a heat treatment of 1 hour at 880°C followed by 6 hours at 600°C (Fig. 3). Tensile properties of the material are given in Table II.

3.3 Fatigue Tests

The form of the specimen used is shown in Fig. 4; the dimensions given are those of the most commonly used test piece. Specimens were machined with their long axes parallel to the rolling direction and their wide faces in the plane of the strip. The specimens were machined to a tolerance of $\pm$ 0. 001 in. on the major dimensions. The specimens were pin loaded through shackles rigidly attached to the loading bars of the machine, and particular attention was paid to positioning the loading pin holes on the centre line of the specimen to ensure axial loading. The design of the specimen and loading shackles was such that the end of the specimen butted hard against the loading shackle, thus preventing rotation of the ends of the specimen and maintaining good alignment throughout the test. Great care was taken in machining the notches; notch depth was controlled to $\pm$0. 001 in. and notch root radius to within $\pm$0. 0005 in. After machining, the specimens were annealed in a vacuum better than 10^{-3} torr and furnace cooled.

Two fatigue testing machines were used. Both were essentially controlled lead screw movement tensile testing machines which had been modified to allow load reversal at pre-set limits. The capacities of the machines were 0 - 10,000 lb f and 0 - 50,000 lb f; the calibration of the load cells and load meters was checked with a Grade I proving ring and found to be accurate to within $\pm 1\%$. The machines allowed independent control of load and frequency, and the control systems were such that the desired load could be attained within the first 10 or 20 cycles of a test at the frequency used. After the first few cycles, load control was within $\pm 2\%$.

Tests were carried out under zero-tension or tension-tension conditions at 0.33 Hz. The loads and specimen dimensions used were such that failure occurred in less than about 3×10^5 cycles; details of the specimen dimensions are given in Table III. The variables investigated were specimen width (W), thickness (B), notch depth (a_o), notch root radius (ρ), stress range ($\Delta\sigma$) and mean stress (σ_m). In order to compare the effect of a microscopically sharp crack with that of notches some tests were carried out in which a fatigue crack was initiated in a notched specimen prior to annealing, and the specimens were re-tested.

3.4 Crack Length Measurement

Of the various methods available for measuring crack length, the electrical potential technique reported by Gilbey and Pearson (1966) was used for the following reasons

a) The method is cheap and simple to use.

b) Continuous measurement of the crack length is possible.

c) Calibration curves are available which relate voltage drop to crack length. No further experimental calibration is necessary.

3.4.1. General Description of the Method

The technique has been reported in detail by Gilbey and Pearson (1966). Briefly, a constant uniform direct current is passed through a specimen containing a crack. The potential drop across the crack (V_a) is compared with that across a unit length of uncracked specimen (V_o) and the crack length (a) is deduced from graphs relating V_a/V_oW to a/W, where W is the width of the specimen. Details of a typical specimen are shown in Fig. 5. A graph of V_a/V_oW versus a/W is shown in Fig. 6. Taking the positive co-ordinates of the points at which V_a is measured as (x, +y) and (x, -y), Fig. 6 relates to only one value of x (in this case 0.1 W) but covers a range of values of y.

Gilbey and Pearson (1966) recommend that at constant current (A) the following measurements be made: V_o, the potential drop across a unit length of uncracked specimen; V_{a_o} the potential drop between the points (x, +y) and (x, -y) with a crack of known length a_o; V_a, the potential drop between (x, +y) and (x, -y) with the crack of unknown length a. The ratio V_{a_o}/V_oW determines

the effective value of y (for a notch this effective value may be different from the measured distance y as the presence of a notch rather than a crack has the same effect as an increase in y) and hence which particular curve in Fig. 6 is appropriate for the rest of the experiment, i. e. for the deduction of a/W from V_a/V_oW. From Fig. 6 it can be seen that the measurement of crack length becomes less sensitive to errors in determining the effective value of y as the crack length increases. Graphs of V_a/V_oW are available for values of x other than that of x = 0. 1W shown in Fig. 6, and the graph for x = 0. 3W is shown in Fig. 7. Comparing Figs. 6 and 7 it can be seen that, at small values of a/W greatest sensitivity to changes in a/W is obtained by using small values of x and y.

3. 4. 2. Experimental Details

Constant current was obtained by using a constant voltage transistorised D. C. power supply unit and passing the current through a suitable external dropping resistance, in this case a length of heavy gauge Nichrome wire. The output voltage was set in the range 1 - 3 volts and the stability of the units was better than 1 part in 4000 over a period of 24 hours after an initial warming up period of about 1 hour. Changes in the resistance of the specimen during crack extension before final fracture were negligible compared with the total series resistance of the circuit, being about 1 part in 5000.

With the specimens used in this work, uniform current was obtained simply by introducing the current through the loading pins via the loading bars. One of the loading bars was electrically insulated from the rest of the machine and the other was earthed. Good earthing was essential and it was found necessary to use a separate remote ground earth rather than the laboratory common earth.

Potential measuring leads were spot welded to the specimen at the appropriate points (See Fig. 5) which had previously been marked out using a scriber and vernier measuring gauge. Accurate positioning of these leads was easy after a little practice. It should be noted that only one of the position co-ordinates of each point is critical; in the case of the V_a leads the effective value of y is deduced from $V_{a_o}/V_o W$ and only the value of x is critical, while in the case of the V_o leads only their longitudinal separation is important since potential is uniformly distributed across the specimen. The V_a leads were positioned on opposite faces of the specimen so that changes throughout the thickness were sensed.

In the initial experiments, either platinum or nichrome potential leads were used. Both gave rise to thermo-electric effects, and for later tests 0.008 in. dia pure iron wire was used. The leads were screened to prevent pick-up which arose due to movement of the leads in the field generated by the specimen current; the screens were earthed to the earthing point on the loading bar. Potential was measured on a potentiometric chart recorder.

The theoretical accuracy and sensitivity of the method are determined by the current and potential measuring instruments used, and can be deduced by reference to Fig. 6. Noting that the graph of V_a/V_oW versus a/W is approximately linear at a/W = 0.2 for leads at x = 0.1 W, y = $\pm$ 0.05 W, the line in Fig. 6 can be represented by

$$\frac{V_a}{V_oW} = 2.25\,\frac{a}{W} \tag{28}$$

Now V_o for unit gauge length is given by

$$V_o = \frac{A\lambda}{BW} \tag{29}$$

where A = specimen current

λ = resistivity of the material

so $$V_a = 2.25\left(\frac{a}{W}\right)\left(\frac{A\lambda}{B}\right) \tag{30}$$

If the accuracy of the recorder is 10^{-6}V and the required accuracy in measurement of a/W is 10^{-3}, then from equation 30 the current required is given by

$$A = 4.44 \times 10^{-4}\left(\frac{B}{\lambda}\right) \tag{31}$$

For mild steel at room temperatures, λ is about 16×10^{-8} ohm. m. and for a 0.2 in. thick specimen the current required is about 14 amps. In the early experiments the accuracy of the recorder was only about 10^{-5}V and the current used was about 15 amps so that crack length measurements were only accurate to about 10^{-2}W. In the later tests, recorders with an accuracy of 10^{-6}V were used and specimen currents were raised to about 25 amps so that the accuracy of the method was about 5×10^{-4}W.

Note that while the absolute accuracy of the technique, especially in the early tests, was not good, the sensitivity to changes in V_a was much higher and crack initiation could be detected with much greater accuracy.

Since resistivity changes with temperature it was necessary to minimise temperature variations in the specimen. This was done by shielding the specimen from draughts and direct sunlight. For mild steel at room temperature, the resistivity is 16×10^{-8} ohm. m., and the change in resistivity per ^{o}C is 9.28×10^{-10} ohm. m. or $5.80 \times 10^{-5}\%$. From Fig. 6, for $x = 0.1W$, $y = 0.05W$ and at $V_a/V_oW = 0.4$, the change in V_a/V_oW for an increase in crack length of $10^{-3}W$ is 2.15×10^{-3} or $5.625 \times 10^{-5}\%$. Thus if the original value of V_o is used to calculate V_a/V_oW the apparent change in crack length for a $1^{o}C$ change in temperature is about $10^{-3}W$.

Pearson (1967) and Gilbey and Pearson (1966) have carried out extensive checks to confirm the accuracy of the method, and found that the results obtained were in agreement with optical measurements on the specimen surface within the accuracy of the optical method, which was about 0.005 in. In the present work, crack lengths on several specimens were measured both by the electrical potential technique and optically at x 50 magnification using a grid superimposed on the specimen surface. Crack initiation was always detected electrically before the crack

could be seen on the specimen surface and during crack growth the crack length measurements were up to about 0.010 in. higher than the optical observations until gross yielding of the specimen took place. Examination of the fracture surfaces showed that the crackfronts were bowed with the centre leading the edge by amounts which could account for these differences, suggesting that electrical potential results represent either the maximum crack length or some average value; the opitcal method was not sufficiently accurate to establish which.

After gross yielding of the specimen the discrepancy increased, and differences of up to 0.050 in. were observed in one case although 0.025 in. was more common. This was probably due to a reduction in W due to gross yielding of the specimen. Noting that V_a/V_oW is independent of changes in W since $V_oW = A\lambda/B$, a difference of 0.025 in. at a crack length of 0.5 in. in a 1 in. wide specimen would result from a change in W of 5%. Examination of failed specimens showed that reductions in W of this amount did, in fact, occur.

During the tests, two effects sometimes occurred which complicated the use of the method. Firstly, strain cycling of the specimen led to cyclic changes in the position of the V_a measuring leads and hence in V_a. This effect was small, and the mean value of V_a was used. Secondly, in tests at high loads, changes in the position of the V_a leads in the first few cycles due to incremental

extension of the specimen gave an increase in the value of V_a. However, V_a stabilised after relatively few cycles and this stable value was taken to be V_{a_o}.

3.5 Compliance Calibration

So that the results of the fatigue tests could be analysed using linear elastic fracture mechanics it was necessary to confirm that the published formula (Gross et. al 1964) for the stress intensity factor of a single edge notched specimen was valid for the fatigue specimen. This was done by a compliance calibration (Sullivan 1967). Specimens with the dimensions shown in Fig. 4, i. e. W = 1. 0 in., B = 0. 2 in. were machined with notch depths from 0 to 0. 6 in. in 0. 1 in. increments. The specimens were loaded in tension in the 10, 000 lb f capacity fatigue machine and the extension across a 2 in. gauge length, symmetrical about the notch, measured with a transducer extensometer. Extension on both sides of the specimen was measured and the mean of the two readings plotted against load on an X - Y plotter. Reproducible straight lines were obtained from specimens with notches up to 0. 5 in. deep. In the case of the 0. 6 in. deep notch the load necessary to take up the slack in the system was greater than the gross yield load of the specimen and no true elastic line could be obtained.

3.6 Other Experimental Work

Standard metallographic techniques were used for the examination of microsections. The fracture surfaces of the specimens were examined

optically at low magnifications, and in the scanning electron microscope at higher magnifications.

4. RESULTS

4.1 Compliance Analysis

The specimen compliance at a particular crack length is ralated to the strain energy release rate G and the stress intensity factor K by the equations (Irwin 1969, Sullivan 1967).

$$BG = \tfrac{1}{2} P^2 \frac{d}{da}\left(\frac{1}{M}\right) \tag{32}$$

$$EG = K^2 \text{ in plane stress} \tag{33}$$

$$\frac{EG}{(1-\nu^2)} = K^2 \text{ in plane strain} \tag{34}$$

where P = load on specimen

E = Young's modulus

ν = Poisson's Ratio

$\frac{1}{M}$ = compliance

a = crack length

For the standard ASTM single edge notched (SEN) specimen loaded in tension (Gross et. al. 1964).

$$K = \sigma a^{\frac{1}{2}} f\left(\frac{a}{W}\right) \tag{35}$$

where σ = stress

$$f\left(\frac{a}{W}\right) = 1.99 - 0.41\left(\frac{a}{W}\right) + 18.70\left(\frac{a}{W}\right)^2 - 38.48\left(\frac{a}{W}\right)^3 + 53.85\left(\frac{a}{W}\right)^4 \tag{36}$$

and for this specimen, equations 32, 34 and 35 give

$$\frac{EBW^2}{2(1-\nu^2)} \cdot \frac{1}{M} = \int a \left(f\left(\frac{a}{W}\right)\right)^2 da \tag{37}$$

and

$$\frac{EB}{2(1-\nu^2)} \cdot \frac{1}{M} = f'\left(\frac{a}{W}\right) + \text{Constant of Integration} \tag{38}$$

On the right hand side of equation 38, $f'\left(\frac{a}{W}\right)$ is related to the displacement due to presence of the crack and the constant of integration is related to the elastic displacement, independent of the crack, over the gauge length across which the compliance $1/M$ is measured.

Equations 37 and 38 have been solved for a standard SEN specimen with W = 1.0 in, B = 0.2 in. The compliance, $^{1}/M$, expressed in units of 10^{-3} in/ 10^{3} lbs as measured over a 2 in gauge length, is shown as the solid line in Fig. 8. The experimental points obtained with the notched fatigue specimens are also shown in Fig. 8, and show satisfactory agreement with the standard SEN specimen up to $^{a}/W = 0.5$. Since all but a few of the fatigue test results are for $^{a}/W \leq 0.5$ it was concluded that the formula for the standard SEN specimen could be used to calculate the stress intensity factor in the fatigue specimens.

4.2 Crack Initiation and Growth

4.2.1 General Description

The results showed that the number of cycles taken to initiate a crack N_i was independent of notch root radius ρ up to a critical value of 0.010 in. This critical value ρ_o was independent of stress σ and notch depth a_o. Tests in which cracks were initiated in specimens which had been pre-cracked, annealed and re-tested showed that N_i for a sharp crack was the same as for a notch of the same length with root radius less than ρ_o. Above the critical root radius, N_i increased with ρ.

After initiation, the early stages of crack growth in many tests was characterised by a decreasing crack growth rate for about the first 0.005 in. of crack growth. This effect was quite definite at intermediate alternating stress levels, but was not well defined at higher stress levels. At low stress levels, crack growth rates were so small that, if the effect were present, the crack length measurement

techniques would not have been sufficiently accurate to detect it. After this initial period of crack growth, the propagation rate increased with crack length until final fracture of the specimen.

At a particular alternating stress level, mean stress had a small but significant effect on both N_i and crack growth rates. Specimen thickness also affected initiation and growth, particularly in specimens less than 0.2 in. thick.

It is convenient to describe first the results of zero-maximum stress tests on 1 in. wide x 0.2 in. thick specimens containing sharp notches, i.e. $\rho < 0.010$ in., followed by a description of the effects of root radius, mean stress and specimen dimensions on this basis data.

4.2.2 Crack Initiation and Growth in 1 x 0.2 in. Specimens Containing Sharp Notches, Tested Under Zero-Maximum Load.

The effect of stress range $\Delta\sigma$ on N_i at various values of notch depth a_o is shown in Fig. 9. A good description of these data was obtained by plotting N_i against the range of stress intensity factor, calculated assuming that the notch behaved as a sharp crack, as shown in Fig. 10. The slope of the line in Fig. 10 is $-\frac{1}{4}$, indicating a relationship

$$N_i \propto \frac{1}{\Delta K^4} \tag{39}$$

Crack growth rates were determined by plotting the crack length a against the number of cycles N and drawing tangents to the curve. A typical plot of a against N at an intermediate stress is shown in Fig. 11. Growth rates were usually determined at intervals of 0.025 in., starting

at a_o + 0.025 in. so that the results were not affected by the initial stages of crack growth from the notch. Crack growth rates at the same stress range and crack length obtained from several tests are shown in Fig. 12 where the growth rate da/dN is plotted against crack length at two stress ranges. The bars represent the extremes of up to 9 determinations of da/dN, while the points are the arithmetic means of these values. The scatter in crack growth rates at the same crack length and stress range was up to a factor of 3. This scatter was not evident in the number of cycles spent in propagating the crack (N_p) in duplicate specimens tested at the same stress range, for which the scatter was typically of the order of $\pm$ 15% about the mean value.

Mean values of crack growth rates at four stress ranges are plotted against the range of stress intensity factor (ΔK) in Fig. 13. At stress ranges of 0 - 20 ksi and above there was no significant effect of stress range, but the 0 - 15 ksi data were consistently lower. All of the data except for the 0 - 15 ksi results at $\Delta K > 65$ ksi $\sqrt{\text{in}}$ fell within a scatter band of slope 3 which covered a factor of 3 on da/dN, indicating a relationship

$$\frac{da}{dN} \propto (\Delta K)^3 \qquad (40)$$

It should be noted that the 0 - 15 ksi results in Fig. 13 which were below the scatter band were obtained at crack lengths greater than 0.5 W and it is therefore possible that the Gross (1964) expression used to calculate ΔK was not valid for these points.

4.2.3 The effect of mean stress

The results of tests on 1 in. x 0.2 in. specimens containing 0.1 in. deep sharp notches at the same alternating stress but with different mean stresses are given in Table IV. There was a small but consistent decrease both in N_i and N_p with increasing mean stress. Assuming a UTS criterion for final fracture, a decrease in N_p would be expected even in the absence of a mean stress effect on crack growth rates since the UTS on the net section would be reached at a smaller crack length as the mean stress increased. This crack length has been calculated for the high mean stress tests and the number of cycles taken to propagate a crack to this value under zero-maximum stress conditions (N'_p) has been determined from plots of a against N for zero-maximum tests at the same stress range. These results are also included in Table IV. Comparing these with the experimental values it can be seen that mean stress did have a real effect on N_p. Crack growth rates from three of these tests are compared with the scatter band from Fig. 13 in Figs. 14(a) and 14(b). Fig 14(a) shows the results of a test in which the ratio of minimum to maximum stress, R, was 0.33; Fig. 14(b) shows the results of two tests for R = 0.50. The data from tests on which the maximum stress did not exceed the general yield stress (35 ksi) of the material fell within the scatter band of the zero-maximum results, while the results of the test in which the maximum stress exceeded the general yield stress were above this scatter band, although by less than a factor of 2.

4.2.4 The Effect of Specimen Thickness

The results of tests on 1 in. wide specimens containing 0.1 in. deep sharp notches are given in Table V, together with the scatter of

data from the tests on 0. 2 in. thick specimens. The results of some of these tests are plotted in Fig. 15 where N_i and N_p are plotted against thickness as a function of alternating stress. The N_i data indicates that N_i is independent of thickness above 0. 2 in. at all stresses although the result of the test at 0 - 17. 5 ksi on a 0. 4 in. thick specimen was a little below the 0. 2 in. thick scatter band. Below 0. 2 in. there was a reduction in N_i, particularly at the higher stress levels.

The N_p data also showed a stress dependent reduction below 0. 2 in. but the results on the 0. 9 in. thick specimen showed an increase in N_p compared with the 0. 2 in. thick data. The N_p results from the 0. 4 in. thick specimens fell within the scatter of 0. 2 in. thick data. Crack growth rates in the 0. 05 in. and 0. 08 in. thick specimen fell at the top or above the scatter in data from 0. 2 in. thick specimens shown in Fig. 13, and are plotted in Figs 16(a) and 16(b). The results for tests in 0. 4 in. thick specimens were within the scatter band in Fig. 13., as shown in Fig 16(c). No crack growth data are available for the 0. 9 in. thick specimens; at the high loads used in the tests electrical interference from the testing machine resulted in poor test records.

4. 2. 5 Other Tests on Specimens Containing Sharp Notches

Tests were carried out on 0. 2 in. thick specimens with W = 2. 0 in. and on 1 in. thick specimen with W = 0. 2 and W = 0. 4 in. Values of N_i and N_p for these tests are given in Table VI. N_i is plotted against ΔK in Fig. 17. The scatter band from Fig. 10 is also included in this plot.

Crack growth rates determined from these specimens were within the scatter band in Fig. 13, as shown in Fig. 18.

4.2.6 The Effect of Notch Root Radius

As stated in 4.2.1, N_i was independent of root radius ρ up to a critical value of 0.010 in. This critical value ρ_o was independent of stress and notch depth. Above the critical value N_i increased with increasing root radius. The results of some of the tests showing this effect are plotted in Fig. 19. At particular values of a_o and σ, the relationship indicated was

$$N_i \propto \rho^2 \qquad (41).$$

By comparison with equation 28, this suggested that N_i should correlate $\Delta K/\rho^{\frac{1}{2}}$. The results of all tests on specimens at thicknesses of 0.2 in. and above are shown in Fig. 20. where N_i is plotted against $\Delta K/(\rho')^{\frac{1}{2}}$, where

$\rho' = \rho$ when $\rho \geq \rho_o$

$\rho' = \rho_o$ when $\rho \leq \rho_o$

Note that the scatter in Fig. 20 is only slightly larger than that in Fig. 10.

There was no effect of root radius on N_p.

4.3 Examination of Specimens

Metallographic examination of microsections through the fracture surface showed that cracks had initiated and propagated in a transgranular manner (Fig. 3). There was no indication of any Stage 1 growth on a plane

at 45° to the tensile axis, propagation being always normal to the tensile axis.

In some of the tests, initiation was observed by viewing the root of the notch through a magnifying glass. Initiation occurred simultaneously at several points distributed across the root of the notch. These points were usually on different planes. As the test progressed, these points spread laterally until they linked and subsequent examination of the fracture surfaces revealed steps on the fracture surface where linking had occurred. These steps disappeared after the crack had grown typically about 0.010 in. and the crack propagated thereafter on a single plane. In some specimens where the load had been changed part way through the test the position of the crack front was clearly marked on the fracture surface. The crack fronts were bowed with the centre leading the edges, usually by about 0.010 in.

The fracture surfaces could conveniently be divided into four parts, as shown schematically in Fig. 21. They were:-

1. A flat region, usually referred to as the tensile or plane strain region, which was normal to the applied stress and the plane of the specimen. This region had small shear lips at the edges; these were often insignificant, particularly at low stresses.

2. A transition region in which the shear lips increased in size until they covered the entire fracture surface. Usually, the shear lips were inclined such that at the end of this region they formed a single plane at 45° to the plane of the sheet (Fig. 18a); on some specimens,

particularly those tested at higher stresses, the shear lips developed into a double 45^{o} shear (Fig. 18b).

3. An inclined region, usually termed the shear or plane stress region, in which the crack propagated on the single 45^{o} plane or on the double 45^{o} planes formed in the second region.

4. A final fracture region.

Qualitatively, the transition from one region to the next occurred at shorter crack lengths at higher stress levels at constant specimen thickness, and at longer crack lengths at greater specimen thickness at constant stress level. The divisions between regions 1 and 2, and between regions 3 and 4 were not well defined and the crack lengths at which they occurred could not be measured. The division between regions 2 and 3 was usually more definite, and the crack length (a_t) which marked the end of the transition region was measured in those specimens where it was sufficiently well defined. The results are listed in Table VII and are plotted as a_t versus alternating stress range in Fig. 22. The stress intensity factor at a_t is also given in Table VII and plotted as log ΔK versus log B in Fig. 23.

Some of the fracture surfaces were examined in the scanning electron microscope. A series of fractographs from one specimen is shown in Figs 24 - 30. The specimen was 1 in. wide x 0.4 in. thick, with a 0.1 in. deep sharp notch, tested at 0 - 30 ksi, and the fractographic features observed were typical of all the specimens examined. In the early stages of crack growth the fracture surface was made up entirely

of fatigue striations or ripples, but as crack length increased a mixed ripple/tensile dimple surface was observed. In the later stage of fracture the surface was almost entirely composed of dimples and was indistinguishable from the final tensile fracture. Ripples were observed at the base of the notch, and also on the shear lips at the edge of the plane strain region. The mixed ripple/dimple fracture surface was first observed at the crack length which marked the end of the transition region, but within the transition region there was no marked difference between the flat region in the centre and the shear lips. Examination of the fracture surfaces of specimens of different thicknesses, or specimens tested at different stresses, gave qualitatively the same results; however the change to the mixed ripple/dimple mode did not always occur at the same length as the transition to the shear region but was generally within the scatter of values of a_t given in Table VII. There was no agreement between crack growth rates in specimens of different thicknesses at the point where dimples were first observed.

The examination of individual ripples at higher magnification often revealed slip markings, usually parallel to them, and it was sometimes difficult to establish whether a particular feature represented a ripple or a slip marking. Ripple spacings were measured on several specimens, and the results are compared with macroscopic crack growth rates obtained from a versus N curves in Table VIII. The results generally show reasonable agreement except at growth rates of less than about 10^{-5} in./cycle, but it should be noted that on some specimens (e. g. Specimen 55, Table VIII) there was apparently little change in ripple spacing over the area examined.

5. DISCUSSION

5.1 Limitations of Experimental Techniques and Analyses

5.1.1 Compliance Calibration

The Gross (1964) expression for the stress intensity factor of a single edge notched specimen was obtained by a boundary collocation procedure and assumed that the tensile load was uniformly distributed across the specimen at a distance from the crack not less than the specimen width. Brown and Srawley (1966) considered that this condition was realised in pin loaded specimens when the separation of the loading pins was not less than three times the specimen width. However, Bloom (1966) has shown that the application of a tensile load to this type of specimen results in combined rotations and displacements of the ends, particularly at high values of a/W. In fracture toughness testing, therefore, it is usual to mount the loading pins in bearings which allow them to rotate freely in order to avoid bending movements due to the restraint of end rotations by frictional effects. In the present work, the specimen was designed to restrain end rotations completely, thus maintaining good alignment of the specimens throughout the fatigue tests. In spite of this, the experimental compliance measurements were in good agreement with theoretical values obtained from the Gross (1964) expression up to a/W = 0.5 as shown in Fig. 8. This observation is also contrary to the work of Pook (1968) who considered the effect of loading pin friction on the stress intensity factor for a single edge notched tension specimen and concluded that an analysis by Harris (1967) for a circumferentially notched tube could be applied to an edge notched specimen with complete end

restraint. This analysis indicates that, at a/W = 0.3 the stress intensity factor is about 30% lower than that given by the Gross expression. However, the present results showed that elastic bending of the specimens occurred, and this would accommodate some of the tendency towards rotation of the ends of the specimen. Bending of this nature is not possible in a circumferentially notched tube, and the Harris analysis can therefore only be applied to an edge notched specimen which is restrained from bending along its entire length rather than one in which only the rotations of the ends are restrained. Thus Pook has considered a special case in which the length: width ratio of the specimen was effectively zero, compared with the Gross expression in which the length:width ratio is effectively infinite. The general case of the finite length:width ratio has been analysed by Bowie and Neal (1965) who used a conformal mapping procedure to obtain stress intensity factors for edge notched specimens with length:width ratios of about 1 and 3. The results showed that the reduction in the stress intensity factor was less at the larger length:width ratio, and that at a/W = 0.3 and a length:width ratio of about 3 the stress intensity factor was reduced by about 15% by end restraint.

The agreement obtained between the experimental results and those predicted from the Gross expression appears to be due to two factors. Firstly, the length:width ratio of the specimens was 8:1 (see Fig. 4) compared with the ratio of about 3:1 considered by Bowie and Neal. Secondly, it is extremely difficult to achieve complete restraint of the end of the specimen in practice, and in the present work the

2 in. dia x 14 in. long loading bars were sufficiently flexible to allow some lateral movement of the loading shackles. This movement, combined with the effect of increased specimen length, was sufficient to accommodate the rotation of the ends of the specimen. The experimental results were limited to a/W = 0.5, and since this covers the majority of the results from the fatigue tests it was not considered necessary to extend the compliance calibration to higher values of a/W. However, there is some evidence from crack growth rates obtained at a/W > 0.5 at low stress ranges (Fig. 13, 0-15 ksi data) that the stress intensity factor was lower than that given by the Gross (1964) expression, although the scatter in the data is too large to draw reliable conclusions.

5.1.2 Crack Length Measurements

The electrical potential technique (Gilbey and Pearson 1966) was used to obtain the data on crack initiation and the a versus N curves from which crack growth rates were derived. Under the conditions used in the later tests the calculated accuracy of the crack length measurements, based on the accuracy of V_a measurements, was better than $\pm$ 0.001 in. and the sensitivity to changes in crack length better than 0.0002 in. In practice, this could not be achieved because of electrical interference from the testing machine and other apparatus, and temperature variations within the laboratory. The accuracy of the crack length measurements, but not the sensitivity to changes in crack length, was further reduced by small errors in positioning the leads used for measuring V_a. Optical measurements of crack length were in agreement with the electric potential measurements to within about 0.010 in. over the majority of a test, and

since the observed bowing of the crack front could account for these differences it was concluded that the electrical potential crack length measurements were within the accuracy of the optical measurements, i. e. within 0. 005 in. The sensitivity of the technique to changes in crack length was greater and it was always possible to detect a crack electrically before it could be seen optically on the surface, and it was considered that a change in crack length of 0. 0005 in. could be detected.

The accuracy of the measurements of N_i can be deduced from the sensitivity to changes in crack length. For example, at a typical initial value of ΔK of 15 ksi $\sqrt{\text{in}}$, N_i from Fig. 10 has a mean value of 5300 cycles and da/dN from Fig. 13 has a mean value of 1.4×10^{-6} in/cycle. If the crack was not detected until it had grown by 0. 0005 in. then it would have been propagating for about 360 cycles i. e. about 7% of the measured value of N_i. This error increases as the initial value of ΔK increases, and at the maximum value of 40 ksi$\sqrt{\text{in}}$ used in this work the corresponding error in N_i is 16%. The observed scatter in measured values of N_i in duplicate tests was about 30%.

The scatter in crack growth rates was much larger than that observed in N_i values, and was up to a factor of 3 (Figs. 12 and 13). This scatter was not reflected in the number of cycles taken to propagate a crack (N_p) in duplicate specimens which varied by approximately $\pm$ 15% about the mean value (Section 4. 2. 2), and was probably due to two factors. Firstly, the errors in crack length measurements were up to about 0. 005 in. and these could lead to large errors in crack growth rates which were typically of the order of 10^{-5} in. /cycle. Secondly, several steps were involved

in obtaining da/dN values from crack length measurements and the errors from each step could be additive. It is likely that the scatter in da/dN values was a result of these factors rather than a real difference in the crack growth rates. In view of this scatter, it is clear that several observations are required to produce a reliable mean value of da/dN; where means are not available it is more useful to use the observed values of N_p to draw conclusions regarding crack growth rates.

5.1.3 Fracture Mechanics Analysis

The use of the stress intensity factor to correlate fatigue crack growth data is now well established, and a correlation of crack initiation data, suggested on theoretical grounds by Weertman (1966) and Bilby and Heald (1968) has been obtained in this work. It is appropriate at this point to discuss the validity of using the stress intensity factor, which arises from an elastic stress analysis, to correlate data obtained at gross section stresses up to and exceeding general yield. In fracture toughness testing, it is usual to restrict the load at fracture to less than $0.8\,\sigma_y$ since as the applied stress approaches the yield stress the errors resulting from large plastic zones become appreciable (ASTM, 1960). However, in a fatigue test the material around the crack tip will work harden (Benham and Ford 1961) rapidly in relatively few cycles of the test leading to a reduction in the size of the plastic zone (Formby 1968). In addition, Rice (1967) has suggested that in calculating the size of the plastic zone in a fatigue test the appropriate value of the yield stress in the

formula (ASTM 1960)

$$r_p = \text{Constant} \left[\frac{K}{\sigma_y}\right]^2 \qquad (42)$$

is twice the monotonic yield stress to take account of the reversed stressing. Thus in the present tests the size of the crack tip plastic zone was probably about an order of magnitude smaller than that in the initial tensile loading to the maximum stress and this difference allows the use of the stress intensity factor at higher loads than in fracture toughness tests.

5.2 General Features

5.2.1 Macroscopic Features

The macroscopic features of the fracture surfaces were similar to those described by Plumbridge and Ryder (1969) and Liu (1964):- a flat (plane strain) region was present at short crack lengths followed by a transition region in which the shear lips increased in size until they covered the entire fracture surface. Finally there was a shear (plane stress) region in which propagation was on planes at 45° to the specimen surface. The crack length at the start and end of the transition region was dependent on both stress range and specimen thickness, high stresses or small thicknesses leading to transitions at shorter crack lengths. In thin (0.050 in. and 0.080 in.) specimens tested at high stress levels the flat (plane strain) region was virtually absent while in the 0.90 in. thick specimens the flat region covered the majority of the fracture surface and there was no shear region.

Liu (1964) has analysed results reported by Weibull (1963) and showed that the transition from flat to shear crack propagation occurred

at a constant stress intensity factor for a particular thickness of specimen. In the present work the transition occurred over a range of crack length and it is not clear whether the transition referred to by Weibull (1963) was the start or end of the transition region. The results presented in Figs. 22 and 23 refer to the end of the transition region and show a large amount of scatter, probably due to the difficulties of specifying accurately the end of a gradual transition.

It is relevant to the present discussion that the fracture mode affected the number of cycles taken to initiate a crack and also the rate of crack propagation. At a particular range of stress intensity factor the number of cycles taken to initiate a crack was independent of specimen thickness above 0.2 in. and it is assumed that under these conditions the material at the notch tip was in plane strain. In specimens in which the conditions at the notch tip were not entirely plane strain there was a reduction in N_i (Fig. 15; Table V). The maximum degree of plane stress in the present tests occurred in a 0.050 in. thick specimen tested at 0-30 ksi and N_i was reduced by a factor of about 4 compared with the plane strain value.

The influence of the fracture mode on crack growth rates can best be inferred from values of N_p given in Table V. At a particular stress range, N_p increased with specimen thickness due to the increasing proportion of N_p spent in the plane strain region. The greatest variation in N_p occurred at the higher stress levels, at which there was no plane strain region in thin specimens and no plane stress region in thick specimens. At lower stresses, there was less variation in N_p since the

major part of N_p was spent at small crack lengths (see Fig. 11) where plane strain conditions prevailed at all thicknesses.

Previous investigators have found that the transition from plane strain to plane stress involved either no change in crack growth rate (Forsyth and Ryder 1960, Liu 1961a) or a reduction in growth rate (McEvily and Johnston 1967) for which the fact that the crack front was bowed with the centre (plane strain) leading the edges (plane stress) was quoted as supporting evidence. Liu (1964) considered that a higher growth rate in plain strain could be caused in high strength materials by bursts of cleavage crack growth in the centre of the specimen where the stress intensity could approach the plane strain fracture toughness of the material; in this case the crack front would be bowed with the centre leading the edges. In the case of lower strength materials Liu concluded that this mechanism did not operate and the crack front should be bowed in the opposite sense.

The present results, which showed that cracks grew faster in plane stress with the centre leading the edges, are in direct conflict with these observations and conclusions. The failure of other investigators to observe a change in crack growth rate is probably due to the fact that the transition from plane strain to plane stress is gradual rather than instantaneous. Possibly an increased crack growth rate in plane stress may have been noted if N_p, or N_f, values had been recorded but most investigations of crack growth rates have been confined to studies of the propagation of established cracks rather than the effect of notches on the fatigue lives of specimens of different thickness as in the present work.

The observed shape of the crack front is apparently in conflict with a higher growth rate in plane stress. However, if fatigue crack growth is regarded as a consequence of plastic deformation in a direction normal to the fracture surface at the crack tip this anomaly is resolved since, whatever the state of stress along the major part of the crack front, lateral contractions at the surface will reduce the degree of crack opening which will, in turn, reduce the crack growth rate at the surface.

5.2.2 Microscopic Features

The fracture surfaces were composed of fatigue ripples at short crack lengths, mixed ripples and dimples in the region of the transition to plane stress, and dimples alone in the region immediately before final fracture.

At macroscopic growth rates of less than about 5×10^{-6} in./cycle, the spacing of the fatigue ripples was greater than the growth rate. Ripples were observed on all specimens immediately adjacent to the notch, even when the growth rate was less than the resolution of the scanning electron microscope and it must be concluded that each ripple was not produced by a single cycle of the fatigue load. At growth rates of between about 5×10^{-6} in./cycle and 10^{-5} in./cycle there was reasonable agreement between ripple spacings and growth rates but the scatter in macroscopic growth rates and the difficulties associated with making accurate measurements on the uneven fracture surfaces does not allow the precise relationship to be determined. In the region where both

ripples and dimples were seen ripple spacings were smaller than the crack growth rate. The size of the dimples was typically about an order of magnitude greater than the ripple spacing.

The results show that the features observed were indicative of the general mode of crack growth; ripples indicating growth in plane strain, dimples growth in plane stress and mixed ripples and dimples the transition from one to the other. It is significant that in the area defined as the transition region there was no difference between the fracture surface in the centre of the specimen and on the shear lips at the edges, suggesting that the appearance of the fracture surface represents the average state of stress along the crack front.

It should be noted that the fractographic examination carried out was not exhaustive as would be the case in a study devoted entirely to the macroscopic features of fatigue crack growth. The results therefore suggest areas in which further work is necessary, and draw attention to the danger of using ripple spacings to indicate crack growth rates in practice.

5.3 Crack Initiation

5.3.1 The Observed Power Relationship

For specimens containing sharp notches (i.e. $\rho \leqslant 0.010$ in.) in plane strain an inverse fourth power relationship was observed between N_i and the range of stress intensity factor. Weertman (1966) and Bilby and Heald 1968) predicted an inverse square relationship, equation 7. A

possible reason for the discrepancy is that Bilby and Heald (1968) obtained their expression for Φ_c, the critical crack tip displacement at which initiation is considered to occur, by linear summation of the displacements resulting from each cycle; these displacements are confined to a single slip plane in this model. In practice, it is likely that deformation occurs randomly on several slip planes. May (1960a, 1960b) and Gittus (1964) have used statistical models in which the accumulation of fatigue damage is proportional to the square of the plastic strain to obtain theoretical justification for the Manson-Coffin relationship. There is also some experimental evidence from results on austenitic steel in high strain fatigue (Dawson et. al. 1967) which can be used to show that N_i is inversely proportional to the square of the plastic strain range for plastic strains of less than about 1%. If in the Bilby and Heald analysis it is assumed that the critical displacement Φ_c is obtained by summation of the squares of the individual displacements i. e. a random rather than a linear summation, their expression becomes

$$N_i \propto (\Delta K)^{-4}$$

which agrees with the present results for sharp notches.

5.3.2 The Effect of Root Radius

Although Bilby and Heald's analysis applies strictly to sharp cracks, Smith (1967) has shown that this treatment should be applicable to notches. Smith's analysis predicts that the displacement Φ at the notch tip is reduced by a factor of about 2 as the root radius increases from 0 to 0. 010 in. for a 0. 1 in. deep edge notch in a semi-infinite plate.

The present results show that experimentally there was no effect of root radius below 0.010 in.

Similar behaviour has been observed in brittle fracture where it has been found (Cottrell 1965, ASTM Committee 1961) that there is a critical root radius below which further sharpening does not reduce the fracture toughness. It is generally assumed that this arises because a particular fracture mechanism requires a minimum volume in which to operate.

Above the critical notch root radius, N_i is a function of $K/\rho^{\frac{1}{2}}$. Thus the effective stress intensity factor (K_{eff}) for a blunt notch is related to that for a sharp notch or crack by

$$K_{eff} = K \left(\frac{\rho_o}{\rho'} \right)^{\frac{1}{2}} \qquad (43)$$

where ρ_o is the critical value of ρ

ρ' is the effective root radius and

$\rho' = \rho$ when $\rho \geq \rho_o$

$\rho' = \rho_o$ when $\rho \leq \rho_o$

Again, similar behaviour is found in fracture toughness testing (ASTM Committee 1961, Weiss and Yukawa 1965). This has been summarised by Tetelman and McEvily (1967) who related the strain on a gauge length ρ to a critical displacement at the root of a notch. This, in turn, was related to the critical strain energy release rate G_c to give

$$G_c = \frac{Kc^2}{E} = 2 \sigma_y \rho' \epsilon_f \qquad (44)$$

where E = Young's modulus

σ_y = yield stress

ϵ_f = fracture ductility

ρ' = effective root radius.

An estimate of the size of the critical element may be obtained by using the work of Weiss and Yukawa (1965) which is based on an analysis of the elastic stress distribution ahead of a notch carried out by Jackson (1963). This analysis shows that the stress distribution for a notch of finite root radius differs from that for a sharp crack of the same length only over a very short distance ahead of the notch tip. Weiss (1962) has developed an approximate expression for the longitudinal stress distribution at a distance r ahead of the notch:

$$\sigma_1 = \sigma_{net} K_t \left[\frac{\rho}{\rho + 4r}\right]^{\frac{1}{2}} \tag{45}$$

where σ_1 is the longitudinal stress

σ_{net} is the net section stress

and K_t is the elastic stress concentration factor.

The distance r_o ahead of the notch tip at which the stress is equal to that for a sharp crack (i.e. $K(2\pi r_o)^{-\frac{1}{2}}$) is therefore obtained from

$$\sigma_1 = \sigma_{net} K_t \left[\frac{\rho}{\rho + 4r}\right]^{\frac{1}{2}} = K(2\pi r_o)^{-\frac{1}{2}} \tag{46}$$

For an infinite plate (Neuber 1958)

$$K_t = 2(a/\rho)^{\frac{1}{2}} + 1 \tag{47}$$

and $K = \sigma(\pi a)^{\frac{1}{2}}$

Weiss's equation for the longitudinal stress reduces to

$$\sigma_1 = \sigma \left[2\left(\frac{a}{\rho}\right)^{\frac{1}{2}} + 1\right]\left[\frac{\rho}{\rho + 4r}\right]^{\frac{1}{2}} \tag{48}$$

and when $a >> \rho$, r

$$r_o = \rho/4 \tag{49}$$

Thus, at the critical root radius of 0.010 in. the distance over which the stress distribution differs from that for a sharp crack in about 0.0025 in. A more detailed calculation gives the value as 0.0016 in. for a half crack length of 0.10 in. This is of the order of the grain size of the material.

When the stress at the end of the critical element is less than that for sharp crack or notch, N_i will increase. The Weiss approximation, in conjunction with the critical element size can be used to develop the modified stress intensity factor which describes crack initiation from a blunt notch.

When $a >> p >> r$,

$$\sigma_1 = 2\sigma (a/\rho)^{\frac{1}{2}} \tag{50}$$

Hence the ratio of stresses σ_a / σ_b arising from notches of root radii ρ_a, ρ_b is given by

$$\frac{\sigma_a}{\sigma_b} = \left(\frac{\rho_b}{\rho_a}\right)^{\frac{1}{2}} \tag{51}$$

At the end of the critical element, the stress for a notch of root radius ρ is given by the stress intensity factor and it follows that for notches of larger root radii

$$\sigma = \frac{K}{(2\pi r)^{\frac{1}{2}}} \left(\frac{\rho_o}{\rho}\right)^{\frac{1}{2}} \tag{52}$$

5.3.3 Comparisons with Other Work

Results which appear to be in accordance with the present work have been reported by Weibull (1954, 1956, 1961) who carried out tests

on geometrically similar centre notched specimens of 24S-T aluminium alloy of different widths. As the width was increased, both notch length $2a_o$ and root radius ρ were increased in proportion. Weibull measured N_i in these specimens, and his results have been re-plotted as ΔK versus N_i in Fig. 31. The value of ΔK, expressed in kg. $mm^{-3/2}$, were calculated assuming that all notches behaved as sharp cracks. The results fall into three groups - a) five points, representing 12 tests (each result is the mean of up to 3 tests) through which a line of slope $-\frac{1}{4}$ can be drawn (line A in Fig. 31). These tests were on specimens with notch root radii of 0.05 mm, 0.10 mm. and 0.15 mm; b) Two points, representing 3 tests on specimens with 0.38 mm root radius notches, through which a line of slope $-\frac{1}{4}$ (line B in Fig. 31) can be drawn and c) three points, representing 6 tests on specimens with notches of 0.05 mm. 0.10 mm. and 0.15 mm. root radius, which were carried out at stress intensity factors of less than about 28 kg. $mm^{-3/2}$ (7.9 ksi $\sqrt{in}$). If the latter group of points at low stress intensity factors is assumed to represent an approach to an assymptotic value of ΔK below which cracks will not initiate, then the other two groups show similar behaviour to that observed in the present work on mild steel. If an effective stress intensity factor of $\Delta K(\rho_o / \rho)^{\frac{1}{2}}$ is assumed, then the value of ρ_o which must be chosen to bring line B into correspondence with line A is about 0.2 mm (0.008 in.). N_i in Weibulls tests on specimens containing sharp notches can be expressed by

$$N_i = 3.59 \times 10^8 (\Delta K)^{-4} \qquad (53)$$

when ΔK is expressed in units of ksi $\sqrt{in}$.

This equation is identical in form to equation 39 obtained in the present work. The mean line in Fig. 10 is given by an equation

$$N_i = 2.63 \times 10^3 \, (\Delta K)^{-4} \qquad (54)$$

Pearson (1966) found that a parameter K/E, where E is Young's modulus could be used to unify crack growth data in a variety of materials. This parameter does not apply to crack initiation; Young's modulus for mild steel is about 3 times that for aluminium alloys and this would imply a ratio of 81 between the constants in equations 54 and 55 compared with the observed ratio of about 1.4.

Pearson (1970) has carried on tests on edge notched aluminium alloy specimens in which crack initiation was detected by the electrical potential method. He found that there was a critical root radius between 0.005 in. and 0.010 in. below which N_i was independent of root radius; this is in close agreement with the value of 0.008 in. deduced from Weibull's work.

The critical element size deduced from the observed critical root radius by the Weiss analysis was of the order of the grain size of the material. Hoeppner (1967) has carried out tests on notched specimens of copper in which the grain size was varied between about 0.058 mm. and 7.0 mm. Although the crack length measurement technique did not allow Hoeppner to measure N_i exactly, he concluded that an increase in the grain size led to a reduction in N_i. If it is assumed that the critical root radius increases with grain size, then Hoeppner's results can be explained in qualitative terms by reference to Fig. 32. In this figure N_i is plotted shematically against root radius for three grain sizes. In

Fig. 32 a), for large grained material, the critical root radius is large and greater than the notch root radius and N_i has the sharp crack value. In Fig. 32 b) for fine grained material, the critical root radius is small and is much less than the notch root radius and the N_i versus ρ graph is moved to the left; in this case N_i is much larger than the sharp crack value. Fig. 32 c represents the situation at an intermediate grain size.

The literature provides little experimental data for N_i in mild steel with which the present results can be compared. However, data reported by Frost and Dugdale (1958) on the formation of non-propagating cracks in mild steel allow reasonable assumptions to be made regarding N_i in their tests. Although these values lie in the range $10^7 - 10^8$ cycles, it can be shown that the present results extrapolate to give reasonable agreement with their data. It is also noted that at $N_i = \frac{1}{2}$ the results extrapolate to a value of ΔK of about 150 ksi$\sqrt{}$ in which is a reasonable value for the fracture toughness of this material. It would be useful if this empirical correlation proved to have general application analogous to the Manson-Coffin relationship in high strain fatigue.

5.3.4. The Effect of Specimen Thickness and Mean Stress

The effect of thickness on crack initiation was considered in section 5.2.1. The effect of mean stress is more conveniently dealt with in the discussion on crack propagation, section 5.4.3.

5.4 Crack Propagation

5.4.1 The Plane Strain-Plane Stress Transition and The Effect of Specimen Thickness

The general features of crack growth were discussed in 5.2.1 where it was concluded that the fracture mode was indicative of the state of stress at the crack tip and that the crack growth rate was dependent upon this state of stress. Liu (1964) and McClintock (1963) have discussed plasticity effects in relation to fatigue crack growth. They derived theoretical expressions in which the crack growth rate is expressed as a function of plastic zone size. The size of the plastic zone is greater in plane stress than in plane strain due to reduced constraint and Liu (1964) has shown that, in plane stress, the plastic zone is about three times as large as in plane strain. Thus it would be expected that the crack growth rate would be greater in plane stress. The present results indicate a relationship (equation 40)

$$da/dN \propto (\Delta K)^3$$

and since the plastic zone size is proportional to $(\Delta K)^2$ (Equation 42) it would be expected that

$$da/dN \propto r_p^{3/2} \qquad (55)$$

From this analysis, the ratio of crack growth rates in plane stress and plane strain would be expected to be about 5. From Table V, the data on 0.90 in. thick specimens extrapolate to a value of N_p at a stress range of 0-30 ksi of about 26×10^3 cycles, while N_p for a 0.05 in. thick specimen at this stress range was 6×10^3 cycles, and the ratio of N_p at 0.90 in. thick to N_p at 0.05 in. thick was about 4.3.

Some indication of the relationship between stress intensity factor and thickness at the start and end of the transition from plane strain to plane stress can be obtained from Figs. 15 and 23. In Fig. 15, crack initiation at a stress range of 0-30 ksi was independent of thickness above about 0.150 in. Assuming that this value represents the start of the transition, and that the size of the plastic zone bears a specific relationship to thickness at this point, i.e.

$$r_p \propto B$$

then since $r_p \propto K^2$

the relationship at the start of the transition indicated in Fig. 15 is

$$K^2 = 2.65 \times 10^3 B \qquad (56)$$

Equation 56 implies that at stress ranges of 0-25 ksi and 0-20 ksi N_i should be independent of thickness down to 0.104in. and 0.067 in. respectively which is not inconsistent with the data in Fig. 15.

The end of the transition from plane strain to plane stress is more difficult to define, but an estimate can be made from the data obtained on 0.2 in. thick specimens given in Fig. 23. This shows that complete plane stress occurs at a stress intensity factor of about 56 ksi $\sqrt{\text{in}}$, giving a relationship

$$K^2 = 1.55 \times 10^4 B \qquad (57)$$

At thicknesses of 0.05, 0.08 and 0.40 in. equation 57 implies that the transition should be complete at stress intensity factors of 28 ksi $\sqrt{\text{in}}$, 35.5 ksi $\sqrt{\text{in}}$ and 80 ksi $\sqrt{\text{in}}$ respectively. These values are in reasonable agreement with the data in Fig. 23 for 0.05 in. and 0.08 in. thick specimens but the figure for the 0.40 in. thick specimens is about a

factor of 2 less than the observed mean figure of about 180 ksi$\sqrt{in}$. However, the transition in these specimens occurred at a crack length of about 0.75 W, and the calculated values of the stress intensity factor can not be considered accurate since the Gross expression is only valid up to a/W = 0.6, and the compliance calibration carried out in the present work did not extend beyond 0.5 W. In addition, the stress intensity factor rises so rapidly above about 0.25W that, even with an accurate compliance calibration, small errors in the measurement of a_t can lead to large errors in the calculated value of K.

5.4.2 The Initial Stages of Crack Propagation

After initiation a decreasing crack growth rate was observed over a short distance in some of the tests, after which the growth rate increased continuously with crack length. This behaviour represents an intermediate stage between the formation of a non-propagating crack and the more usually observed continuous increase in growth rate after initiation. Frost (1955) has discussed the formation of non-propagating cracks in reversed stress tests and showed that the length of non-propagating cracks corresponded to the distance ahead of the notch tip at which the stress distribution from the notch fell off to the fatigue limit of the material. In the present work the decreasing crack growth rate was observed in zero-maximum stress tests. It seems unlikely that under these conditions the formation of a crack at the notch root would not affect the stress distribution and it is expected that the stress at the crack tip would increase continuously as the crack grows. Frost's explanation cannot

therefore be applied to these tests.

Richards (1970) has observed analogous behaviour during fatigue crack growth tests on mild steel. His tests were conducted at constant stress intensity factor range, and the crack growth rate reached a constant equilibrium value. If the stress intensity factor range was then increased there was an immediate large increase in crack growth rate but this rate quickly decreased to a new equilibrium value. Richards has suggested that, at constant ΔK the plastic zone reaches an equilibrium size. When ΔK is increased the plastic zone will extend into material that has not been work hardened to the same extent as that within the equilibrium plastic zone. The increase in plastic zone size will thus be greater than would be calculated from the increase in ΔK, leading to an exaggerated increase in crack growth rate. As the plastic zone shrinks the growth rate will reduce to its new equilibrium value. This mechanism explains the observations in the present work, and if it is assumed that cracks will initiate at a lower value of ΔK, or equilibrium plastic zone size, than is required to propagate them, non-propagating cracks under zero-tension and fully reversed stressing can also be explained.

5.4.3 The Effect of Mean Stress

Mean stress had a small but significant effect both on crack initiation and crack growth. Tests were carried out over a limited range since the low cyclic frequency of the testing machines dictated that tests should be completed in less than about 3×10^5 cycles (about 10 days),

which in turn limited the minimum stress range to about 0-15 ksi for the specimen geometries used. Since the yield stress of the material was about 30 ksi, there was clearly little scope for varying mean stress while remaining in the pseudo-elastic range. Within the range studied, the effect of mean stress was small compared with the general scatter of results and has not been included in the equations describing N_i and da/dN. This effect must clearly be incorporated in a complete analysis, since N_i becomes zero and da/dN infinite when the maximum value of the stress intensity factor is equal to the fracture toughness. Forman, Kearney and Engle (1966) have proposed an equation for the crack growth rate (equation 15)

$$\frac{da}{dN} = \frac{A(\Delta K)^n}{(1-R)K_c - \Delta K}$$

and it is possible that a similar equation, such as

$$N_i = \left[\frac{(1-R)\ K_c - \Delta K)}{B(\Delta K)^{\beta}}\right]^{\alpha} \qquad (58)$$

would describe N_i, but more data than are at present available would be needed to confirm this.

5.4.4 Comparison with Other Work

The most recent comprehensive review of crack growth rates in steels was presented by Crooker and Lange (1970) at a recent conference. They represented crack growth rates for plain carbon and low alloy steels having yield strengths in the range 34 - 127 ksi by a single scatter band on a da/dN vs ΔK plot as shown in Fig. 33. This scatter band included results obtained by Brothers (1968) and Gurney (1969) on similar materials

to that used in the present work and their results are given in Fig. 33. The scatter band from Fig. 13 is also included in this figure.

The results obtained in the present work bracketed the upper boundary of Crooker and Lange's scatter band. However, the results obtained by Brothers and Gurney were on thick specimens which were presumably in plane strain, while the results in Fig. 13 were on 0.2 in. thick specimens in which, from equations 56 and 57, the transition from plane strain to plane stress took place between about 23 ksi$\sqrt{}$ in and 56 ksi $\sqrt{}$in. Since the present results on 0.9 in. thick specimens showed that the average growth rate was about a factor of two slower than in the 0.2 in. thick specimens it is considered that these results are in agreement with the published work summarised in Fig. 33.

6. APPLICATION OF RESULTS

6.1 Calculation of Fatigue Lives of Notched Specimens

The results of zero-maximum stress tests on specimens containing sharp notches showed that crack initiation and propagation could be represented by the equations

$$N_i = 2.63 \times 10^{8} (\Delta K)^{-4} \tag{54}$$

$$\frac{da}{dN} = 5 \times 10^{-10} (\Delta K)^{3} \tag{59}$$

From these equations, it is possible to calculate the fatigue life of any sharply notched or pre-cracked specimen for which the stress intensity factor is known. N_i is obtained simply by substituting the appropriate value of ΔK in equation 54. The number of cycles taken to propagate the crack (N_p) from the starting notch or crack of length a_o to the crack length at which failure occurs, a_f, is obtained by integration of equation 59:-

$$N_p = \int_{a_o}^{a_f} \frac{da}{5 \times 10^{-10} (\Delta K)^{3}} \tag{60}$$

Substituting equation 25 into equation 60:-

$$N_p = \frac{1}{5 \times 10^{-10} (\Delta\sigma)^{3}} \int_{a_o}^{a_f} \frac{da}{\left\{a^{\frac{1}{2}} f(a/W)\right\}^{3}} \tag{61}$$

When f(a/W) is expressed in polynomial form (equation 26) equation 61 cannot be solved analytically since no closed form solution to the integral is known. In the present work, a computer programme was used to obtain N_i and N_p, and hence N_f, for particular values of a_o, a_f, σ and W. The accuracy of the programme was checked by calculating the fatigue lives of the specimens; good agreement was obtained.

6.2 Results of Typical Calculations

The computer programme was used to calculate the fatigue lives of edge and centre notched mild steel plates (Fig. 34), assuming that in all cases the notches were sharp. The final crack length was taken to be that crack length at which the net section stress reached a UTS of 60 ksi; stress intensity factors were calculated from the polynomial expressions given by Brown and Srawley (1966). The forms of equations 54 and 61 do not allow an easy assessment of the life of a particular specimen, or of the relative contribution of N_i and N_p to that life. Accordingly, examples have been chosen to illustrate points of particular interest.

Fig. 35. shows the effect of tensile stress range on N_i and N_f for 1 in. wide specimens containing single edge notches (Fig. 34a) of various depths. These are essentially S - N curves for notched specimens. In carrying out the calculations, no account was taken of a possible fatigue limit. Harrison (1969) has indicated that, for mild steel, cracks will not propagate at a range of stress intensity factor less than about 3 ksi $\sqrt{\text{in}}$, and the stress (σ_L) appropriate to this value is shown for notch depths of 0.010in. and 0.025 in. in Fig. 35. At notch depths of 0.10 in. and 0.25 in., σ_L was less than 5 ksi, and is therefore not shown in Fig. 35.

The effect of specimen width on N_i and N_f at three tensile stress ranges for specimens containing 0.025 in. deep edge notches is shown in Fig. 36. N_i is virtually constant at widths above about 0.5 in.; this effect is general since when a/W is less than about 0.05, f(a/W) in

equation 26 approaches A_o, and ΔK and N_i will be insensitive to W. N_f increases continuously with W since the number of cycles spent in propagating the crack increases as the distance over which the crack must grow becomes greater. However, the relative effect of W on N_f is small when W is greater than about 1 in., for example at 0 - 20 ksi, N_f increases by an order of magnitude as W increases from 0.1 in. to 1 in., but only by about a factor of 2 as W increases from 1 in. to 10 in. Again this effect is general since for any specimen the major part of the integral in equation 61 is accumulated near a_o and N_p will be only weakly dependent on W provided that, say, $2a_o/W$ is less than about 0.05.

Some of the data from Fig. 36 have been replotted in Fig. 37a to show the relative proportions of N_f spent in initiating and propagating the crack. Fig. 37a relates to specimens of various widths containing 0.025 in. deep edge notches at a stress range of 0 - 10 ksi. For comparison, the effect of width on specimens containing a 0.10W deep edge notch at 0 - 10 ksi is shown in Fig. 37b. Note that although these specimens are geometrically similar the proportion of N_f spent in initiating the crack varies from about 90% at W = 0.1in. to about 2% at W = 10 in.

The effect of specimen geometry and type of loading is shown in Table IX where N_i, N_p and N_f for single edge notch plates in tension and bending, and centre notched plates in tension are given. Specimen width is in all cases 1.0 in., and for the three geometries considered,

specimens are compared at constant total notch length i. e. at constant net cross section area. Results are given for stress ranges of 0 - 10 ksi and 0 - 20 ksi.

6.3 Discussion

Fatigue lives of specimens containing notches down to 0. 010 in. deep have been calculated. There must be some reservations regarding the application of equations 54 and 61 to notches of this size since no specimen containing notches less than 0. 020 in. deep have been tested and there is no evidence in the literature that the expressions used to calculate the stress intensity factors are valid at small values of a/W. However, the results give a good indication of general trends in notched fatigue lives and, bearing in mind these reservations, can be applied to practical cases.

A variety of crack like defects can exist in commercial welds, ranging from small slag inclusions found at the toes of welds (Signes et. al. 1967) to major defects found in pressure vessel welds. In most cases the root radii of these defects are such that they can be treated as sharp notches so that the fatigue life can be calculated from equations 54 and 61. Mild steel plate specimens containing welds with lack of root penetration defects have been tested at Berkeley Nuclear Laboratories (Priddle 1970). The specimens were tested in zero-tension loading with the stress axis normal to the weld with the lack of root penetration defect across the wide face of the plate. N_i and N_p were calculated using the data for annealed mild steel. The specimen width was taken to be the

plate thickness plus the weld reinforcement and the plate was assumed to behave as a single edge notched tension specimen; the measured fatigue life is plotted against the calculated life in Fig. 38. Since tests on laboratory specimens containing autogenous weld runs (Jack 1969) have shown that N_i and N_p for the weld material were increased by about a factor of two compared with the annealed material, it is considered that Fig. 38 shows good agreement between the measured and predicted lives.

It is often assumed that in calculating fatigue lives it is legitimate to neglect crack initiation (Maddox 1970). The results of the present calculations show that this is true only for large defects in thick sections. For small defects in thin sections, for example a 0.1W defect in a 0.1 in. wide plate Fig. 37b, initiation can occupy 90% of the fatigue life. In intermediate ranges it is necessary to consider both crack initiation and propagation to obtain the most accurate prediction of fatigue life, although in many instances either could be ignored and the result still fall within the normal scatter of fatigue data. In specifying defect standards it can be argued that ignoring N_i results in conservative estimates of the life of a structure. However, when considering individual defects in terms of the integrity of a structure it is better to consider both initiation and propagation. For simple situations, computation is not difficult and can be reduced to a convenient graphical form. This is shown for a single edge notched specimen in Fig. 39, and has been derived as follows:-

From equation 26,

$$K = \sigma W^{\frac{1}{2}} \left[A_o (a/W)^{\frac{1}{2}} + A_1 (a/W)^{3/2} + A_2 (a/W)^{5/2} + \ldots\ldots \right]$$

$$= \sigma W^{\frac{1}{2}} f'(a/W) \qquad (62)$$

Thus from equation 54

$$N_i = \frac{2.63 \times 10^8}{(\Delta\sigma)^4 W^2} \left[\frac{1}{f'(a/W)}\right]^4$$

$$= \frac{2.63 \times 10^8}{(\Delta\sigma)^4 W^2} \Phi \qquad (63)$$

where $\Phi = \left[\frac{1}{f'(a/W)}\right]^4$

Similarly from equation 61

$$N_p = \frac{1}{5 \times 10^{-10} (\Delta\sigma)^3 W^{\frac{1}{2}}} \int_{a_{o/W}}^{a_{f/W}} \frac{d(a/W)}{[f'(a/W)]^3}$$

$$= \frac{1}{5 \times 10^{-10} (\Delta\sigma)^3 W^{\frac{1}{2}}} \chi \qquad (64)$$

where $\chi = \int_{a_{o/W}}^{a_{f/W}} \frac{d(a/W)}{[f'(a/W)]^3}$

Values of Φ and χ are plotted against a/W in Fig. 39. In order to make the presentation general, the values of χ plotted were obtained by evaluating the integral between a/W and $a_{f/W} = 1$. Noting that

$$\int_{a_{o/W}}^{a_{f/W}} = \int_{a_{o/W}}^{1} - \int_{a_{f/W}}^{1} \qquad (65)$$

the most accurate value of N_p is obtained by subtracting χ at $a_{f/W}$ from χ at $a_{o/W}$ and substituting the difference in equation 64. However, the major part of the integral is accumulated near to $a_{o/W}$, so that in general

$$\int_{a_{o/W}}^{1} \gg \int_{a_{f/W}}^{1} \qquad (66)$$

and N_p can be calculated directly from the value of χ at $a_{o/W}$. As an example, for an initial edge defect 0.1 in. deep in a 1 in. wide plate at a stress range of 20 ksi,

$$a_{o/W} = 0.1, \quad \Phi = 5, \quad \chi = 2.3 \times 10^{-1}$$

$$N_i = \frac{2.63 \times 10^{8}}{16 \times 10^{4} \times 1} \times 5 = 8.23 \times 10^{3} \text{ cycles}$$

$$N_p = \frac{1}{5 \times 10^{-10} \times 8 \times 10^{3} \times 1} \times 2.3 \times 10^{-1} = 5.75 \times 10^{4} \text{ cycles}$$

$N_f = N_i + N_p = 6.57 \times 10^{4}$ cycles.

In cases where a_f is close to a_o the relationship indicated in equation 65 does not apply and it is necessary to consider χ at $a_{f/W}$ to obtain an accurate value for N_p.

Fig. 39 can also be used to determine how far a defect will grow in a particular number of cycles. In the above example, N_i was 8.23×10^{3} cycles. It may be necessary to assess how far the crack will have extended after, say 5×10^{4} cycles:-

$$N_p = 5 \times 10^{4} - N_i = 4.177 \times 10^{4}$$

From equation 64

$$4.177 \times 10^{4} = \frac{1}{5 \times 10^{-10} \times 8 \times 10^{3} \times 1} \chi$$

whence $\chi = 0.167$

At $a/W = 0.1$ $\quad \chi = 0.23$

Thus at a_f/W $\quad \chi = 0.063$

whence $a_f = 0.20$

i. e. the crack will have extended to a length of 0.20 in. after 5×10^4 cycles. Similar curves can be constructed for any geometry for which the stress intensity factor is known, and for different values of the exponents in equations 54 and 59.

6.4 The Original Problem

The present work was part of a co-ordinated research programme within the C. E. G. B. The aim of this programme was to specify defects which could be tolerated in boiler tube butt welds i. e. defects which would not lead to failure within the expected service life of the boiler. Using the formulae for circumferentially notched tubes given by Harris (1967) it is clear that an analysis of the type shown above can be used to calculate the critical size of a continuous external lack of root penetration defects, which is the worst case encountered in practice. Tests on tubular specimens containing this type of defect are to be carried out elsewhere in the C. E. G. B. to confirm these predictions.

7. CONCLUSIONS

7.1 Crack Initiation

7.1.1 Fatigue crack initiation from notches was independent of notch root radius below a critical value of 0.010 in. Above this critical value, N_i increased with root radius.

7.1.2 For sharp notches (i.e. $\rho \leqslant 0.010$ in.) under plane strain conditions, N_i was inversely proportional to the fourth power of the range of stress intensity factor. Above the critical notch root radius, N_i could be described by a modified stress intensity factor.

7.1.3 At particular values of applied stress range and notch depth, N_i was independent of specimen thickness above a critical value. Below this value, N_i reduced with decreasing thickness. This effect has been related to a plane strain - plane stress transition.

7.1.4 Mean stress had a small but significant effect on N_i.

7.1.5 Limited evidence in the literature suggests that similar behaviour is observed in other materials.

7.2 Crack Propagation

7.2.1 There was a large amount of scatter in individual measurements of crack growth rates, but mean values indicated that the crack growth rate was proportional to the third power of the stress intensity factor.

7.2.2 Crack growth rates in plane stress were faster than in plane strain by a factor of about 4.

7.2.3 The state of stress at the crack tip determined both the plane on which the crack grew and the microscopic features of the fracture surface.

7.2.4 Measurements of the distances between adjacent fatigue ripples on the fracture surfaces were not always in agreement with macroscopic crack growth rates, particularly at growth rates below about 10^{-6} in/cycle. There was evidence that at low growth rates each ripple was produced by several cycles of the fatigue load.

7.2.5 The results were in general agreement with crack growth rates for mild steel given in the literature.

7.3 Application of Results

7.3.1 Good agreement was obtained between the observed fatigue lives of specimens containing welds with lack of root penetration defects and lives calculated from equations derived from the present work.

7.3.2 The correlations observed have been used to illustrate the effects of specimen size, geometry and type of loading on the fatigue life of notched specimens. A simple graphical aid to calculations of fatigue life has been described.

8. RECOMMENDATIONS FOR FURTHER WORK

8.1 Crack Initiation

8.1.1 Extension of Present Work

The low cyclic frequency of the testing machines used in the present work dictated that tests should be completed in less than about 3×10^5 cycles (about 10 days at 0.33 Hz). This limited the work on the effects of mean stress and also prevented investigation of the range over which the $N_i - \Delta K$ correlation was valid. Further tests should be carried out on high frequency testing machines to clarify these points.

More work is needed on the effect of thickness on N_i in order to obtain quantitative relationships. Also, it is possible that there is a critical thickness (or stress intensity factor - thickness relationship) below which further reductions will not affect N_i; this should be investigated.

8.1.2 New Work

Limited evidence in the literature suggests that the behaviour observed in mild steel is general. A research programme on crack initiation and growth in notched copper specimens has been started in C. E. G. B. (Midlands Region) and work on crack initiation from notches in aluminium alloys is being carried out at the Royal Aircraft Establishment. Further work should be carried out on other materials.

8.2 Crack Propagation

8.2.1 Microscopic Features

The relationship between fatigue ripple spacings and macroscopic crack growth rates should be investigated further. This work is of

considerable importance since ripple spacings are frequently used to deduce crack growth rates (and hence applied stresses and lives to failure) in service failures.

8.2.2 Macroscopic Features

Many of the conclusions regarding crack growth rates in the present work were based on values of N_p since small but significant effects were obscured by the large scatter in crack growth rates determined from a versus N curves. Further work should be carried out, preferably at constant ΔK, to clarify the effects of mean stress and the plane strain - plane stress transition.

8.3 Application of Results

The use of crack initiation and growth data in the investigation of service failures, and in the specification of allowable defect sizes, is conditional upon the availability of expressions for the stress intensity factor for the geometry involved. There is a need for the development of computer programmes which will calculate stress intensity factors for the complex geometries encountered in practice.

REFERENCES

ASTM (1960) First Report of Special ASTM Committee on Fracture Testing of High Strength Materials. ASTM Bulletin 243, January 1960.

ASTM Committee (1961) Mats. Res. and Standards 1, 877.

Bellow, D. G. and Long, B. R. (1966) Canadian Met. Q. 5, 19.

Benham, P. P. and Ford, H. (1961) J. Mech. Eng. Sci. 3, 119.

Bilby, B. A., Cottrell, A. H. and Swinden, K. H. (1963) Proc. Roy. Soc. A272, 304

Bilby, B. A. and Heald, P. T. (1968) Proc. Roy. Soc. A305, 429.

Bloom, J. N. (1966) Int. J. Fract. Mech. 2, 597.

Bowie, O. L. and Neal D. M. (1965) Technical Report AMRA TR 65 - 20.

Brothers, A. J. (1968) AEC Research and Development Report GEAP - 5607

Brothers, A. J. and Yukawa, S. (1966) ASME Paper 66 - MET - 2

Broek, D. and Schijve, J. (1963) NLR - TR M2111

Brown, W. F. and Srawley, J. E. (1966) ASTM Special Technical Publication STP-410.

Burgess, N. T. and Glossop, B. A. (1970) International Institute of Welding. Memorandum to Annual Assembly 1970.

Carman, C. M. and Katlin, J. M. (1966) Trans. ASME, J. Basic Eng. 88, 792.

Cottrell, A. H. (1965) Proc. Roy. Soc. A285, 10

Crooker, T. W. and Lange, E. A. (1970) Fatigue of Welding Structures Conference, Brighton. The Welding Institute.

Dawson, R. A. T., Elder, W. J., Hill, G. J. and Price, A. T. (1967) Thermal and High Strain Fatigue. International Conference 1967. Metals and Metallurgy Trust Monograph and Report No. 325, p 239.

Dixon, J. R. and Pook, L. P. (1969) Nature 224, 166.

Ewing, Sir J.A. and Humfrey, J.W.C. (1903) Phil. Trans. A200, 241.

Fenner, A.J., Owen, N.B. and Phillips, C.E. (1951) Engineering 171, 637.

Forman, R.G., Kearney, V.E. and Engle, R.M. (1966) ASME Paper 66 - WA MET - 4

Formby, C.L. (1968) C.E.G.B. Report RD/B/N1050

Forsyth, P.J.E. (1956) International Conference on the Fatigue of Metals, London. Institution of Mechanical Engineers.

Forsyth, P.J.E. (1961) Proceedings of the Crack Propagation Symposium, Cranfield. p 76.

Forsyth, P.J.E. and Ryder, D.A. (1960) Aircraft Engineering 32, 96.

Forsyth, P.J.E. and Ryder, D.A. (1961) Metallurgia 63, 117.

Frost, N.E. (1955) Engineer 200, 464

Frost, N.E. and Denton, K. (1966) NEL Report No. 260

Frost, N.E. and Dixon, J.R. (1967) Int. J. Fract. Mech. 3, 301.

Frost, N.E. and Dugdale, D.S. (1958) J. Mech. and Phys. of Solids 6, 92.

Frost, N.E. and Greenan, A.F. (1964) NEL Report 132.

Gilbey, D.M. and Pearson, S. (1966) Royal Aircraft Establishment Tech. Rep. 66402.

Gittus, J.H. (1964) Nature 202, 788.

Gough, H.J. and Hanson, D. (1923) Proc. Roy. Soc. A104, 538.

Griffith, A.A. (1920) Phil. Trans. A221, 163

Gross, B. Srawley, J.E. and Brown, W.F. (1964) NASA TN D-2395

Gurney, T.R. (1969) Metal Construction 1, 91.

Ham, R.K. (1966) Nature 212, 1568.

Harris, D.O. (1967) Trans. ASME, J. Basic Eng. 89D, 49.

Harrison, J.D. (1969) Welding Institute Report E20/3/69

Head, A.K. (1953) Phil. Mag. 44, 925.

Hoeppner, D.W. (1967) ASTM Special Technical Publication STP - 415 p 486.

Hudson, C.M. and Scardina, J.T. (1969) Eng. Fract. Mech. 1, 429.

Irwin, G.R. (1948) Fracturing of Metals, ASM (Cleveland).

Irwin, G.R. (1958) Encyclopedia of Physics (Ed: S. Flugge) Volume VI. Elasticity and Plasticity. Springer (Berlin)

Irwin, G.R. (1960) Structural Mechanics (Eds: Goodier and Hoff) Pergamon Press p 557.

Jack, A.R. (1969) Unpublished work

Jackson, L.R. (1963) DMIC Memo 178. Battelle Memorial Institute. Columbus, Ohio.

Kennedy, A.J. (1962) Processes of Creep and Fatigue in Metals. Oliver and Boyd, London.

Krafft, J.M. (1964) Applied Mats. Research. April 1964, 88.

Krafft, J.M. (1965) Trans. ASM. 58, 691.

Laird, C. and Smith, G.C. (1962) Phil. Mag. 7, 847.

Liu, H.W. (1960) ASME Paper 60 - MET - 11.

Liu, H.W. (1961a) Proceedings of the Crack Propagation Symposium, Cranfield p. 514.

Liu, H.W. (1961b) ARL Report 58.

Liu, H.W. (1964) Applied Mats. Research, October 1964 p 229.

McClintock, F.A. (1963) Fracture of Solids. Interscience Publishers. (New York)

McEvily, A.J. and Illg, W. (1958) NACA - TN 4394

McEvily, A.J. and Johnston, T.L. (1967) Int. J. Fract. Mech. 3, 45.

McMillan, J.C. and Pelloux, R.M.N. (1967) ASTM Special Technical Publication STP-415, p 505.

Maddox, S.J. (1970) Welding Construction 2, 327.

May, A. N. (1960a) Nature 185, 303

May, A. N. (1960b) Nature 188, 573.

Miller, G. A. (1968) Trans. ASM. 61, 442

Neuber, H. (1958) Theory of Notch Stresses. Springer (Berlin).

Orowan, E. (1939) Proc. Roy. Soc. A171, 79.

Orowan, E. (1950) Fatigue and Fracture of Metals (MIT Symposium 1950) John Wiley and Sons, New York.

Paris, P. C., Gomez, M. P. and Anderson, W. E. (1960) The Trend in Engineering 13, 9.

Paris, P. C. and Erdogan, F. (1963) Trans. ASME. 85, 121.

Pearson, S. (1966) Nature 211, 1077

Pearson, S. (1967) Private Communication

Pearson, S. (1969) Royal Aircraft Establishment Technical Report 69195.

Pearson, S. (1970) Private Communication.

Plumbridge, W. J. and Ryder, D. A. (1969) Metals and Materials 3, 321.

Pook, L. P. (1968) Int. J. Fract. Mech. 4, 295.

Priddle, E. K. (1970) C. E. G. B. Report RD/B/M1757.

Rice, J. R. (1967) ASTM Special Technical Publication STP 415 p 247.

Richards, C. E. (1970) Private Communication

Rolfe, S. T. and Munse, W. H. (1963) Welding Research Supplement, June 1963.

Signes, E. G., Baker, R. G., Harrison, J. D. and Burdekin, F. M. (1967) British Welding Journal. 14, 108.

Smith, E. (1967) Proc. Roy. Soc. A299, 455.

Srawley, J. E. and Gross, B. (1967) Mats. Research and Standards. 7, 155.

Sullivan, A. M. (1967) Mats. Research and Standards. 7, 20.

Tetelman, A. S. and McEvily, A. J. (1967) Fracture of Structural Materials. John Wiley and Sons. (New York).

Thomson, N, Wadsworth, N. J. and Louat, N. (1956) Phil. Mag. 1, 113.

Weertman, J. (1966) Int. J. Fract. Mech. 2, 460.

Weertman, J. (1969) Int. J. Fract. Mech. 5, 13.

Weibull, W. (1954) SAAB. TN25

Weibull, W. (1956) The Aeronautical Research Institute of Sweden. FFA Report 65.

Weibull, W. (1961) Proceedings of Crack Propagation Symposium, Cranfield p 271.

Weibull, W. (1963) Acta. Met. 11, 745.

Weiss, V. (1962) ASME Paper 62-WA-270

Weiss, V. and Yukawa, S. (1965) ASTM Special Technical Publication STP 381.

Westergaard, H. M. (1939) Trans ASME, J. Appl. Mech. 61, 49.

Zappfe, C. A. and Worden, C. O. (1951) Trans. ASM. 43, 958.

TABLE I Composition of Mild Steel

C	Si	S	P	Mn	Ni	Cu	Sn
0.23%	0.15%	0.03%	0.018%	0.45%	0.07%	0.07%	0.011%

TABLE II Tensile Properties of Annealed Material

Yield Point	U. T. S.	Elong. on 1in.	R. in A.	E
15.5 tsi	27.2 tsi	43%	59%	29.9×10^6psi

TABLE III Details of Specimen Dimensions

Width W (in)	Thickness B (in)	Notch Depth a_o (in)	Notch Root Radii, thou.
1	0.05	0.10	5
1	0.08	0.10	5
1	0.2	0.05	2
1	0.2	0.10	2, 5, 10, 15, 20, 25, 50
1	0.2	0.15	2
1	0.2	0.20	5, 15, 30
1	0.2	0.30	2, 20, 50
1	0.4	0.10	5
1	0.9	0.10	5
0.2	1	0.02	2
0.4	1	0.04	5
2	0.2	0.10	5

TABLE IV The Effect of Mean Stress on N_i and N_p in 1 in. wide x 0.2 in. thick specimens containing 0.1 in. deep sharp notches.

Stress Range ksi	Mean Stress ksi	N_i k cycles	N_p k cycles	N'_p k cycles
15	7.5	30	189	
		26	-	
		35	252	
	22.5	16	134	217
	32.5	10	-	208
20	10	8	52	
		7	64	
	20	4	49.5	57
		5	47	
	30	4	25	53

Note: N'_p is the number of cycles, under zero-maximum stress conditions, to propagate a crack to the length at which failure occurs in high mean stress tests.

TABLE V The effect of specimen thickness on N_i and N_p in 1 in. wide specimens containing 0.1 in. deep sharp notches.

Specimen Thickness in.	Stress Range ksi	N_i k cycles	N_p k cycles	Scatter band from 0.2in. thick specs.	
				N_i	N_p
0.05	0 - 20	7	62	7.5-13	54-81
	0 - 25	3	21	2.2-4.8	21-32
	0 - 30	0.25	6	0.8-2.1	13-18.5
0.08	0 - 20	7	-	7 - 13	54 - 81
	0 - 25	3.5	29	2.2-4.8	21 - 32
	0 - 30	0.5	8	0.8-2.1	13-18.5
0.40	0 - 17.5	11	123	14-24	110-160
	0 - 25	2.7	35	2.2-4.8	21-32
	0 - 30	1	15.5	0.8-2.1	13-18.5
0.90	0-22.22	4-8	71-75	4.1-8.2	34-52
	0-27.78	2.5	30	1.3-3	15-22

TABLE VI Miscellaneous Results

Width W(in)	Thickness B(in)	Stress Range ksi	Notch Depth a_o(in)	Notch Root Radius p (in)	N_i k cycles	N_p k cycles	
2	0.2	20	0.1	0.005	21	131	*
		25	0.1	0.005	2	53	
		25	0.1	0.005	1.75	59	
0.2	1	30	0.02	0.002	27	35	
		35	0.02	0.002	10.5	16.5	
0.4	1	30	0.04	0.005	13	21	
		35	0.04	0.005	5	13	

* Poor test record N_i is max. figure, N_p is min. figure.

TABLE VII

Specimen Thickness, in.	Stress Range ksi	a_t in.	K ksi$\sqrt{in}$
0.05	25	0.138	20.7
0.08	25	0.197	26.6
	30	0.197	32.0
0.20	15	0.550	66.2
	18	0.691	155.7
	18	0.611	103.1
	20	0.433	54.2
	20	0.500	70.9
	22.5	0.400	53.1
	22.5	0.355	44.7
	25	0.235	31.4
	25	0.355	49.7
	27	0.355	53.6
	27	0.355	53.6
	30	0.315	51.3
0.4	17.5	0.711	159.3
	17.5	0.750	197.1
	30	0.472	93.8

TABLVE VIII. Ripple spacings and macroscopic crack growth rates.

Specimen 36. 0 - 15 ksi 1 in. wide x 0.2 in. thick specimen
0.1 in. deep sharp notch.

Crack length	0.125	0.200	0.300	0.400	0.500	0.600
Ripple spacing	8.7	6.7	10.5	13.5	22.7	127
Growth Rate	0.427	1.35	4.25	14.45	37.0	

Specimen 55 0 - 30 ksi 1 in. wide x 0.08 in. thick specimen
0.1 in. deep sharp notch.

Crack length	0.1	0.125	0.150	0.175	0.200	0.225
Ripple spacing	8.3	13.5	17.1	17.5	14.3	13.6
Growth rate	-	14.4	19.6	26.6	37.6	50.4

Specimen 65 0 - 30 ksi 1 in. wide x 0.40 in. thick specimen
0.1 in. deep sharp notch

Crack length	0.1	0.125	0.175	0.250	0.350	0.425
Ripple spacing	17.4	16.5	18.5	24.6	27.2	27.2
Growth rate		10	17.2			

Specimen 87 0 - 20 ksi 1 in. wide x 0.05 in. thick specimen
0.1 in. deep sharp notch.

Crack length	0.10	0.20	0.30	0.40	0.50	
Ripple spacing	17	10.4	24.9	30.5	66.7	
Growth rate		6.62	16.4	41.0		

Crack lengths in inches
Ripple Spacings and Growth Rates in 10^{-6} inches/cycle.

TABLE IX The effect of specimen geometry, loading configuration and stress on the fatigue lives of 1 in. wide specimens.

Stress Range ksi	Total Notch length in.	Edge Notch-Tension			Edge Notch-Bending			Centre Notch-Tension		
		N_i	N_p	N_f	N_i	N_p	N_f	N_i	N_p	N_f
10	0.025	2.68×10^6	2.03×10^6	4.71×10^6	2.99×10^6	2.87×10^6	5.86×10^6	1.69×10^7	4.93×10^6	2.18×10^7
	0.100	1.35×10^5	4.70×10^5	6.05×10^5	2.23×10^5	1.00×10^6	1.22×10^6	1.02×10^6	1.72×10^6	2.74×10^6
	0.250	8.34×10^3	7.27×10^4	8.10×10^4	3.11×10^4	2.78×10^5	3.09×10^5	1.48×10^5	6.02×10^5	7.50×10^5
20	0.025	1.67×10^5	2.53×10^5	4.20×10^5	1.87×10^5	3.57×10^5	5.43×10^5	1.06×10^6	6.09×10^5	1.67×10^6
	0.100	8.41×10^3	5.87×10^4	6.71×10^4	1.40×10^4	1.25×10^5	1.39×10^5	6.40×10^5	2.11×10^5	2.75×10^5
	0.250	5.21×10^2	9.05×10^3	9.57×10^3	1.94×10^3	3.43×10^4	3.62×10^4	9.24×10^3	7.09×10^4	8.01×10^4

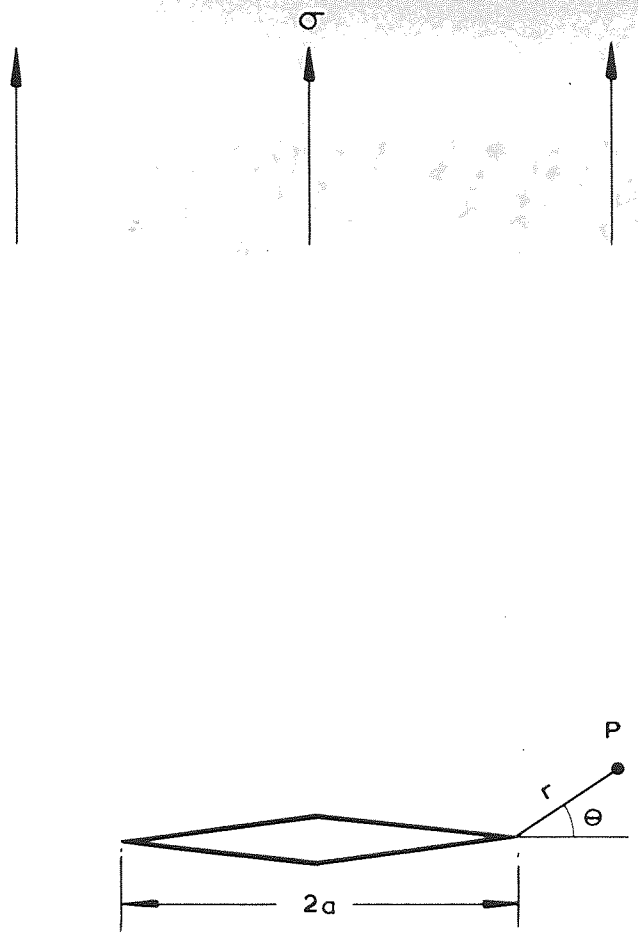

FIG. 1 A CRACK OF LENGTH $2a$ IN AN INFINITE PLATE UNDER A UNIFORM TENSILE STRESS σ

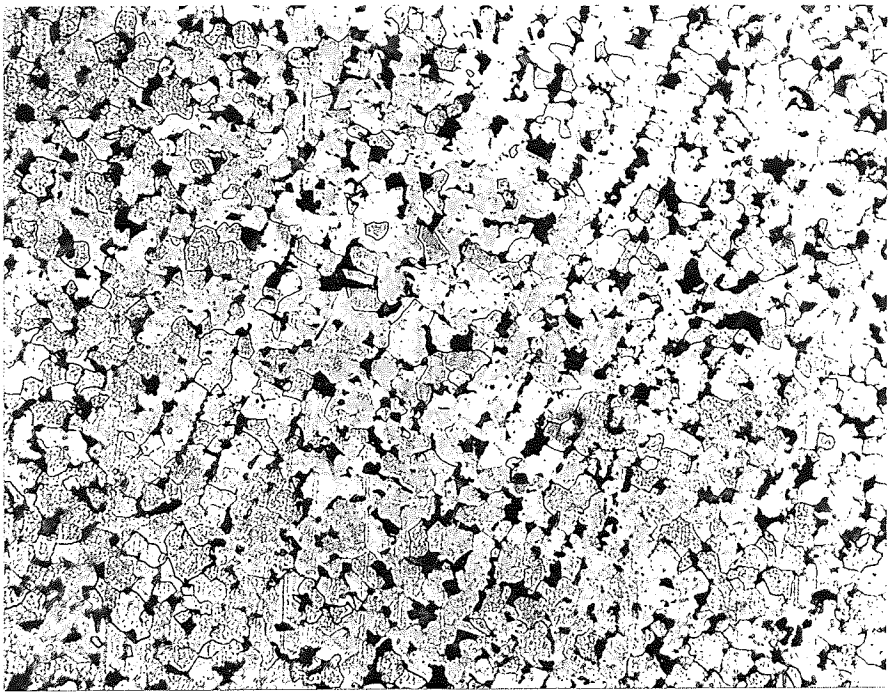

Fig.2. Microstructure of economiser tube. x200

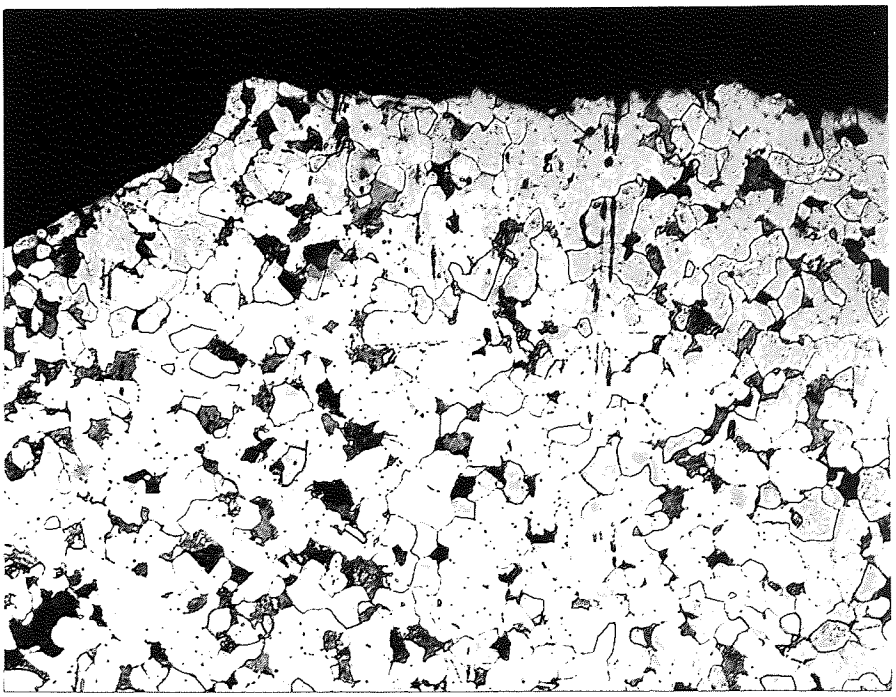

Fig.3. Section through fracture surface of annealed specimen. x200

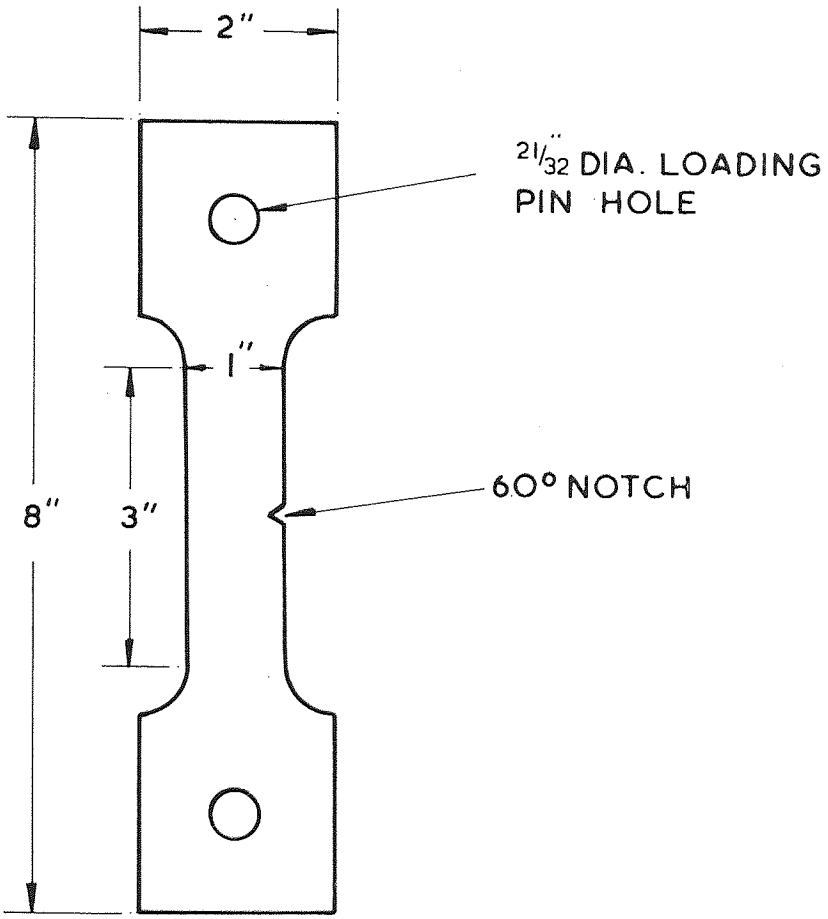

FIG.4. FORM OF TEST SPECIMEN. THE DIMENSIONS SHOWN ARE THOSE MOST COMMONLY USED.

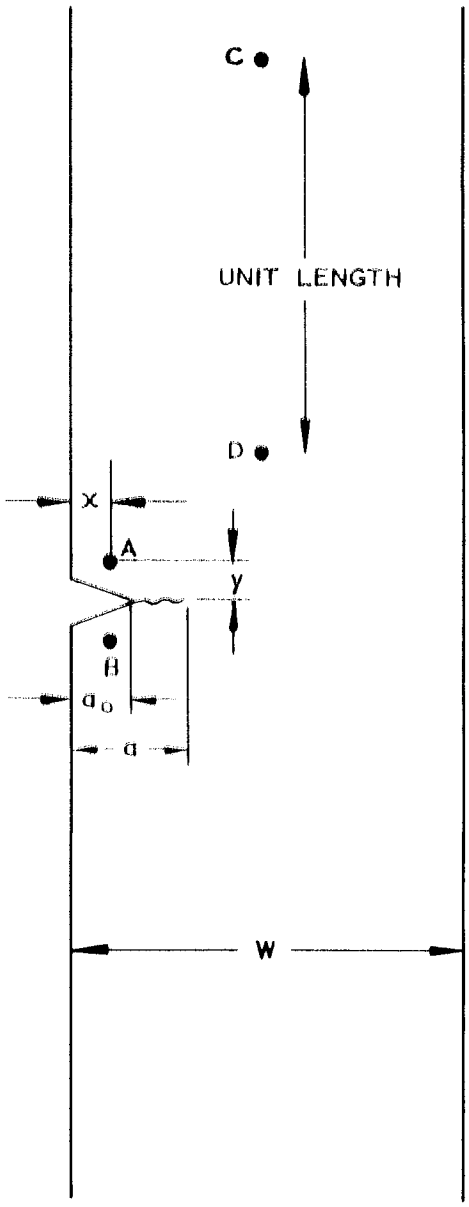

A.B. POTENTIAL POINTS FOR MEASURING V_a

C.D. POTENTIAL POINTS FOR MEASURING V_0

FIG. 5 DETAILS OF SPECIMEN SHOWING A CRACK OF LENGTH a GROWING FROM A NOTCH OF LENGTH a_0

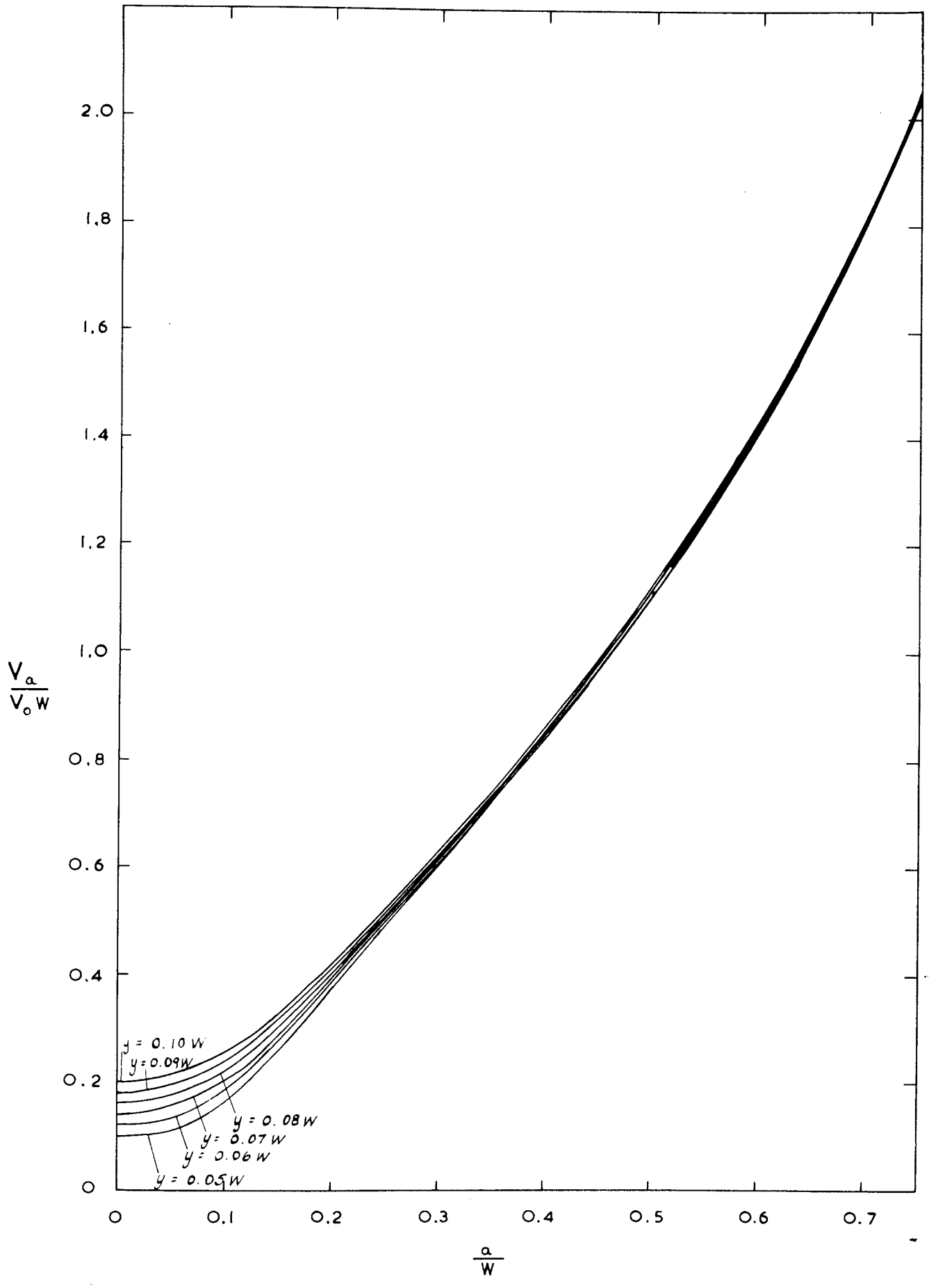

FIG. 6. GRAPH OF $\frac{V_a}{V_o W}$ VERSUS $\frac{a}{W}$ FOR POTENTIAL MEASURING POINTS AT $x = 0.10W$. $y = \pm$ VALUES SHOWN.

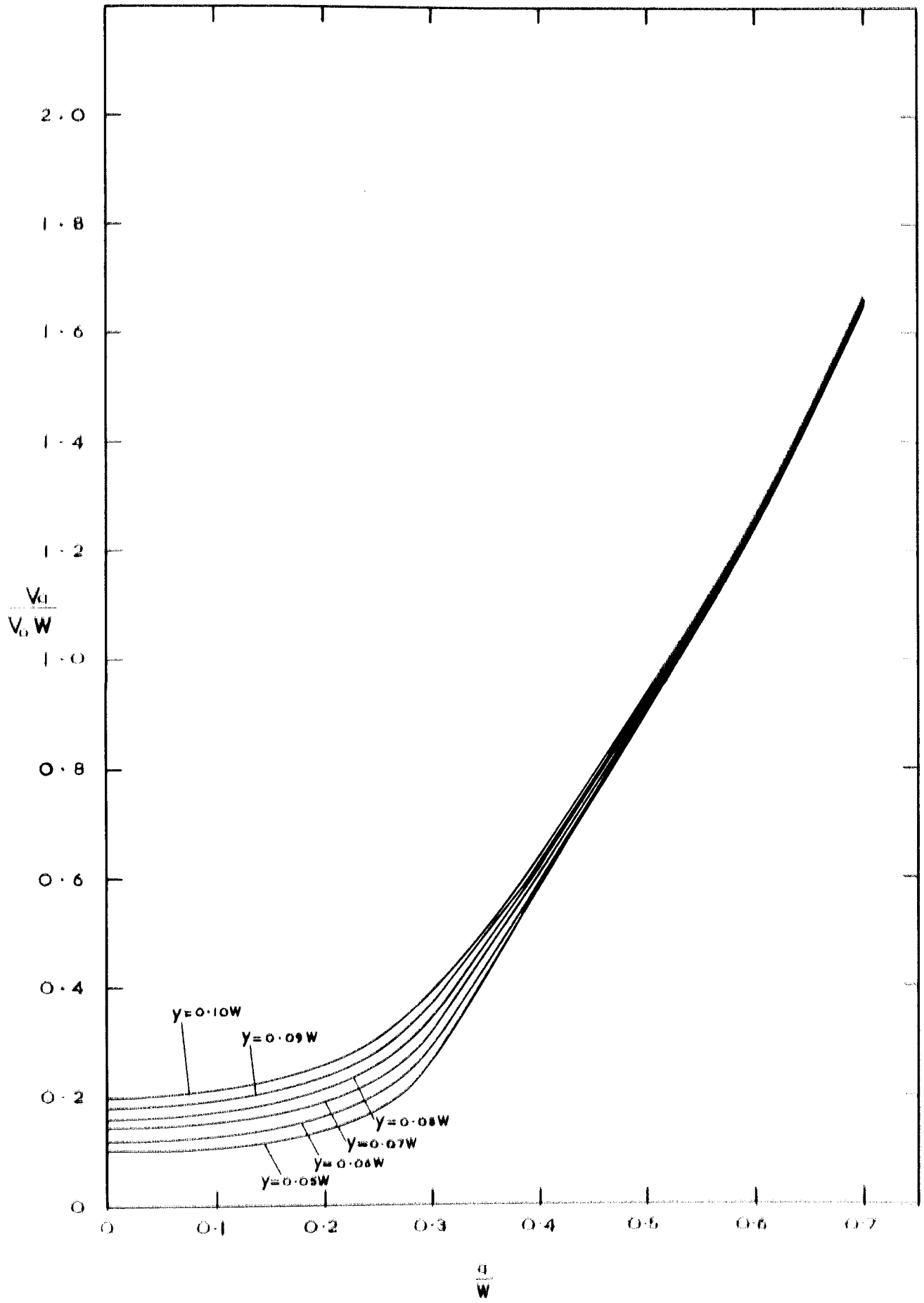

FIG. 7 GRAPH OF $\frac{V_q}{V_0 W}$ VERSUS $\frac{q}{W}$ FOR POTENTIAL MEASURING POINTS AT $X = 0 \cdot 30W$, $y = \pm$ VALUES SHOWN.

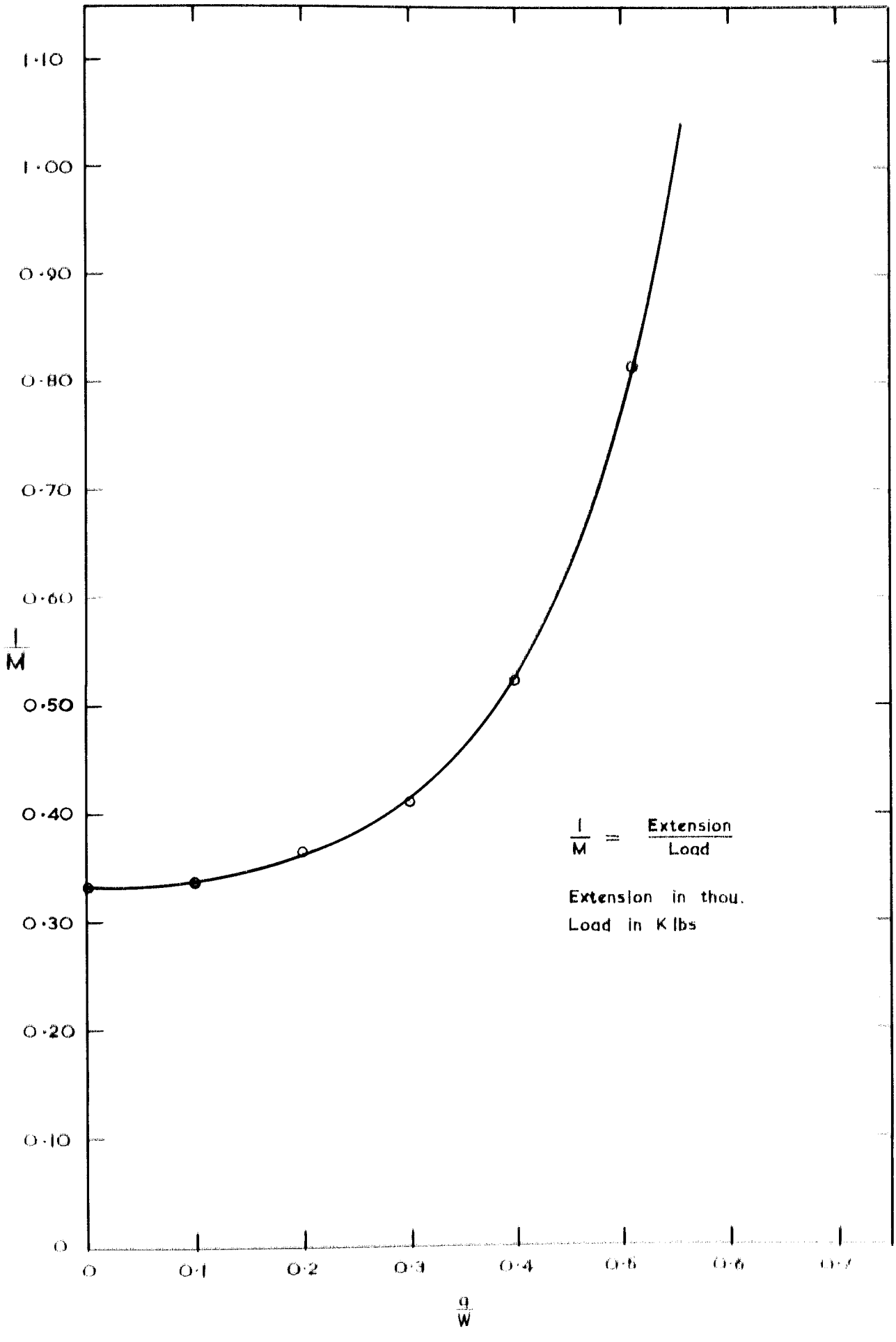

FIG 8 COMPLIANCE CALIBRATION FOR FATIGUE SPECIMEN

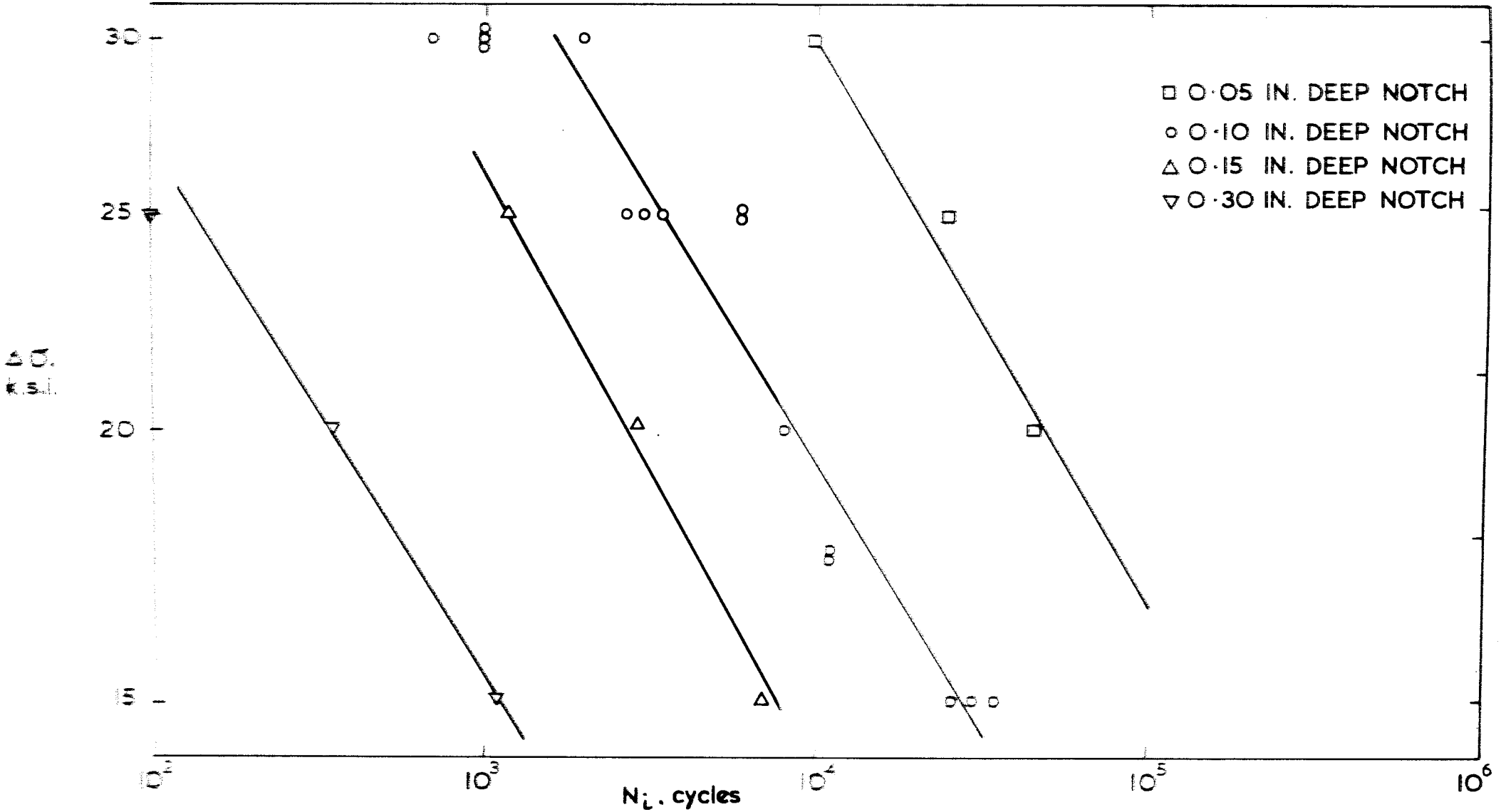

FIG 9. THE INFLUENCE OF STRESS RANGE($\Delta\sigma$) ON THE NUMBER OF CYCLES TO INITIATE A CRACK (N_i) FROM SHARP NOTCHES IN 1·0 IN. WIDE SPECIMENS.

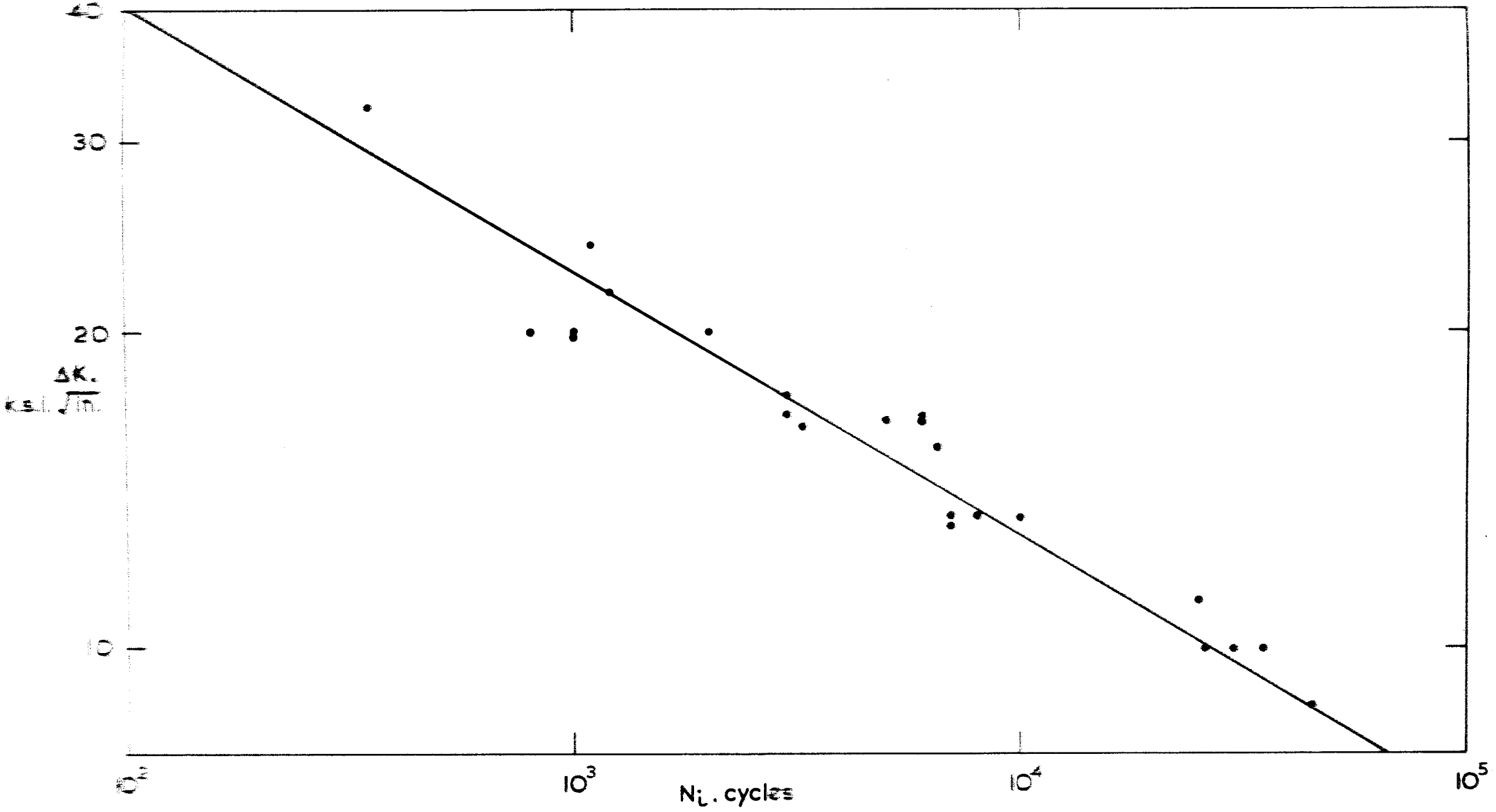

FIG. 10. THE INFLUENCE OF THE RANGE OF STRESS INTENSITY FACTOR (ΔK) ON THE NUMBER OF CYCLES TO INITIATE A CRACK (N_i) FROM SHARP NOTCHES IN 1·0 IN. WIDE × 0·2 IN. THICK SPECIMENS.

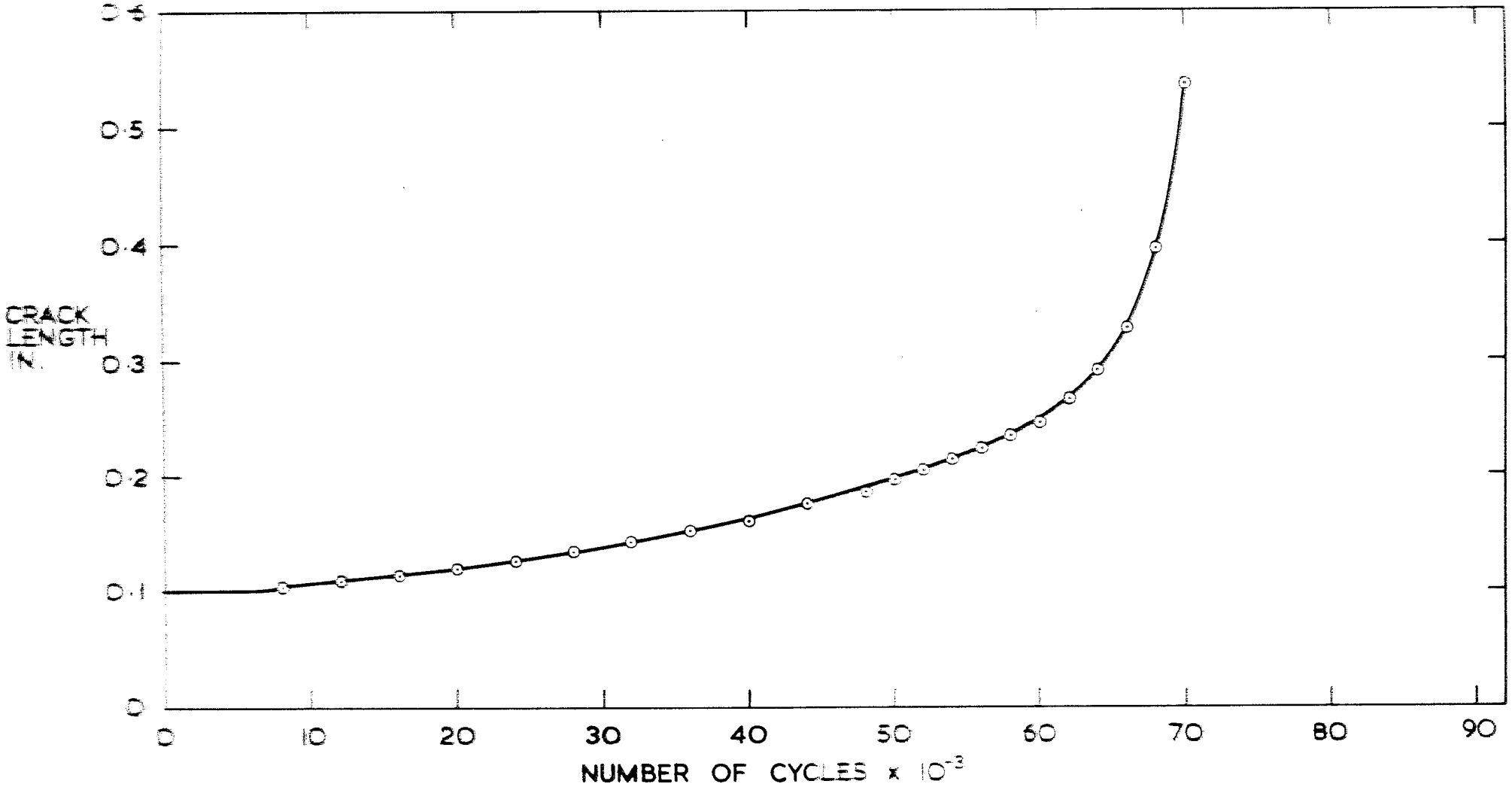

FIG. 11. CRACK LENGTH VERSUS NUMBER OF CYCLES. SPECIMEN No. 42
STRESS RANGE: 0-20 k.s.i. SPECIMEN: W = 1·0 IN., B = 0·2 IN. NOTCH: a_0 = 0·10W, ρ = 0·002 IN

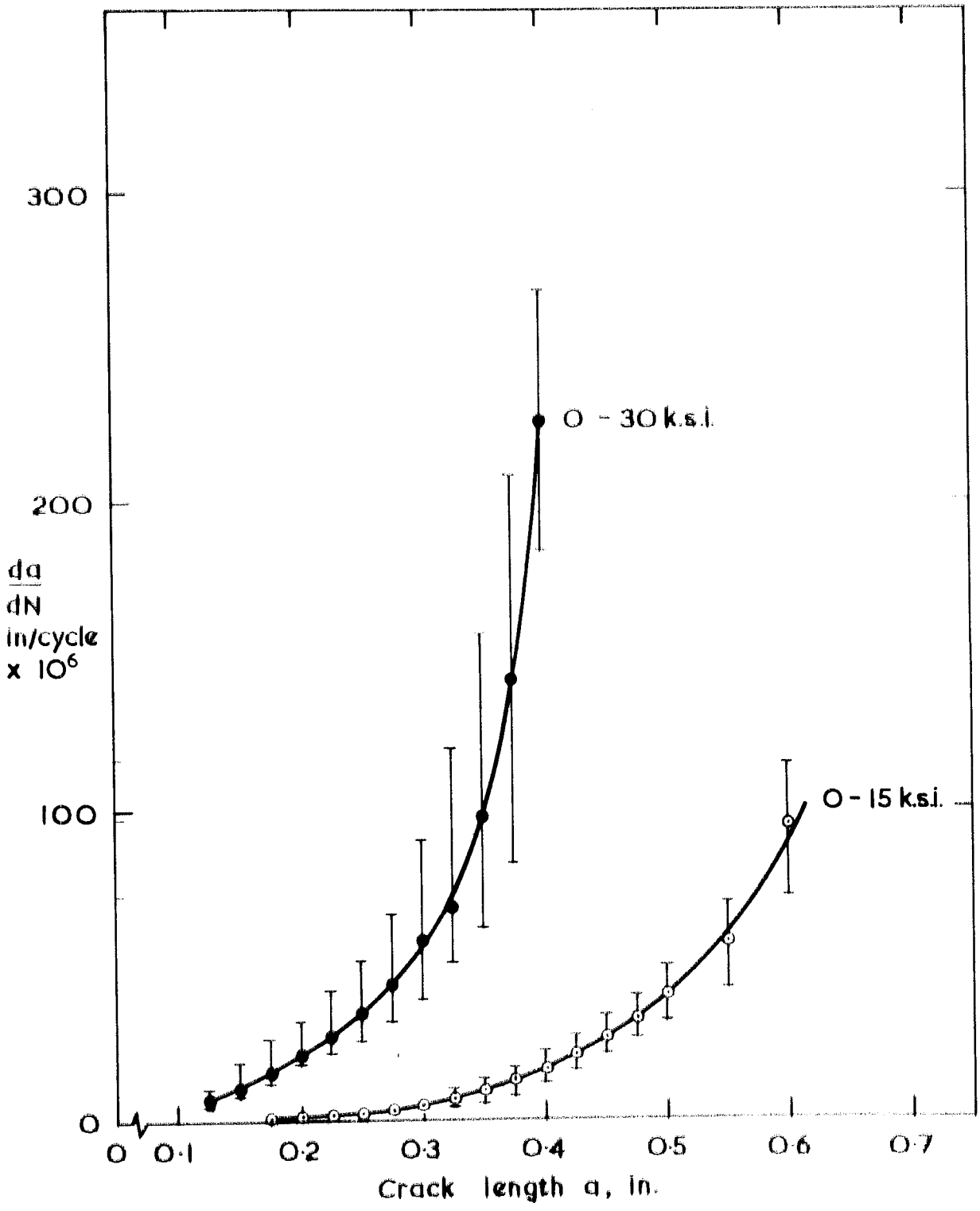

FIG. 12. THE RATE OF CRACK PROPAGATION (da/dN) AS A FUNCTION OF CRACK LENGTH FOR 1·0 IN. WIDE x 0·2 IN. THICK SPECIMENS.

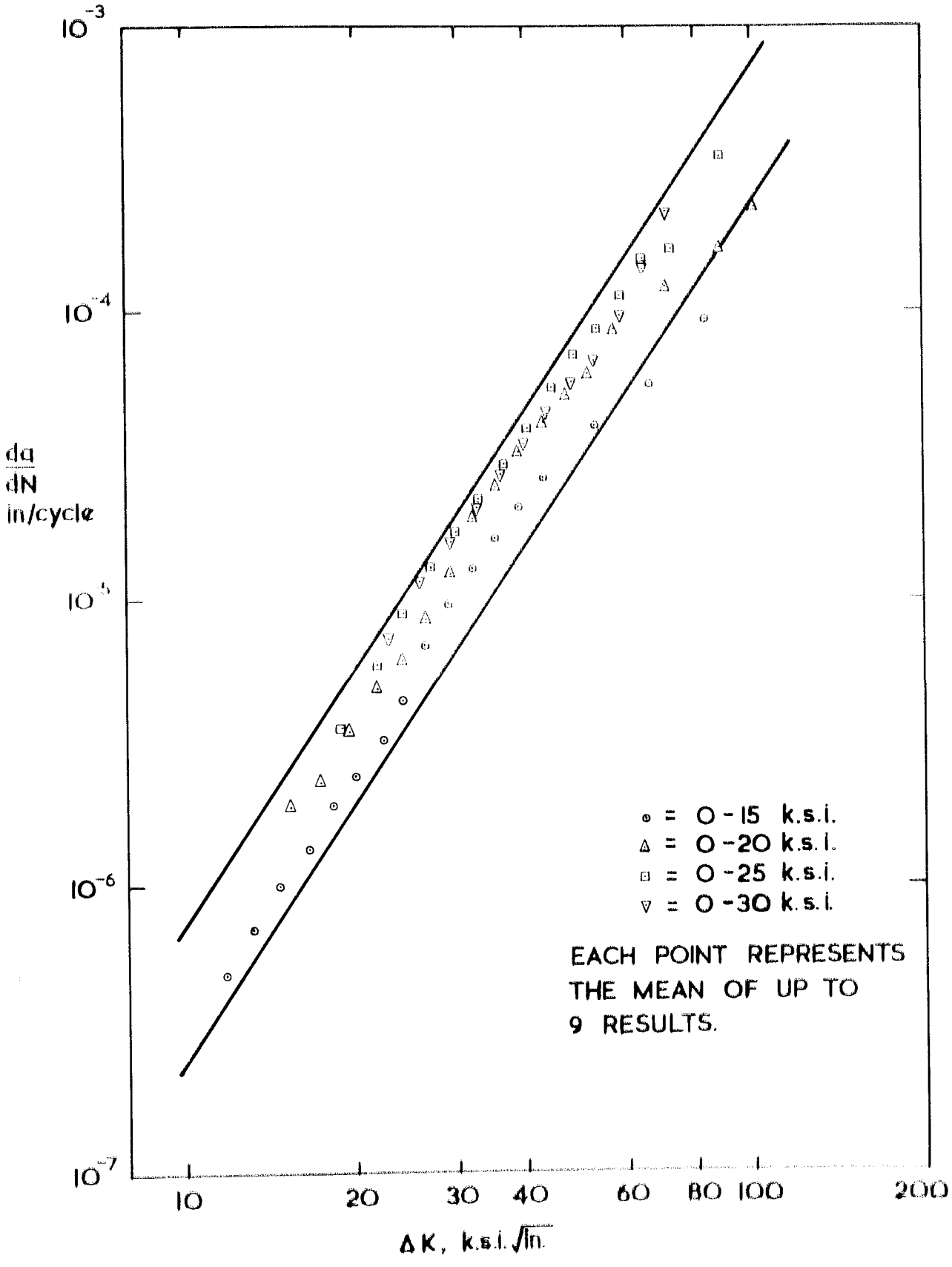

FIG. 13. da/dN VERSUS ΔK AS A FUNCTION OF STRESS RANGE FOR 1·0 IN WIDE x 0·2 IN THICK SPECIMENS.

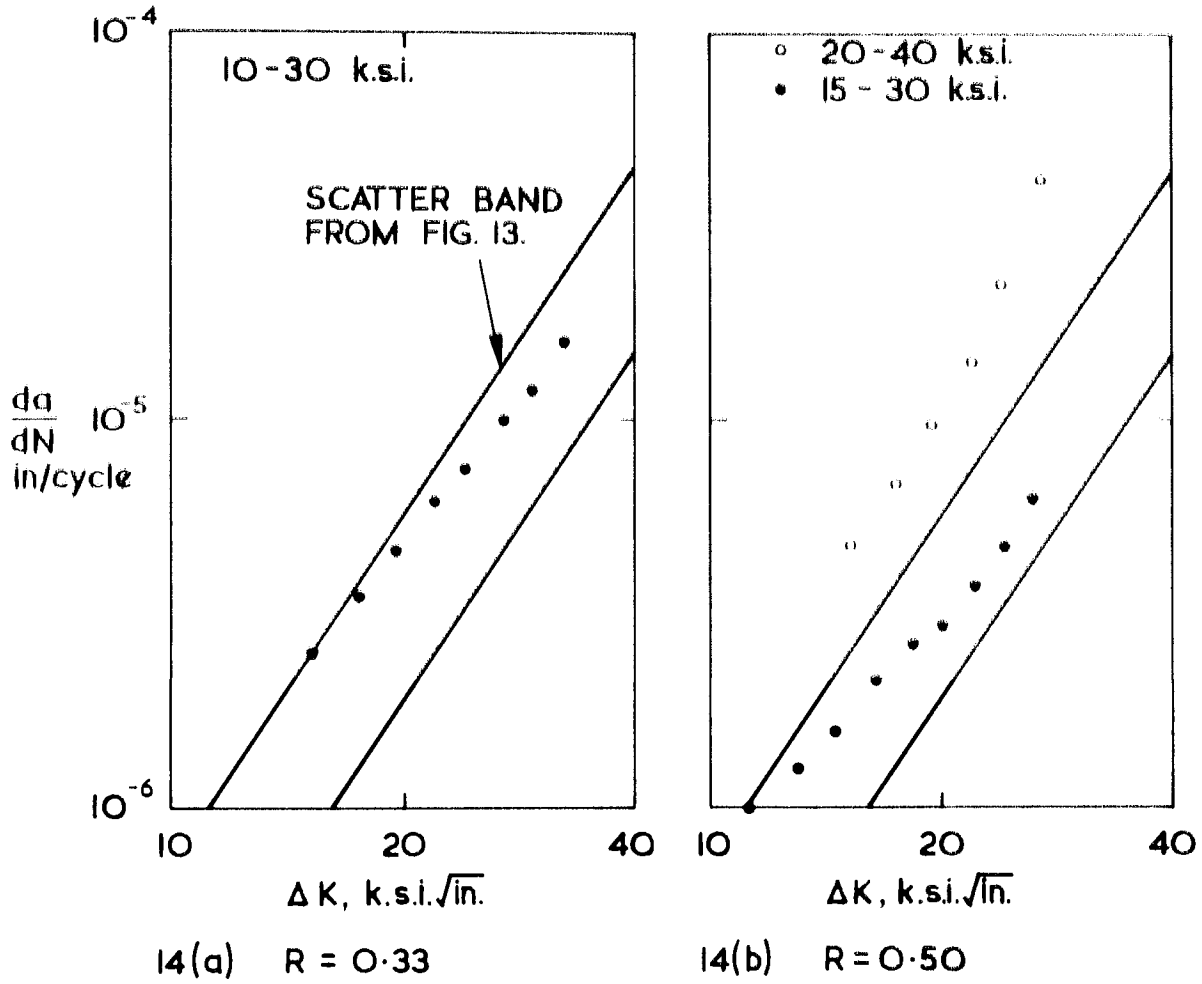

FIG. 14. CRACK GROWTH RATES VERSUS THE RANGE OF STRESS INTENSITY FACTOR FOR 1·0 IN. WIDE x 0·2 IN THICK SPECIMENS – THE EFFECT OF MEAN STRESS.

(a) R = 0·33
(b) R = 0·50

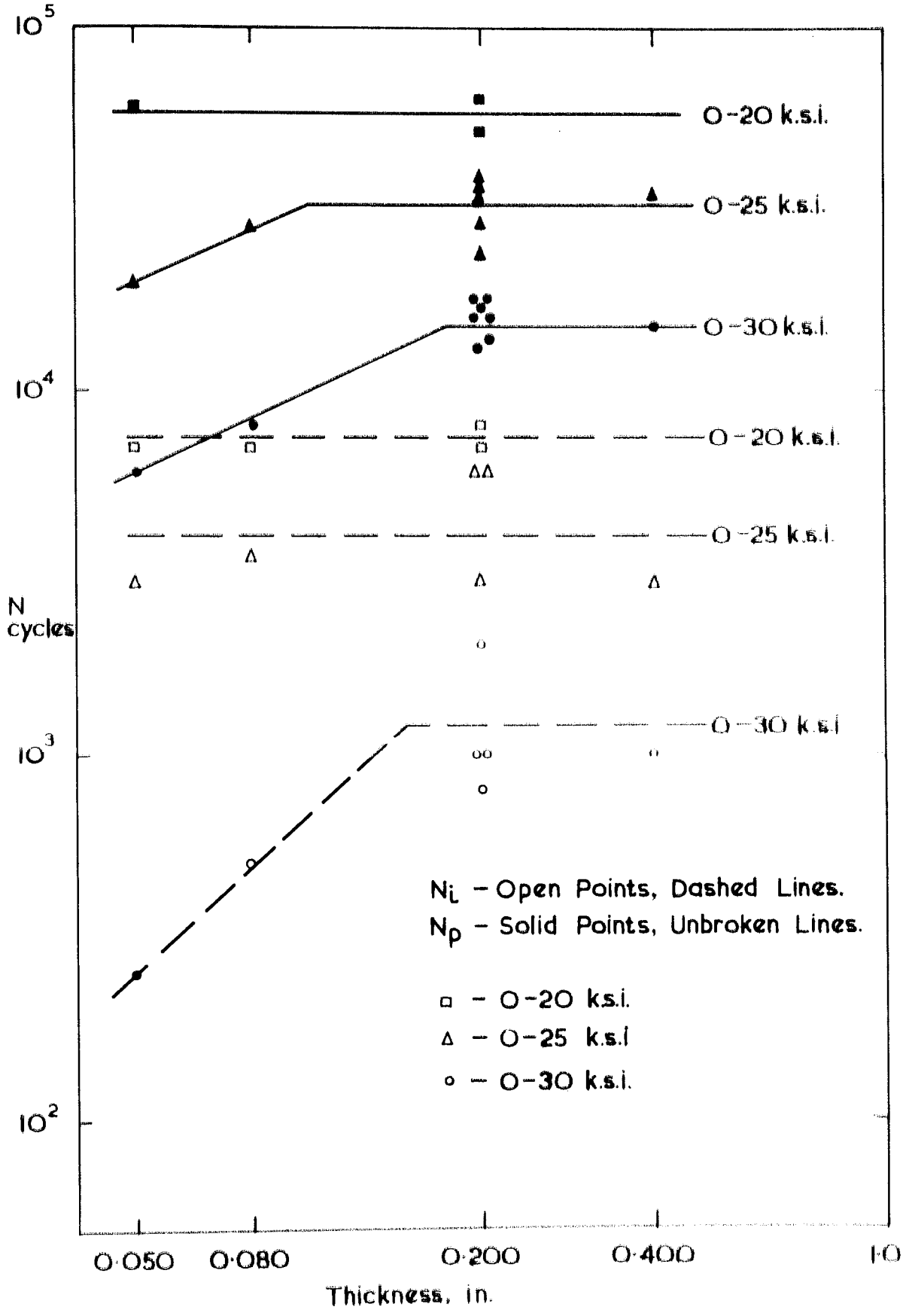

FIG 15. THE EFFECT OF THICKNESS ON N_i AND N_p IN 1·0 IN WIDE SPECIMENS CONTAINING 0·1 IN. DEEP EDGE NOTCHES AT THREE STRESS RANGES.

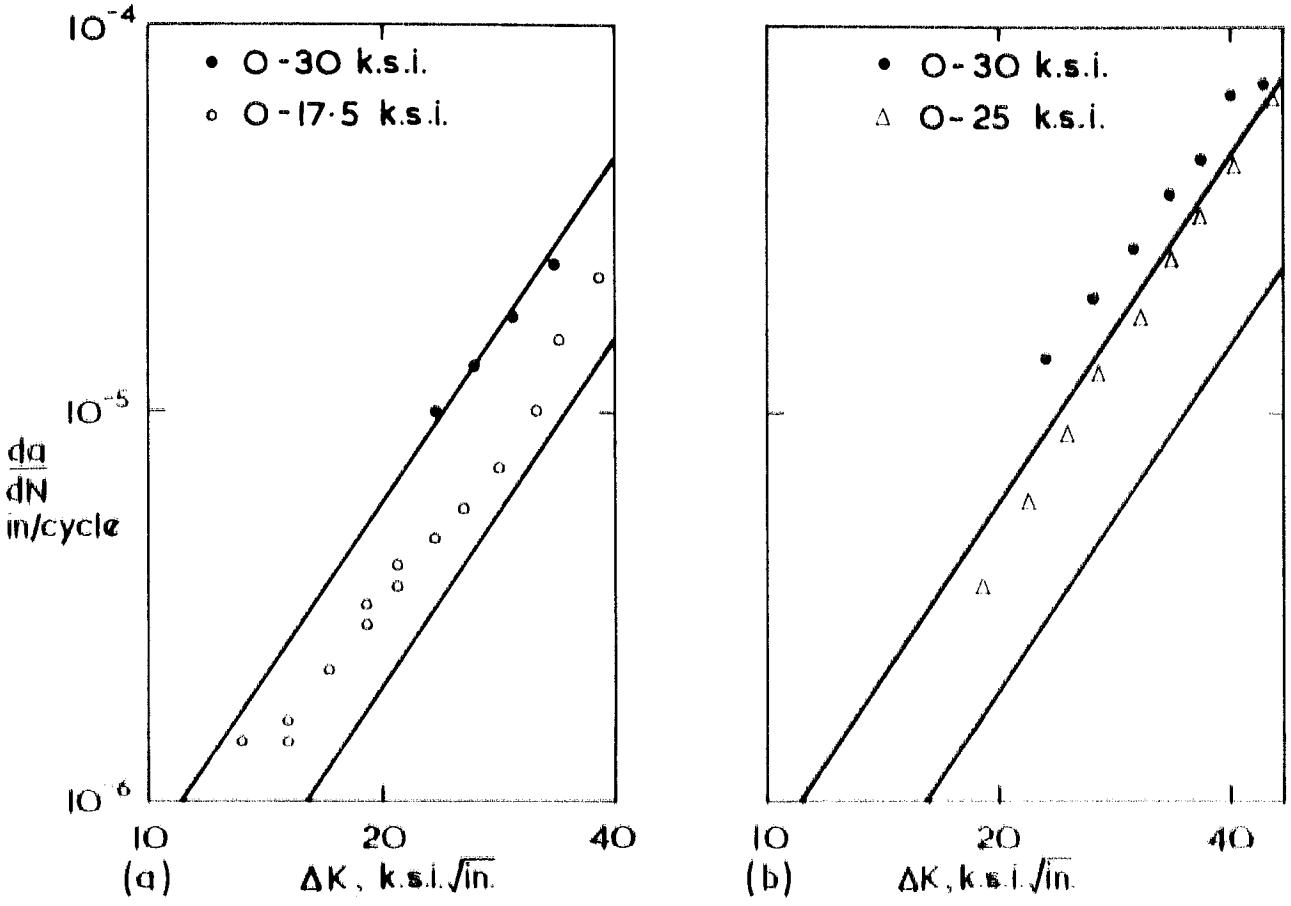

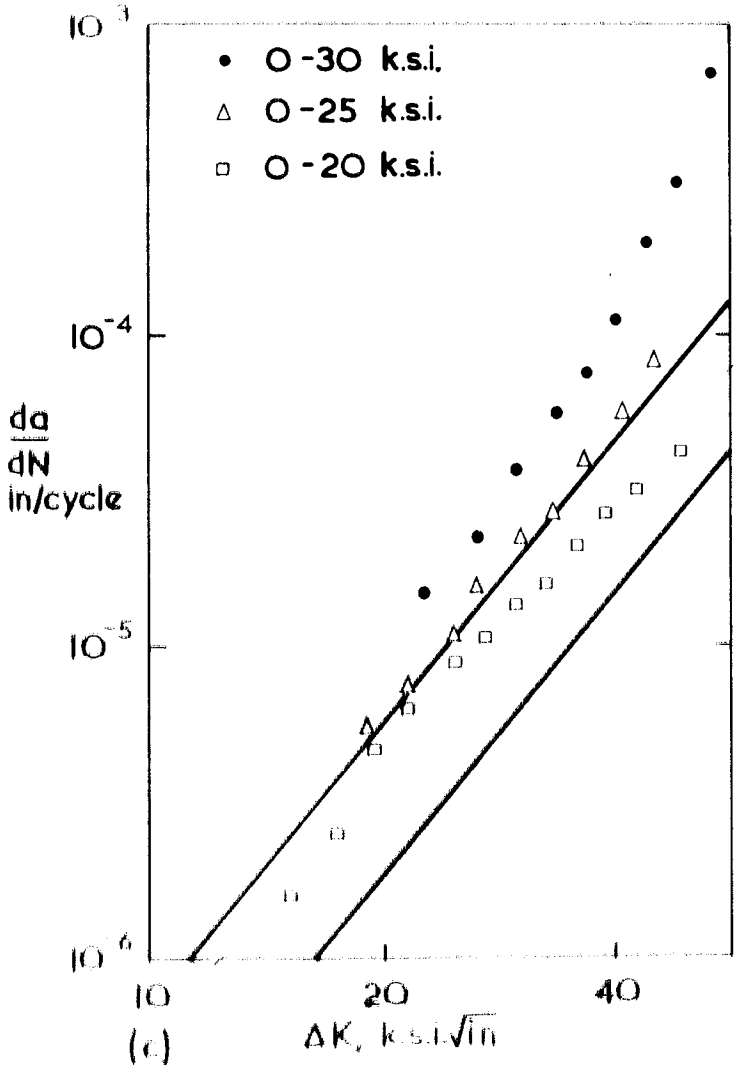

FIG. 16.
THE EFFECT OF SPECIMEN THICKNESS ON CRACK GROWTH RATES IN 1·0 IN. WIDE SPECIMENS.
(a) 0·40 IN. THICK.
(b) 0·08 IN. THICK.
(c) 0·05 IN. THICK.
THE SCATTER BAND FROM FIG. 13 IS SHOWN FOR COMPARISON.

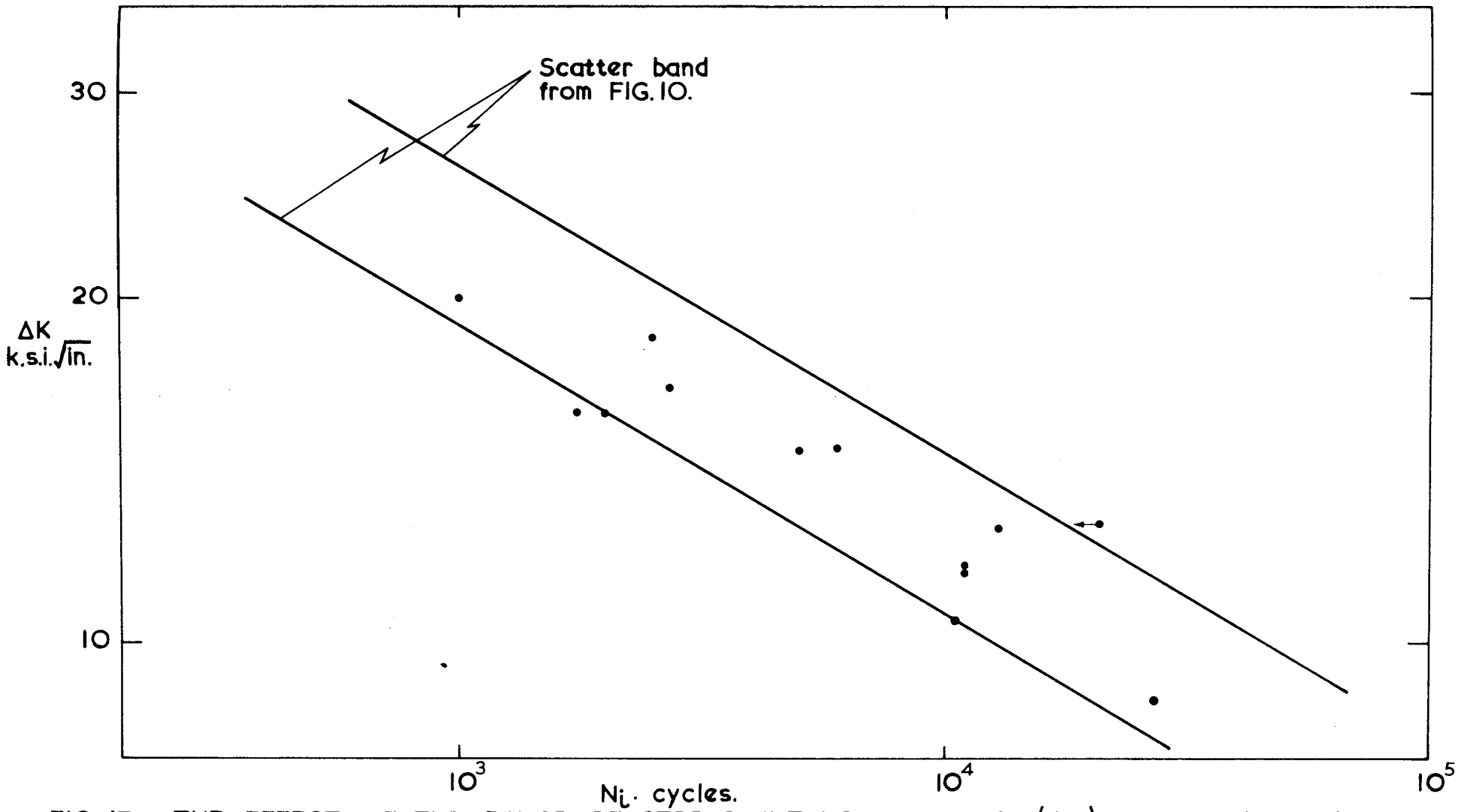

FIG. 17. THE EFFECT OF THE RANGE OF STRESS INTENSITY FACTOR (ΔK) ON THE NUMBER OF CYCLES TO INITIATE A CRACK FROM A SHARP NOTCH (N_i) — MISCELLANEOUS RESULTS.

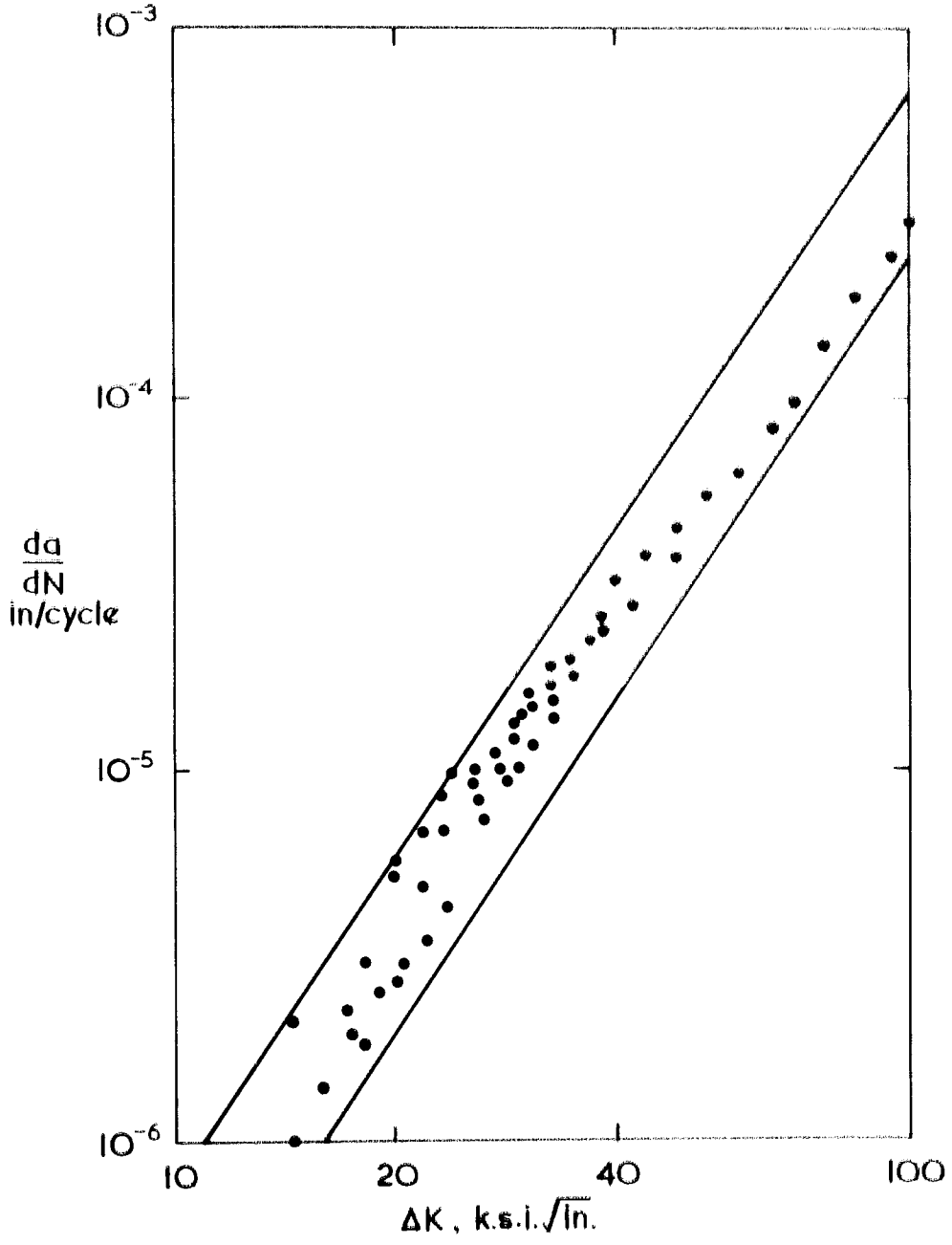

FIG. 18. CRACK GROWTH RATE (da/dN) VERSUS THE RANGE OF STRESS INTENTENSITY FACTOR (ΔK) MISCELLANEOUS RESULTS COMPARED WITH THE SCATTER BAND FROM FIG. 13.

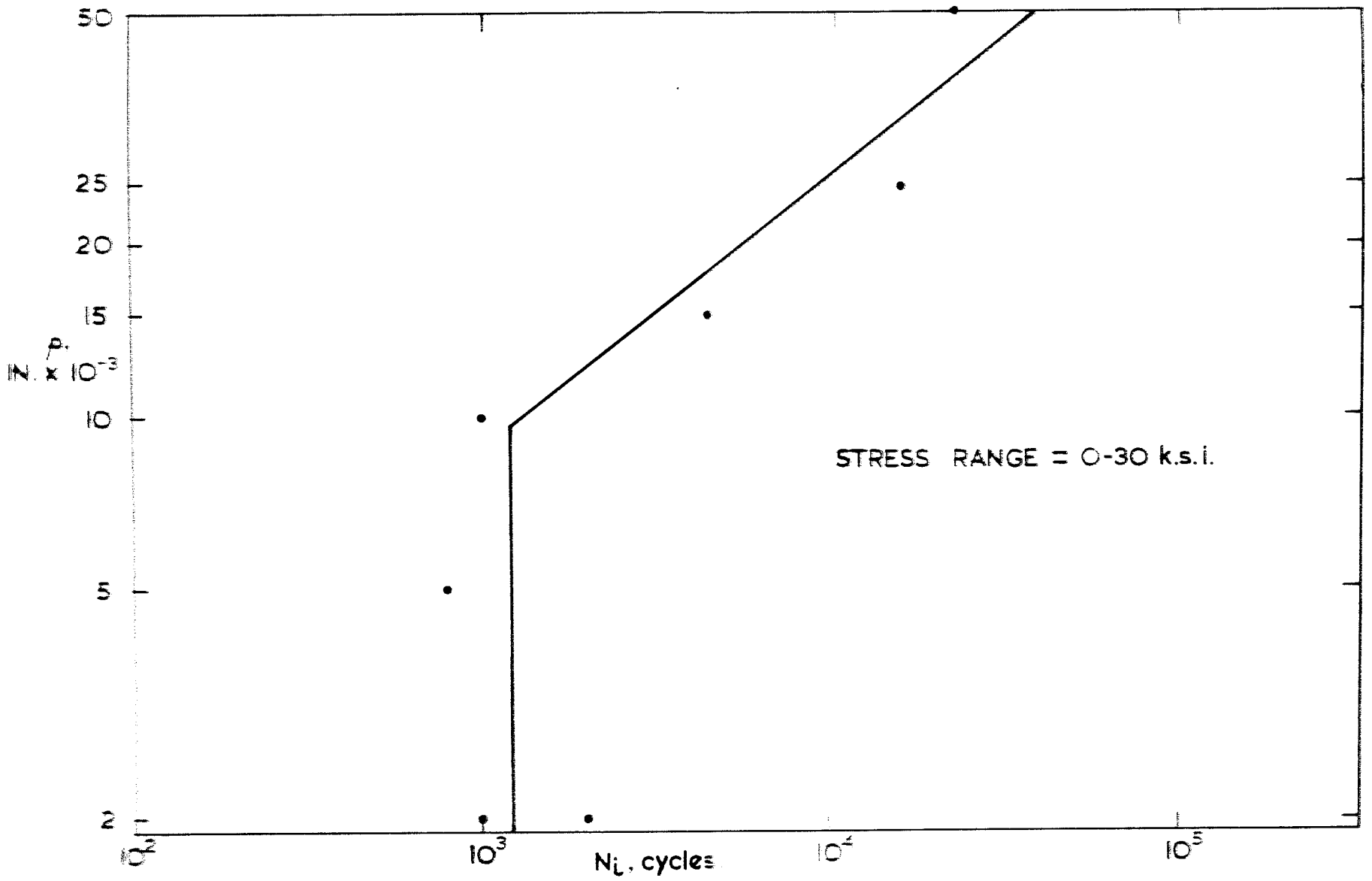

FIG 9 THE INFLUENCE OF NOTCH ROOT RADIUS (ρ) ON THE NUMBER OF CYCLES TO INITIATE A CRACK (N_i) FROM A 0·1 IN. DEEP NOTCH IN A 1·0 IN WIDE SPECIMEN.

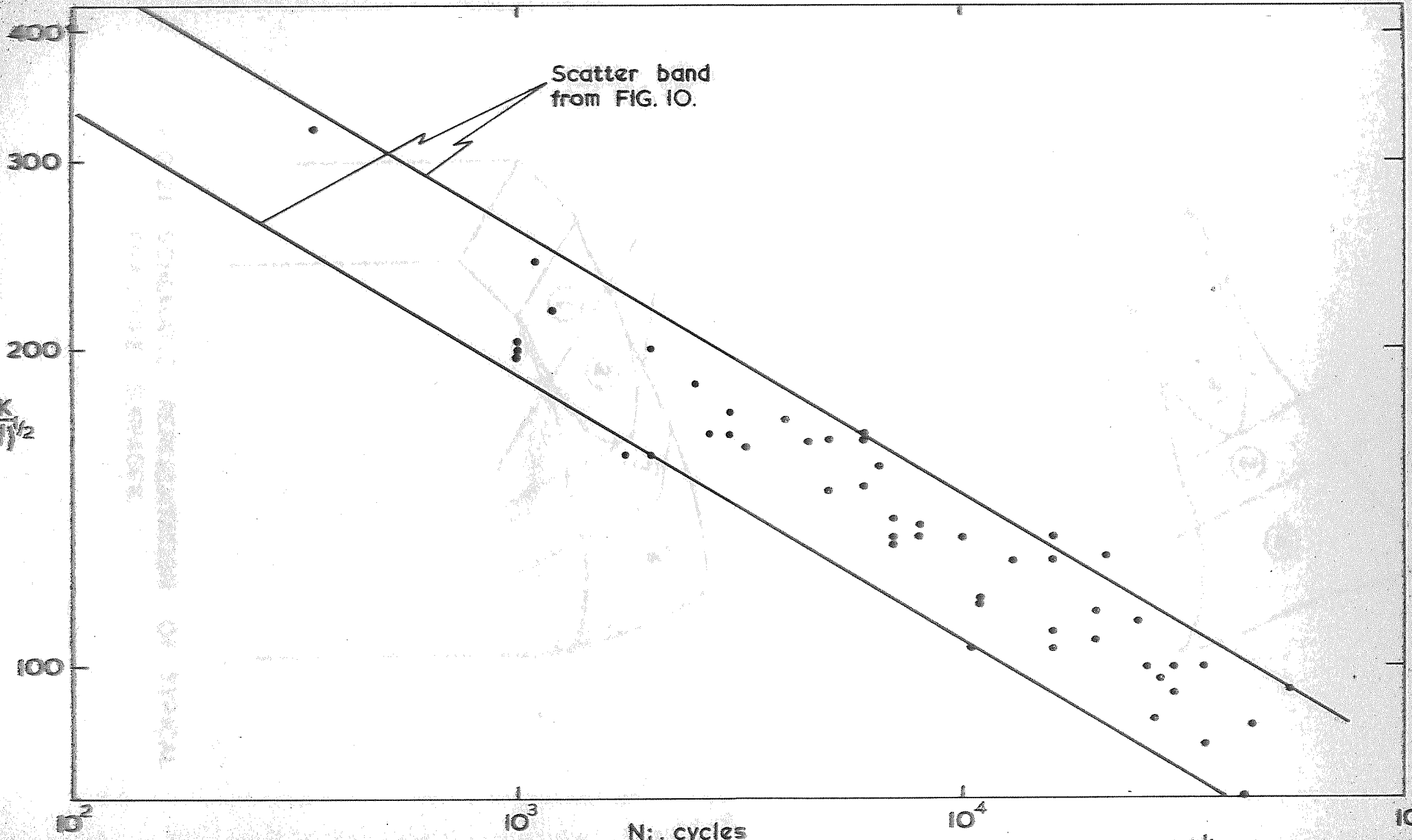

FIG 20. THE INFLUENCE OF THE RANGE OF EFFECTIVE STRESS INTENSITY FACTOR $[\Delta K/(\rho)^{1/2}]$ ON THE NUMBER OF CYCLES TO INITIATE A CRACK (N_i) FROM NOTCHES IN SPECIMENS $\geq$ 0·2 IN THICK

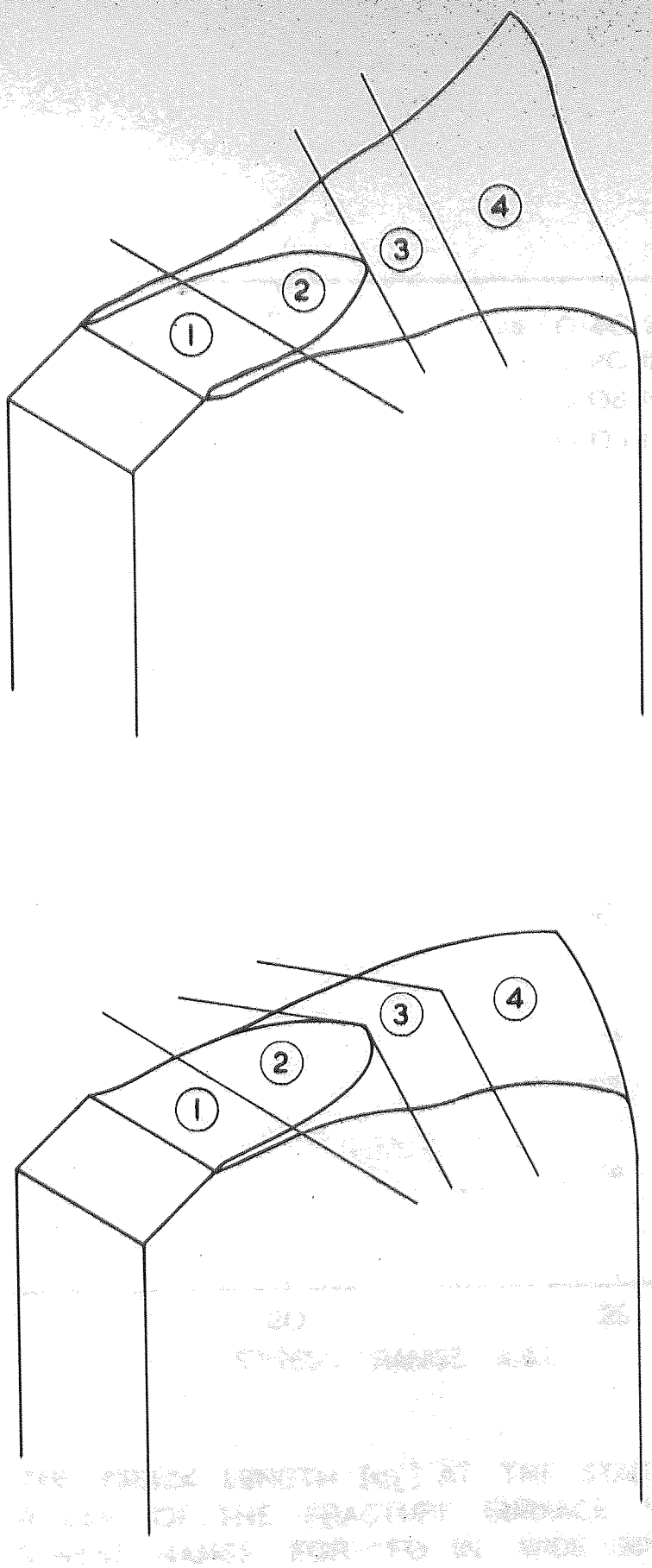

FIG 21. SCHEMATIC RERESENTATION OF TYPICAL FRACTURE SURFACES.

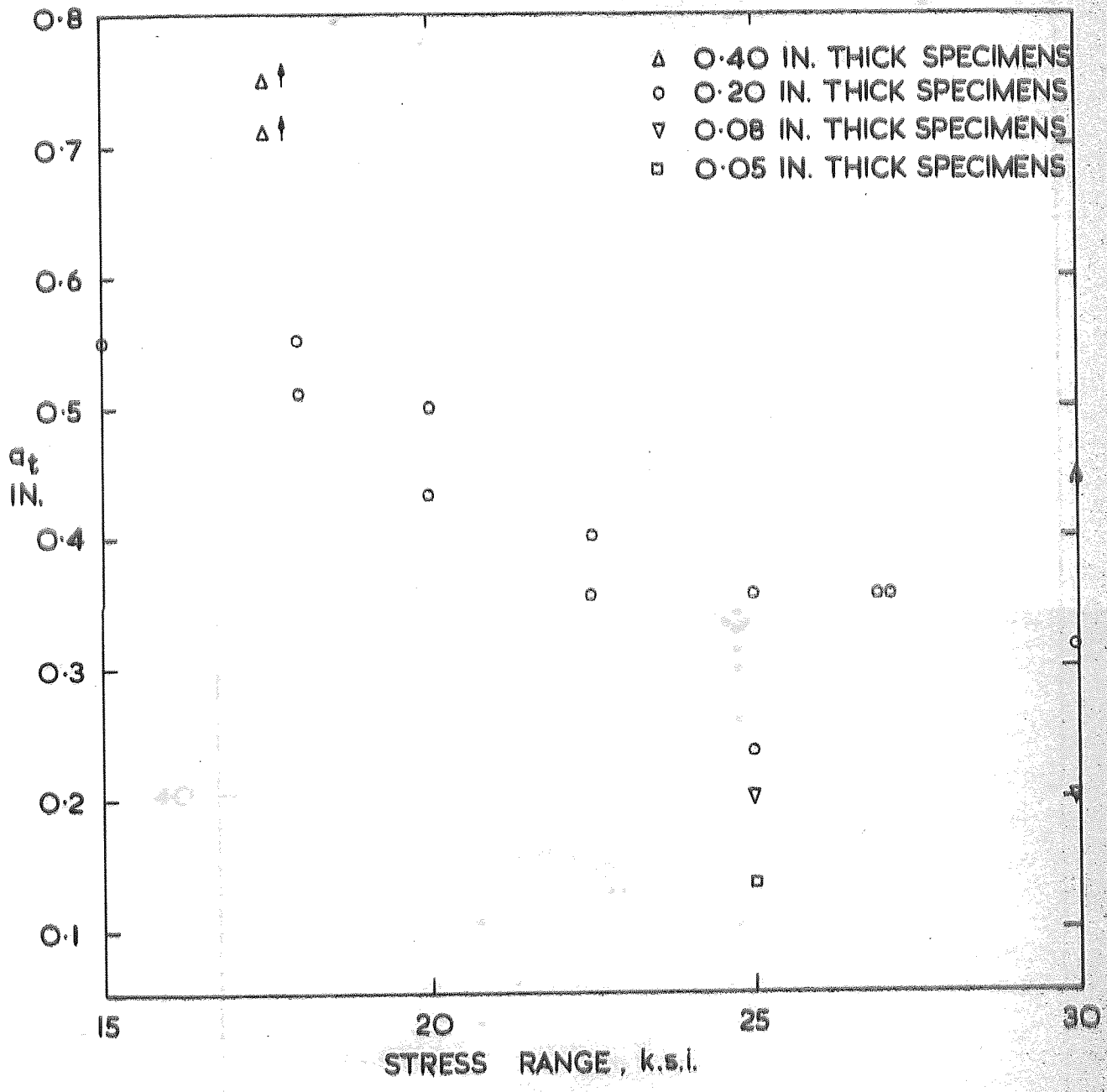

FIG. 22. THE CRACK LENGTH (a_t) AT THE START OF THE SHEAR REGION OF THE FRACTURE SURFACE VERSUS APPLIED STRESS RANGE FOR 1·0 IN. WIDE SPECIMENS.

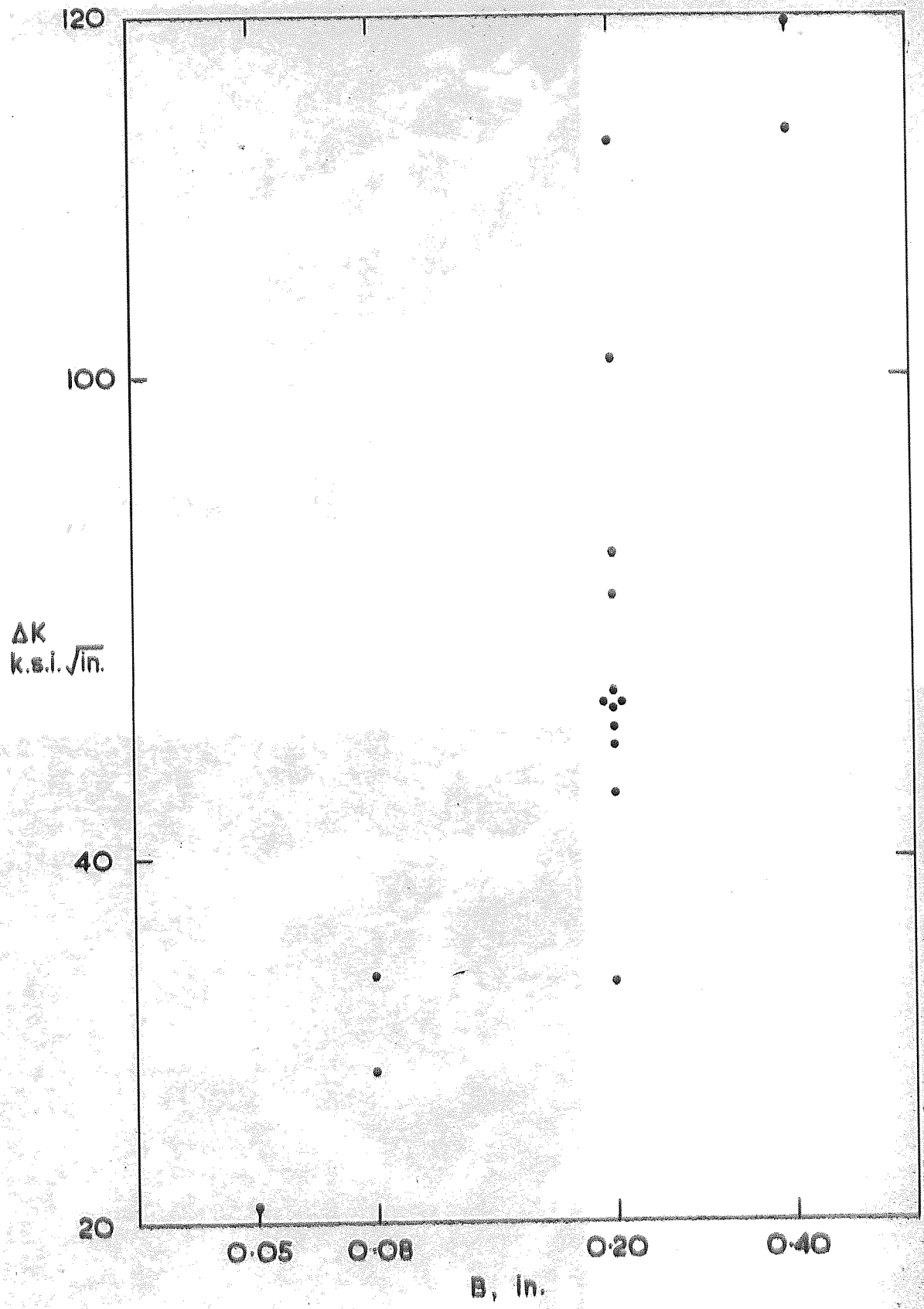

FIG. 23. THE RANGE OF STRESS INTENSITY FACTOR (ΔK) AT a_t VERSUS SPECIMEN THICKNESS (B)

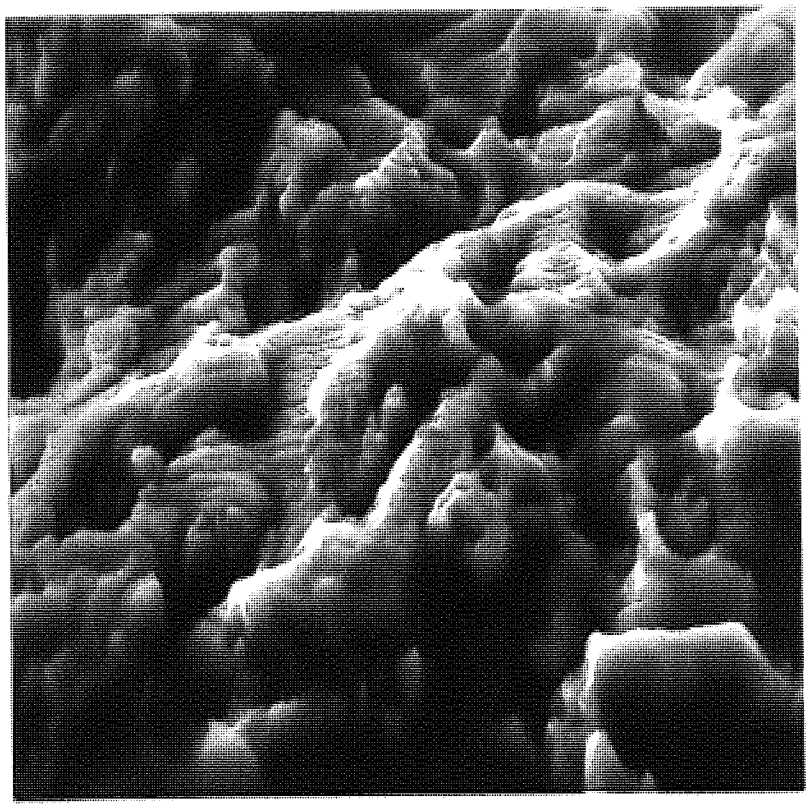

Fig.24. Specimen 65. Fracture surface adjacent to root of notch. x2,900

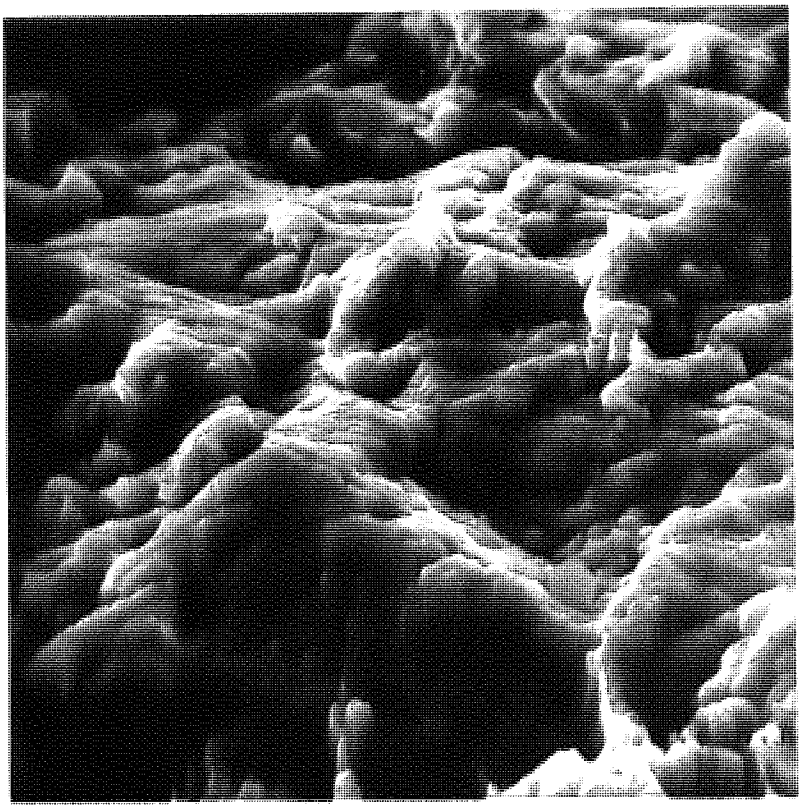

Fig.25. Specimen 65. Fracture surface at a = 0.125 in. x2,900

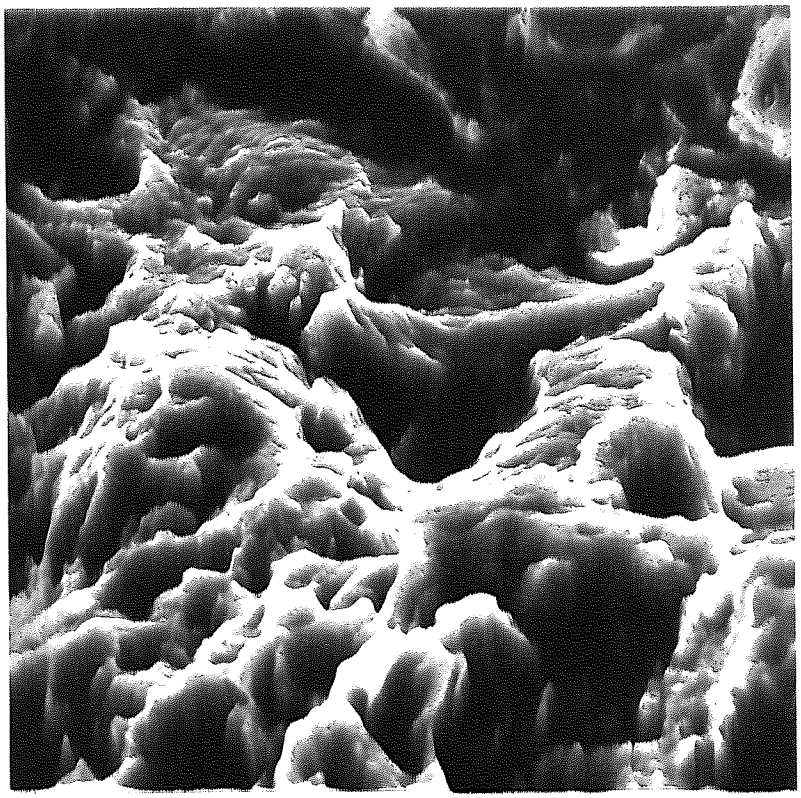

Fig.26. Specimen 65. Fracture surface at a = 0.250 in. x2,600

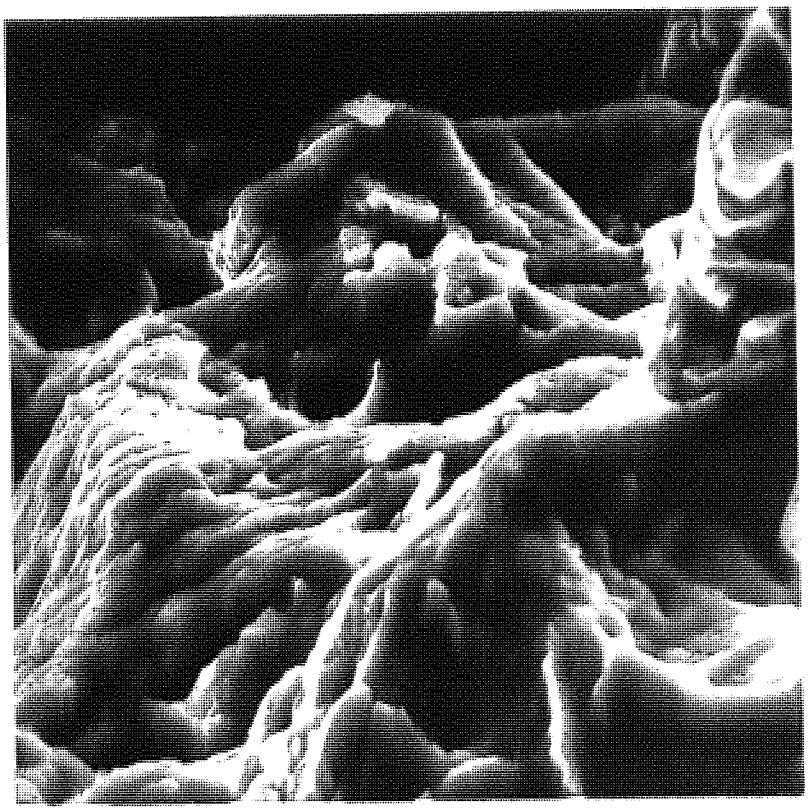

Fig.27. Specimen 65. Fracture surface at a = 0.350 in. x2,400

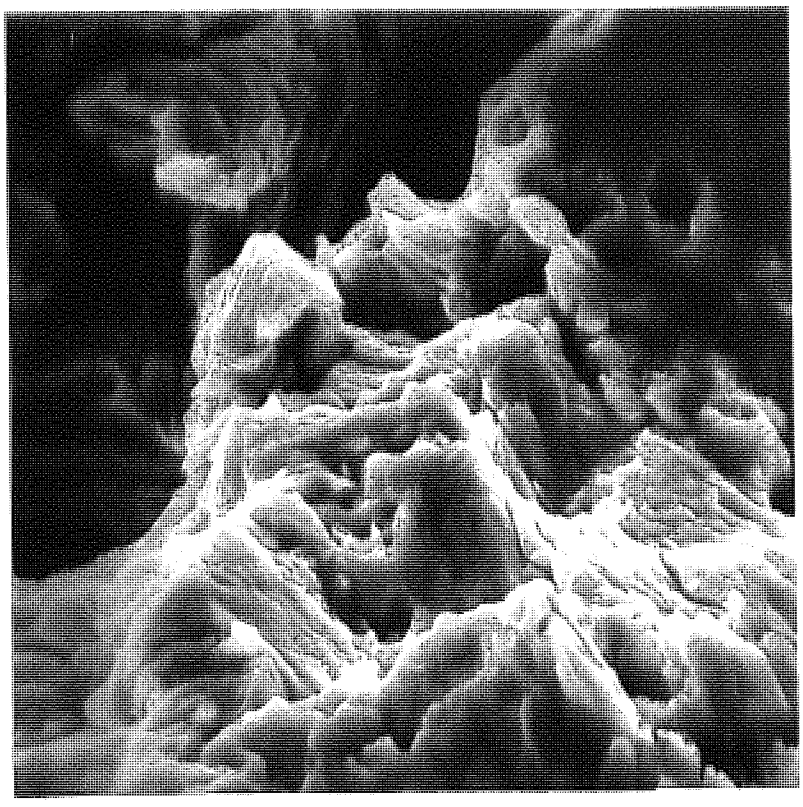

Fig. 28. Specimen 65. Fracture surface at a = 0.425 in. x 2,250

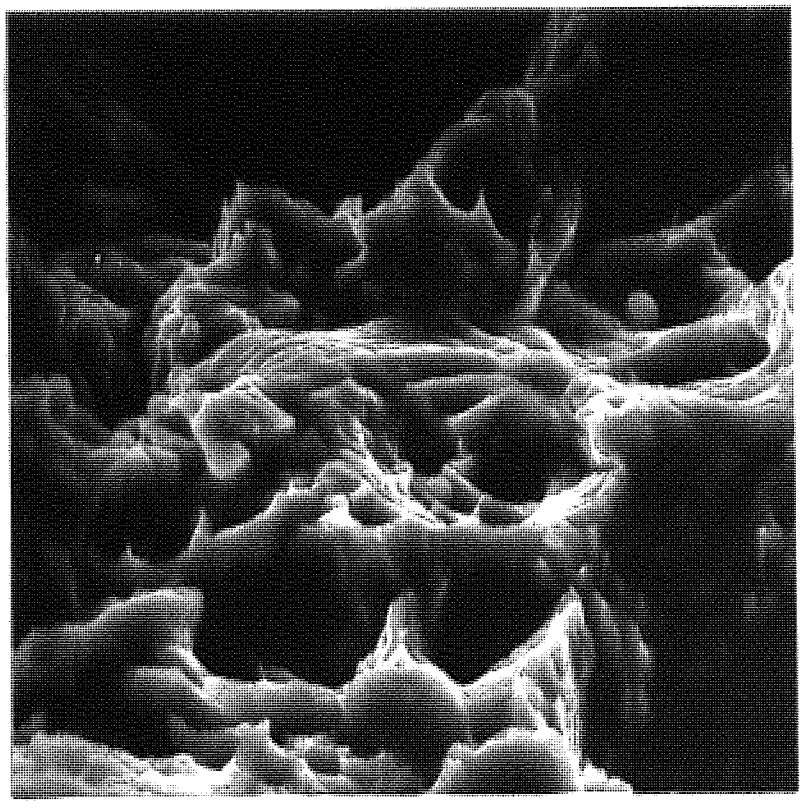

Fig. 29. Specimen 65. Fracture surface at a = 475 in. x2,100

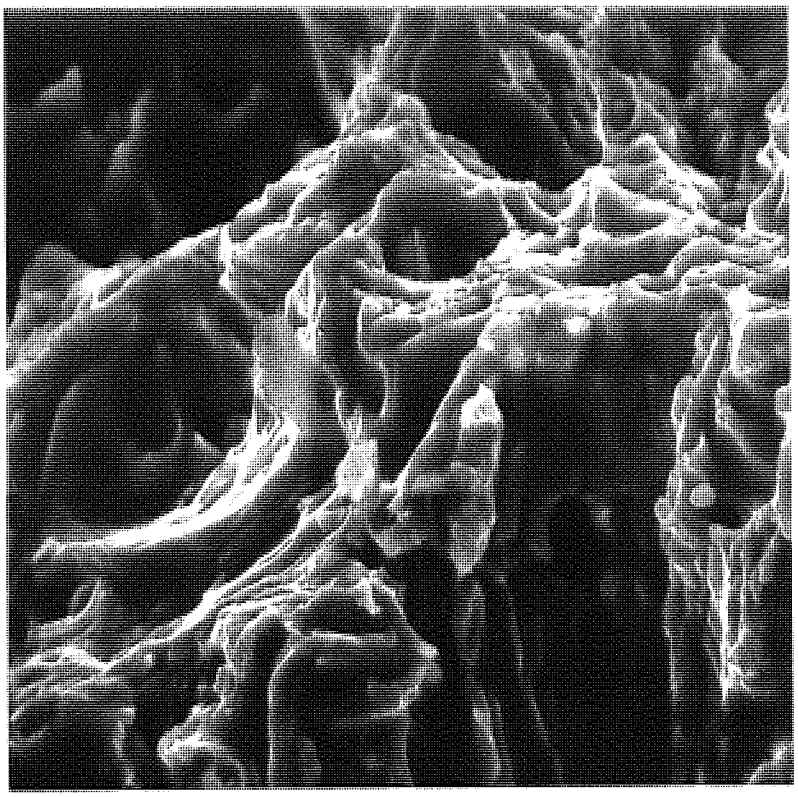

Fig.30. Specimen 65. Fracture surface at a = 0.50 in. x2,100

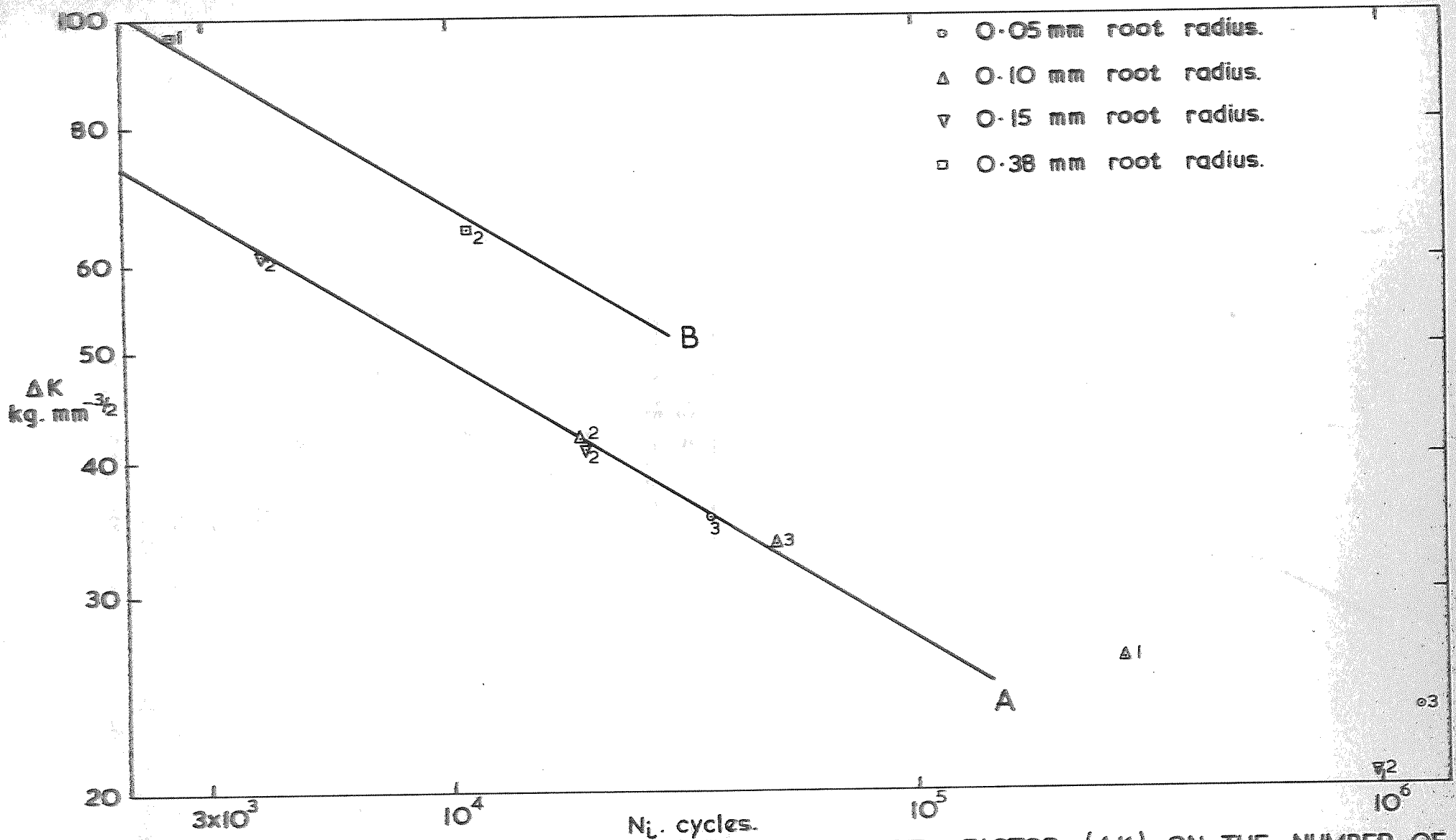

FIG. 31. THE INFLUENCE OF THE RANGE OF STRESS INTENSITY FACTOR (ΔK) ON THE NUMBER OF CYCLES TO INITIATE A CRACK (N_i) FROM NOTCHES OF VARIOUS ROOT RADII IN 24 S-T ALUMINIUM ALLOY (WEIBULL 1961.)

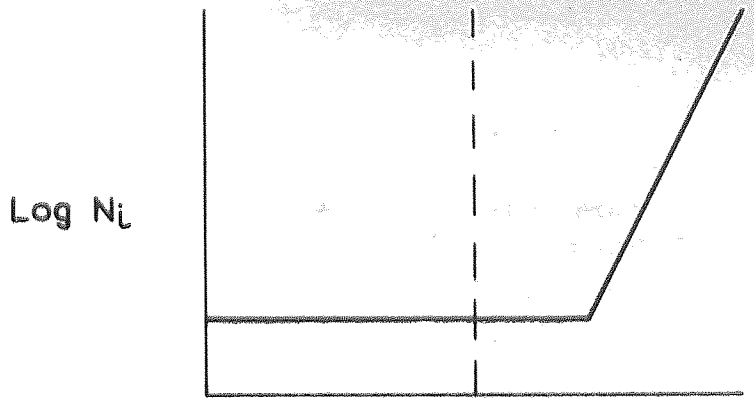

(a) LARGE GRAIN SIZE. $\rho_o > \rho$

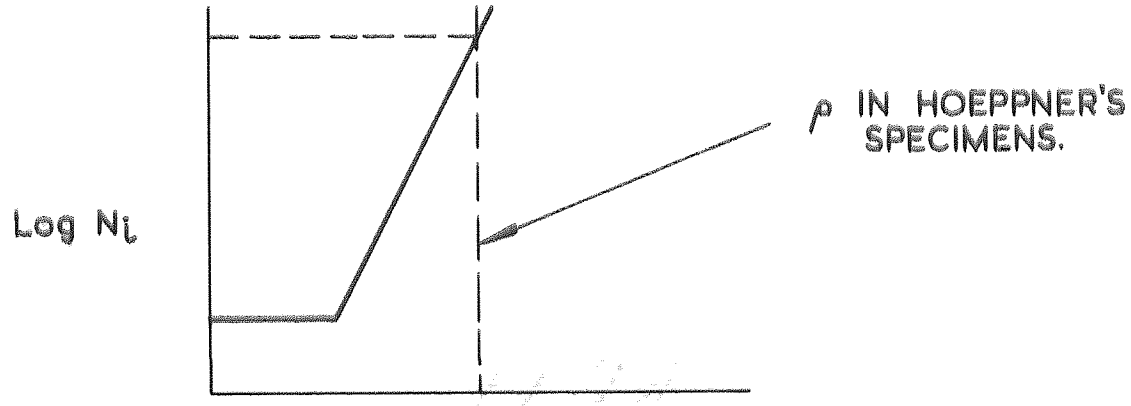

(b) SMALL GRAIN SIZE. $\rho_o < \rho$

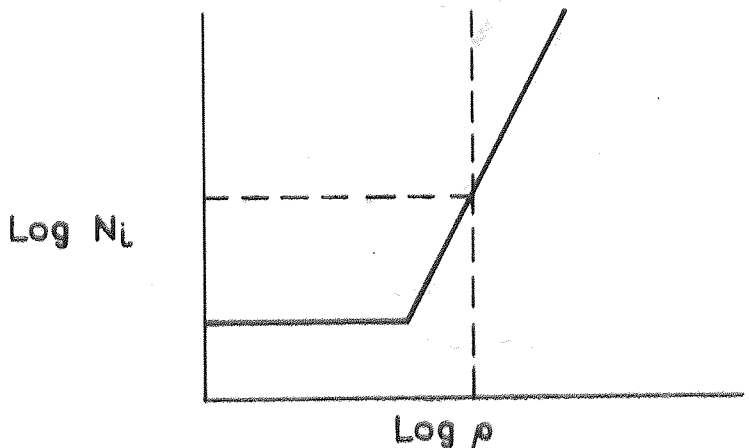

(c) INTERMEDIATE GRAIN SIZE.

FIG. 32. SUGGESTED EXPLANATION FOR THE EFFECT OF GRAIN SIZE ON CRACK INITIATION IN NOTCHED COPPER SPECIMENS OBSERVED BY HOEPPNER. (1967.)

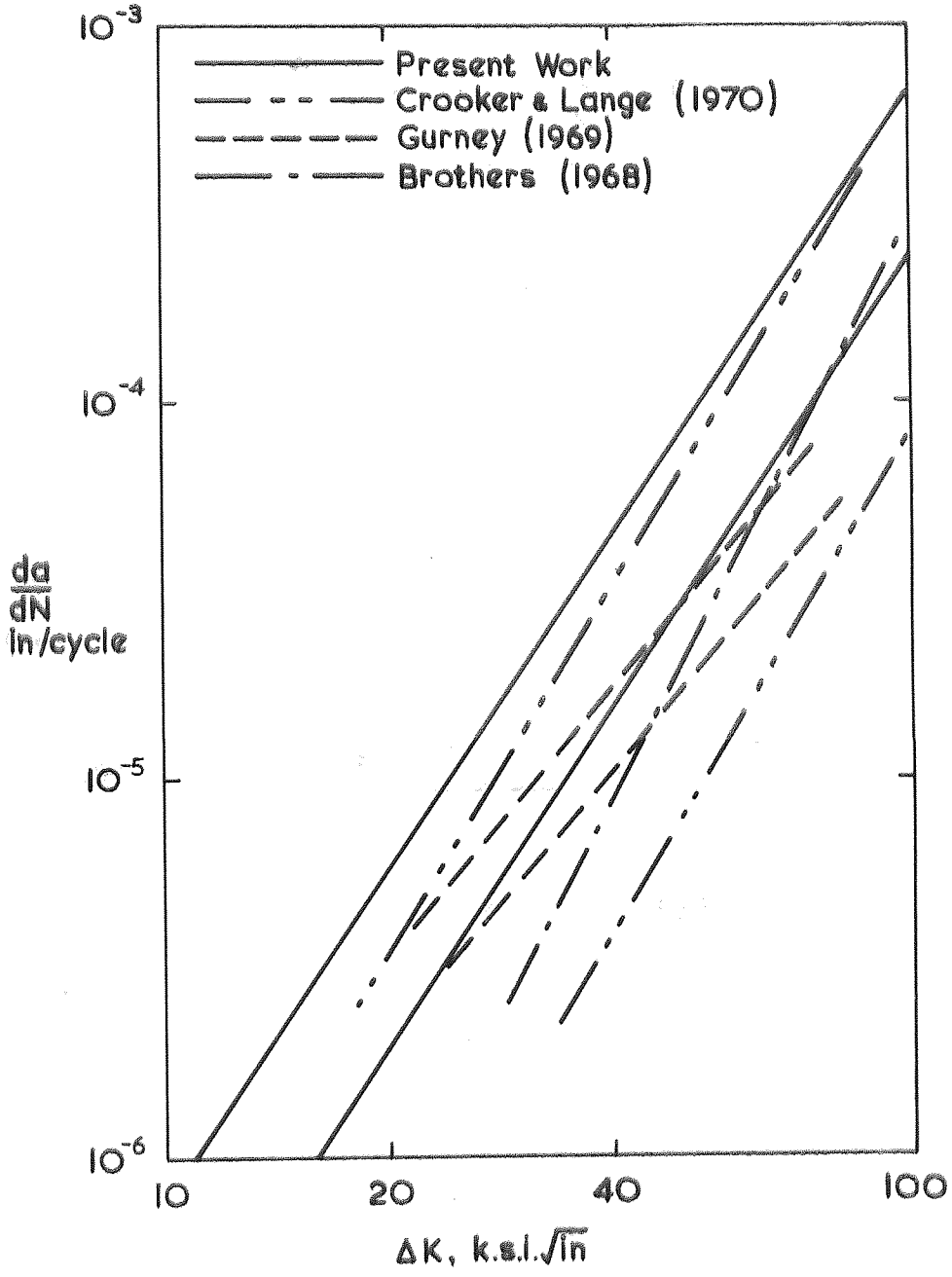

FIG. 33. COMPARISON OF PUBLISHED CRACK GROWTH RATES WITH SCATTER BAND FROM FIG. 13.

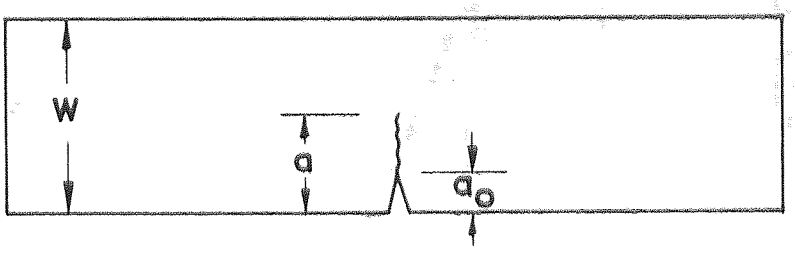

(a)

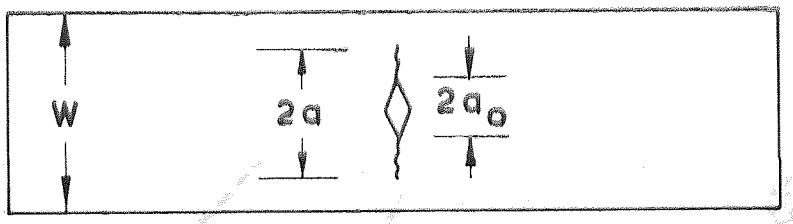

(b)

FIG. 34. (a) SINGLE EDGE NOTCHED PLATE.

(b) CENTRE NOTCHED PLATE.

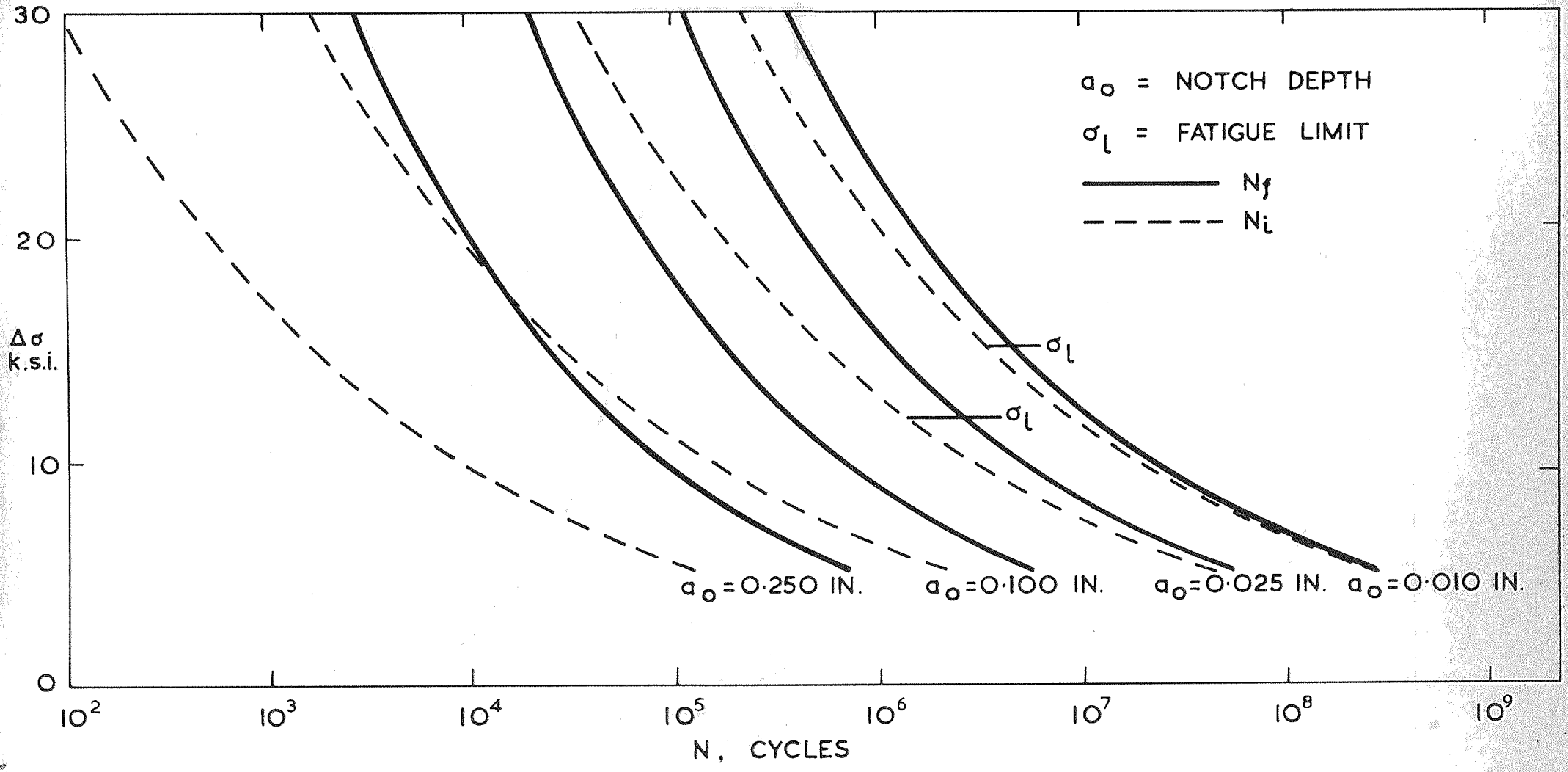

FIG. 35. THE EFFECT OF STRESS RANGE ($\Delta\sigma$) ON N_i AND N_f FOR 1·0 IN. WIDE PLATES CONTAINING SHARP EDGE NOTCHES OF VARIOUS DEPTHS.

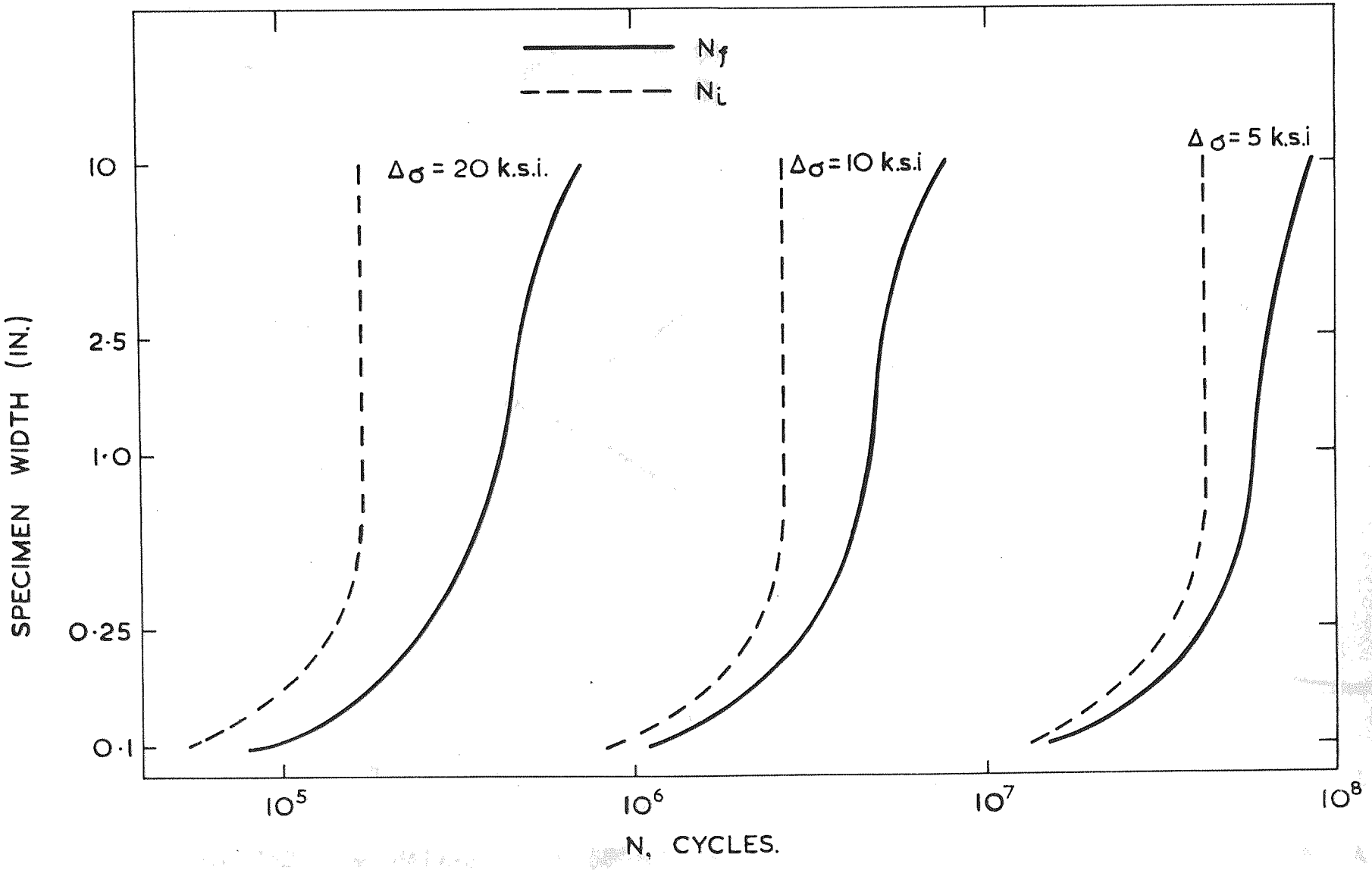

FIG. 36. THE EFFECT OF SPECIMEN WIDTH ON N_i AND N_f FOR SPECIMENS CONTAINING 0·025 in. SHARP EDGE NOTCHES AT THREE STRESS RANGES.

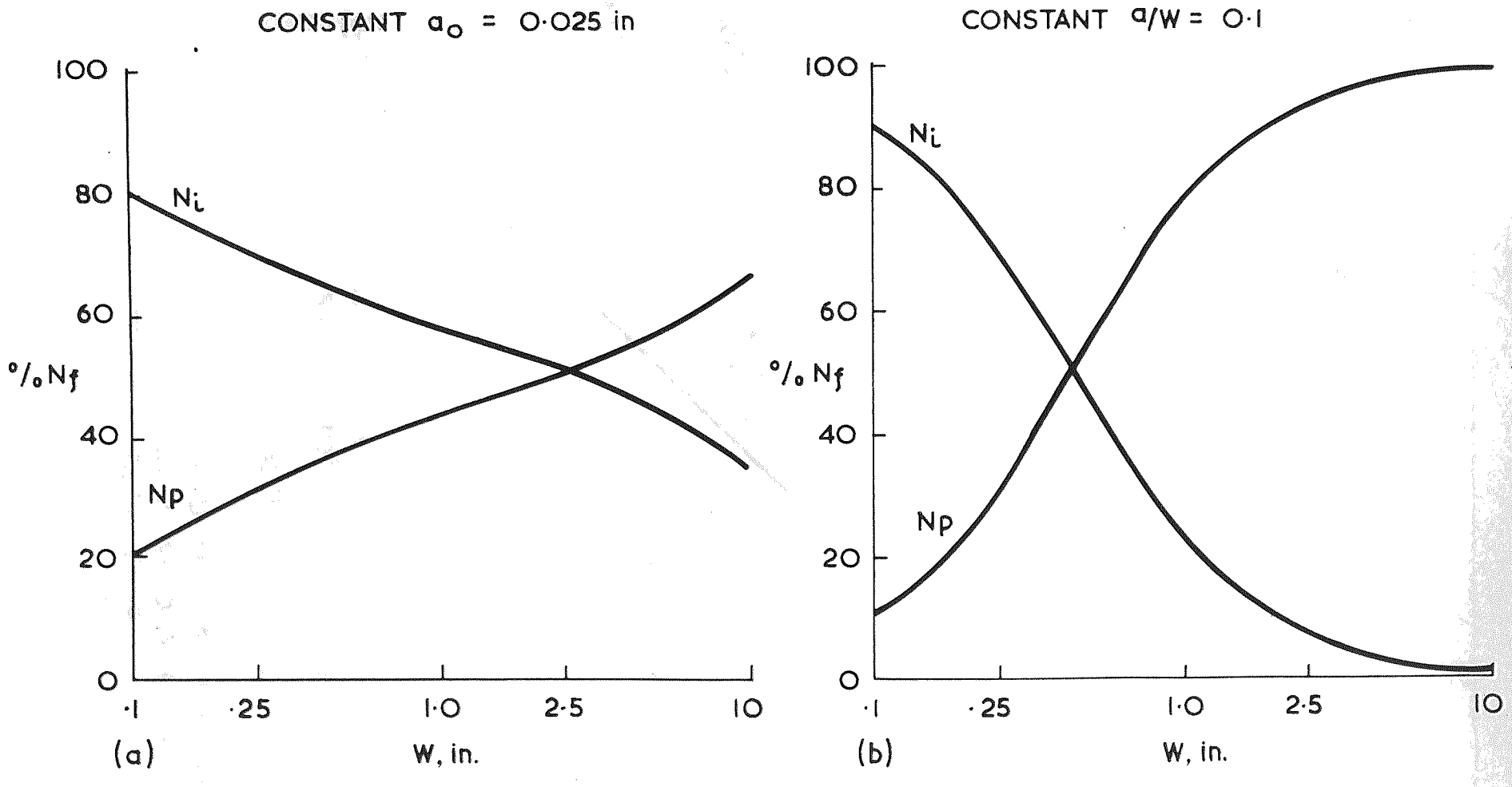

FIG. 37. THE FRACTION OF FATIGUE LIFE SPENT IN CRACK INITIATION AND PROPAGATION AS A FUNCTION OF SPECIMEN WIDTH.

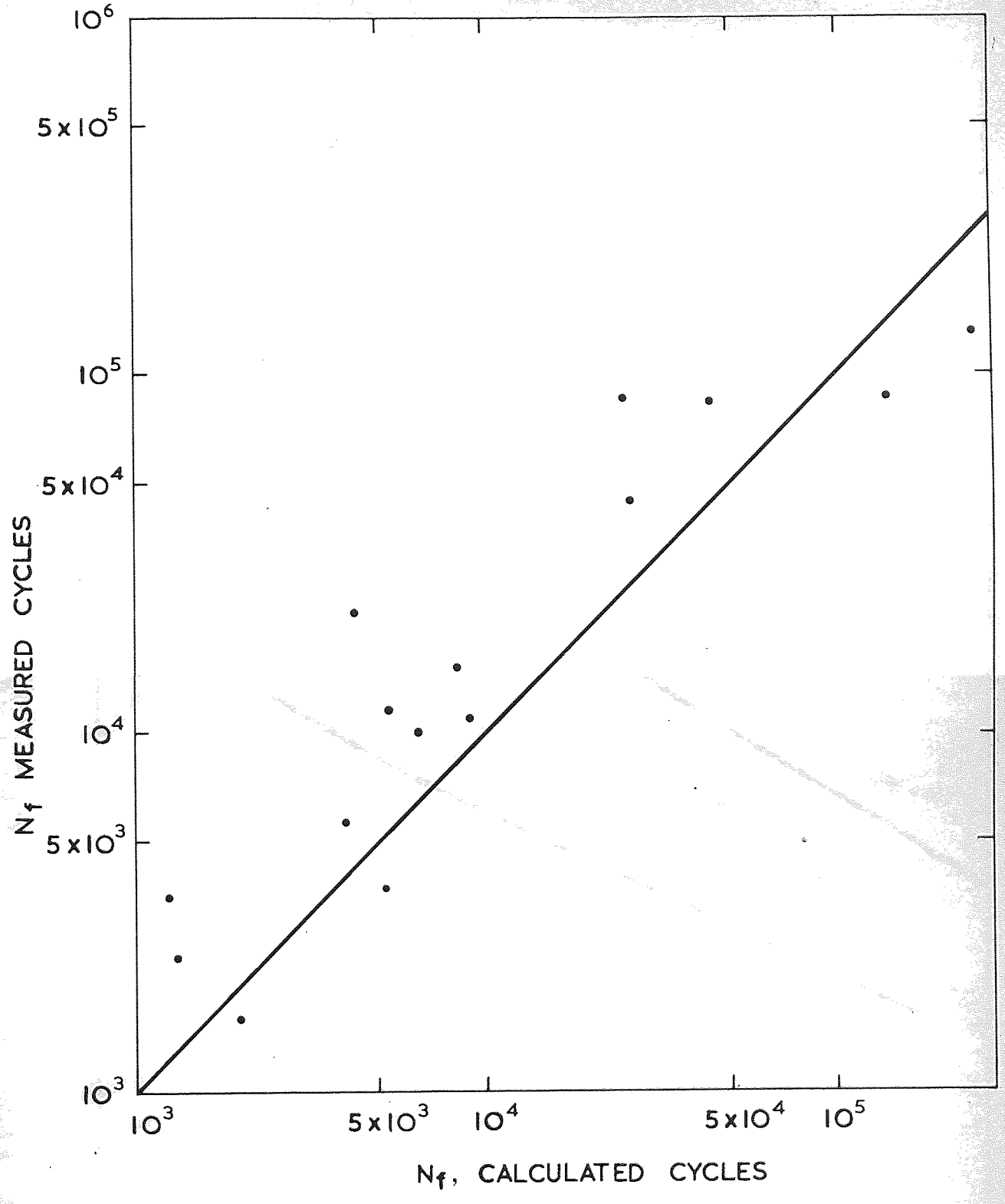

FIG. 38. MEASURED VERSUS CALCULATED FATIGUE LIFE OF SPECIMENS CONTAINING A WELD WITH A LACK OF ROOT PENETRATION DEFECT.

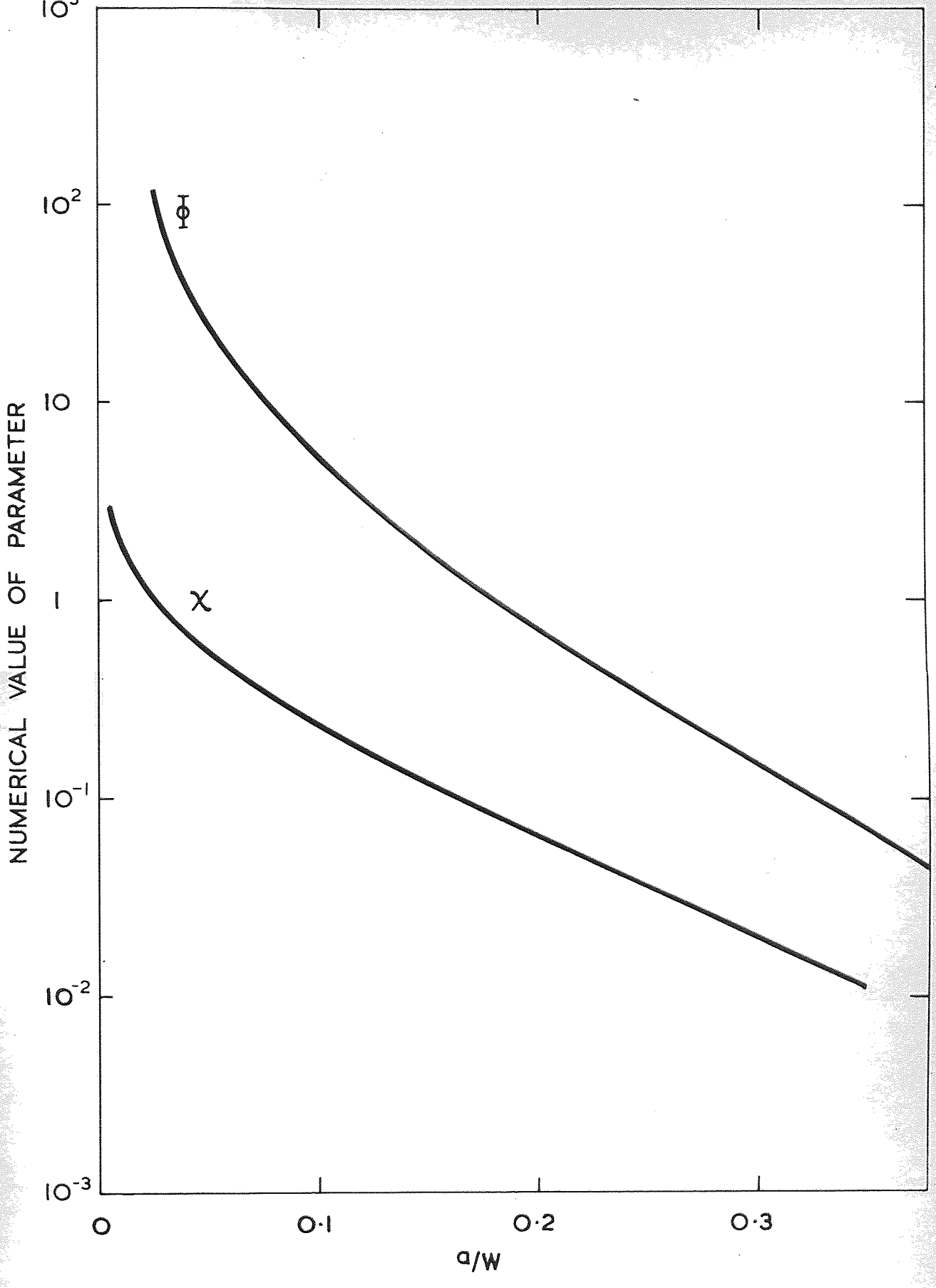

FIG. 39. FUNCTIONS USED IN CALCULATING N_i AND Np